JYVÄSKYLÄ STUDIES IN BIOLOGICAL AND ENVIRONMENTAL SCIENCE
337

Yufei Gu

Sunlit Surface Waters

Exploring the Photochemical Reactivity of Dissolved Organic Carbon

JYVÄSKYLÄN YLIOPISTO

JYVÄSKYLÄ STUDIES IN BIOLOGICAL AND ENVIRONMENTAL SCIENCE 337

Yufei Gu

Sunlit Surface Waters

Exploring the Photochemical Reactivity of Dissolved Organic Carbon

Esitetään Jyväskylän yliopiston matemaattis-luonnontieteellisen tiedekunnan suostumuksella
julkisesti tarkastettavaksi Ambiotica-rakennuksen salissa YAA303,
marraskuun 23. päivänä 2017 kello 12.

Academic dissertation to be publicly discussed, by permission of
the Faculty of Mathematics and Science of the University of Jyväskylä,
in building Ambiotica, hall YAA303, on November 23, 2017 at 12 o'clock noon.

UNIVERSITY OF JYVÄSKYLÄ

JYVÄSKYLÄ 2017

Sunlit Surface Waters

Exploring the Photochemical Reactivity of Dissolved Organic Carbon

JYVÄSKYLÄ STUDIES IN BIOLOGICAL AND ENVIRONMENTAL SCIENCE 337

Yufei Gu

Sunlit Surface Waters

Exploring the Photochemical Reactivity of Dissolved Organic Carbon

UNIVERSITY OF JYVÄSKYLÄ

JYVÄSKYLÄ 2017

Editors
Anssi Lensu
Department of Biological and Environmental Science, University of Jyväskylä
Pekka Olsbo, Ville Korkiakangas
Publishing Unit, University Library of Jyväskylä

Jyväskylä Studies in Biological and Environmental Science
Editorial Board

Jari Haimi, Anssi Lensu, Timo Marjomäki, Varpu Marjomäki
Department of Biological and Environmental Science, University of Jyväskylä

Cover photo by Yufei Gu.

Permanent link to this publication: http://urn.fi/URN:ISBN:978-951-39-7252-3

URN:ISBN:978-951-39-7252-3
ISBN 978-951-39-7252-3(PDF)

ISBN 978-951-39-7251-6 (print)
ISSN 1456-9701

Jyväskylä University Printing House, Jyväskylä 2017

ABSTRACT

Gu, Yufei
Sunlit surface waters: exploring the photochemical reactivity of dissolved organic carbon
Jyväskylä: University of Jyväskylä, 2017, 53 p.
(Jyväskylä Studies in Biological and Environmental Science
ISSN 1456-9701; 337)
ISBN 978-951-39-7251-6 (print)
ISBN 978-951-39-7252-3 (PDF)
Yhteenveto: Pintavedet auringonpaisteessa: liuenneen orgaanisen hiilen valokemiallisen reaktiivisuuden vaihtelu
Diss.

In surface waters, solar radiation can photochemically mineralise the dissolved organic carbon (DOC, a measure of dissolved organic matter, DOM) to dissolved inorganic carbon (DIC). This DIC photoproduction constitutes an essential yet vague flux in the aquatic carbon cycling. The present thesis is based on the empirical assessment of the DOC photochemical reactivity, which was determined as the spectral apparent quantum yields (AQY) for DIC photoproduction. First, AQYs were determined in DOM solutions to quantify the impact of pH and DOM-associated iron. Then boreal lake waters were used for assessing the alteration of DOC photoreactivity due to water quality and catchment property. By simulating DIC production, further, AQYs were used to approximate the photomineralisation of terrigenous DOC (tDOC) in coastal waters. Finally, the experimental protocols determining AQY were compared by four laboratories. The results demonstrated the variation of AQYs triggered by the laboratory-specific procedures was less than that across the examined inland waters. Up to 86 % of the DIC photoproduction in DOM solutions can be justified by iron-stimulated photoreactions with acidic pH, while the effect was negligible at pH > 7. This interaction between iron and acidity was similarly influential on DOC photoreactivity in boreal lake waters. Across lakes, the DOC photoreactivity was varied relevant to the water quality and catchment land use patterns. A high DOC photoreactivity can be expected when the contents of DOC and chromophoric DOM are high, more so in small lakes enriched by peaty soils. Although DOC photoreactivity in lakes was higher, the estimates revealed that solar radiation mineralised far more tDOC in marine waters, which may be attributed to the extensive spreading of tDOC during mixing over the coastal ocean.

Keywords: Apparent quantum yields; boreal lakes; catchment land use; dissolved organic matter; iron; photomineralisation; water quality.

Yufei Gu, University of Jyväskylä, Department of Biological and Environmental Science, P.O. Box 35, FI-40014 University of Jyväskylä, Finland

Author's address Yufei Gu
Department of Biological and Environmental Science
P.O. Box 35
FI-40014 University of Jyväskylä
Finland
yufei.y.gu@jyu.fi

Supervisors Dr. Anssi V. Vähätalo, Senior Lecturer
Department of Biological and Environmental Science
P.O. Box 35
FI-40014 University of Jyväskylä
Finland

Professor Jussi Kukkonen
Department of Biological and Environmental Science
P.O. Box 35
FI-40014 University of Jyväskylä
Finland

Reviewers Professor Andrew Rose
Southern Cross GeoScience
Southern Cross University
Lismore, NSW 2480
Australia

Associate Professor Amit Bhatnagar
Department of Environmental Science
University of Eastern Finland
Yliopistonranta 1E, Snellmania
FI-70211 Kuopio
Finland

Opponent Professor Davide Vione
Department of Chemistry
University of Turin
Via Pietro Giuria 5
10125 Torino
Italy

CONTENTS

LIST OF ORIGINAL PUBLICATIONS

This thesis is based on the following original articles, which will be referred to in the text by their Roman numerals I–IV. Contributions of authors in each article:

In I, YG & AV planned the study, collected water sample and designed experiment, YG conducted the experiment, SP & YG analysed iron samples, YG, AL & AV made statistical analyses, all authors contributed to manuscript preparation.

In II, YG, MT & AV planned the study, KV & YG collected water samples, YG & AV designed the experiment, YG conducted the experiment, SP & YG analysed iron samples, KV & AV collected catchment data, YG made statistical analyses, all authors contributed to manuscript preparation.

In III, BK & LT planned the study, BK led the experimental design and coordination, RC, KE, AV & CW contributed to water samples collection, RC & CW contributed to chemical characterisation, YG & AV contributed to iron analysis, KE, YG, LP, CW designed and conducted the experiment, BK led the data analyses and writing, LP and WM contributed to nitrite actinometry, all authors contributed to data analyses and manuscript preparation.

In IV, AV & HA planned the study, HA, AV & YvesG organised water sampling, HA conducted the experiment, HA & AV made data analyses, YG & V-MP made AQY modelling, all authors contributed to manuscript preparation. This study was included in the doctoral thesis of H. Aarnos. The manuscript enclosed here has been majorly revised.

I Gu Y., Lensu A., Perämäki, S., Ojala A. & Vähätalo A.V. 2017. Iron and pH regulating the photochemical mineralization of dissolved organic carbon. *ACS Omega* 2: 1905–1914.

II Gu Y., Vuorio K., Perämäki, S., Tiirola M. & Vähätalo A.V. Linking photochemical reactivity of dissolved organic carbon to catchment property and water quality in boreal lakes. Manuscript.

III Koehler B., Miller W.L., Cory R.M., Einarsdottir K., Gu Y., Powers L.C., Vähätalo A.V., Ward C.P. & Tranvik L.J. An inter-laboratory comparison of the apparent quantum yield for photochemical dissolved organic carbon mineralization in inland waters. Manuscript.

IV Aarnos H., Gélinas, Y., Kasurinen V., Gu Y., Puupponen V. & Vähätalo A.V. Photochemical mineralization of terrigenous DOC to dissolved inorganic carbon in ocean. Submitted manuscript.

ABBREVIATIONS

AQY	Apparent Quantum Yields
ASW	Artificial SeaWater
a_λ	CDOM spectral absorption coefficient at λ nm
CDOM	Chromophoric Dissolved Organic Matter
CO_2	carbon dioxide
DIC	Dissolved Inorganic Carbon
DICpr	photoproduction rate of DIC
DOC	Dissolved Organic Carbon
DOM	Dissolved Organic Matter
ϕ_λ	spectral apparent quantum yields for DIC photoproduction at λ nm
Fe	iron
[Fe]	iron concentration
Fe(II)	ferrous iron
Fe(III)	ferric iron
HMW	High Molecular Weight
HO·	hydroxyl radical
λ	wavelength
LMW	Low Molecular Weight
NOM	Natural Organic Matter
PAR	Photosynthetically Active Radiation
pr	areal rate of DIC photoproduction
ROS	Reactive Oxygen Species
SPE	Solid Phase Extraction
SPE-DOM	Solid Phase Extracted Dissolved Organic Matter
S_R	Slope ratio
SUVA	Specific UV absorbance at 254 nm
tDOC	Terrigenous Dissolved Organic Carbon
UVR	Ultraviolet Radiation
UV-B	Ultraviolet B

1 INTRODUCTION

1.1 Dissolved organic matter in freshwater

1.1.1 Terrestrial dissolved organic matter

Studies on naturally occurring organic substances have become more prevalent since its recognisable significance in the soil-forming process and fertility for agriculture in the 1800s (Kononova 1966). Wallerius (1761) used humus to describe its formation from decomposed plant and its ability to absorb water and nutrients. In an aquatic environment, the dissolved fraction of the organic substance is dissolved organic matter (DOM), which operationally is defined as a fraction passes through filters between 0.2–0.7 µm (Danielsson 1982, Zsolnay 2003, Potter and Wimsatt 2005). Although the nominal pore size of 0.2–0.7 µm to separate DOM is arbitrary, the 0.45 µm is almost a universal consensus (Danielsson 1982, Zsolnay 2003, Potter and Wimsatt 2005). DOM is typically introduced into the aquatic environment via 1) terrestrial material leached from decayed plants residues or animal tissues in the soil, 2) autochthonous matter derived from phytoplankton and other aquatic organisms, and 3) anthropogenic sources (Mostofa *et al.* 2013), despite the classification can be varied (McDowell and Likens 1988, Qualls and Haines 1991, Zsolnay 1996).

DOM is an important element in the freshwater system. It can interact with natural colloids and engineered particles (Philippe and Schaumann 2014), thus may involve in nutrient cycling, microbial metabolism (Baña *et al.* 2014, Kamjunke *et al.* 2015), or alter the fate of emerging contaminants (Kim *et al.* 2003, Bolan *et al.* 2011) and carbon dioxide (CO_2) fluxes between geosphere, hydrosphere and atmosphere (Mayorga *et al.* 2005, Lapierre *et al.* 2013). Quantification of DOM is commonly based on its carbon component, dissolved organic carbon (DOC) (Hopkinson and Vallino 2005).

In recent years, efforts to construct inland water carbon fluxes promoted the vital role of DOC in carbon biogeochemistry (Cole *et al.* 2007). Inland water permeates into terrestrial ecosystem. Although it covers less than 2 % of the

planet's surface, the collective contribution of lakes, reservoirs and peatlands to the global carbon flux is substantial compared with that of the ocean (71 % Earth's coverage) ecosystems (Cole *et al.* 1994, 2007, Battin *et al.* 2009, Downing *et al.* 2012). DOC constitutes the largest share of total organic carbon (TOC) in boreal lake waters (Kortelainen *et al.* 2006, Cole *et al.* 2007), e.g., over 90 % of TOC is in the form of DOC in Finnish rivers (Mattsson *et al.* 2005). Increased export of terrigenous DOM into the boreal aquatic regime can modify the in-lake carbon inventory (Lapierre *et al.* 2013).

1.1.2 Global browning and iron

DOM is partially chromophoric (CDOM), characterises the DOM pool with increasing light-absorption towards the UV–visible spectral region and causes a yellow-brownish colour of lake and stream waters. Since the 90's, enhanced terrestrial DOC export into surface waters has caused the brownification (Graneli 2012) of lakes and streams in North America, northern Europe and the UK, which largely can be ascribed to the recovery from environmental acidification and increased temperature (Forsberg 1992, Evans *et al.* 2005, Skjelkvåle *et al.* 2005, Vuorenmaa *et al.* 2006, Monteith *et al.* 2007, Löfgren and Zetterberg 2011), cf. (Hruška *et al.* 2009). This browning process strongly drove CDOM to absorb solar radiation at short wavelength (i.e., UV-visible range) of the spectrum, thus reduced the availability of light, e.g., to aquatic plants in lakes and other freshwater ecosystems (Morris *et al.* 1995). In a study on 168 Norwegian lakes, rising DOC contents had led to a negative impact on the number of brown trout (Finstad *et al.* 2014), which suggested that lasting brownification could disturb the structure and function of the aquatic ecosystem.

In addition to the rise in DOC, an increasing iron (Fe) concentration has been observed in Finland, Sweden and UK along with the brownification of inland waters (Neal *et al.* 2008, Kritzberg and Ekström 2012, Sarkkola *et al.* 2013). Ferric iron (Fe(III)) has a brown colour similar to that of DOM (Xiao *et al.* 2013, 2015), hence it is suspected that Fe contributes similarly to the brownification as DOC. Further studies have proven a positive relation between Fe concentration and water colour, considering Fe is mainly organically bound in humic waters (Shapiro 1964, Heikkinen 1990, Kritzberg and Ekström 2012). Increased DOC and Fe concentrations are relevant to enhanced absorption of ultraviolet radiation (UVR; 280–400 nm), photosynthetically active radiation (PAR; 400–700 nm) and CDOM absorbance (Poulin *et al.* 2014), which could plausibly initiate photochemical reaction. Therefore, loading DOM and Fe in freshwaters were analogues in the sense that both of whom absorb light, enhance water colour, and potentially serve photochemical reaction.

1.2 Photochemistry of DOM

1.2.1 CDOM absorbance and photobleaching

Light must be absorbed by the system for the occurrence of a photochemical reaction, which is the first law of photochemistry attributed to Grotthnus (1819) and Draper (1841). In shallow freshwater and estuary, CDOM is the dominant light absorber compared to other absorbing agents, e.g., water, phytoplankton and non-biogenic detritus (Hoge *et al.* 1993, Branco and Kremer 2005). CDOM absorption increases from the visible towards the UV-part of the spectrum. No method is currently available to quantify CDOM concentration because it consists of heterogeneous chromophores. Instead, light absorption is used as a proxy for CDOM concentration (Hu *et al.* 2002). It is derived from Beer-Lambert law that formulated a relation between the light attenuation and the properties of the medium thorugh which light travels, given by,

$$A = \log_{10} \frac{P_\lambda^0}{P_\lambda} = \varepsilon\, c\, l \quad (1)$$

where A = absorbance, P_λ^0 = radiant intensity of light passing through the blank, P_λ = radiant intensity of light passing through the sample, ε = molar absorption coefficient, c = concentration of a homogeneous medium and l = optical path length (McNaught and Wilkinson 1997). However, absorbance is not good for comparison because it is proportional to the compound concentration and optical path length. Absorption coefficient (a) is frequently used to indicate the light absorption. Unlike absorbance, the a of CDOM is normalised with the path length and is independent of illumination conditions. It is crucial for spectrophotometry in general, which can be derived as:

$$a = \ln(10)\, A_{\text{sample}}\, l^{-1} \quad (2)$$

where a = absorption coefficient, and A_{sample} = apparent absorbance of sample. Often a is closely related to the concentration of DOC and therefore, can be applied to, e.g., estimate DOC concentrations in river-influenced ocean margins (Ferrari *et al.* 1996, Fichot and Benner 2011, Inamdar *et al.* 2012). The wavelength-dependent characteristic of a can be used to describe the spectral optical property. For instance, deriving from a, the spectral slope coefficient at 275–295 nm ($S_{275\text{–}295}$) and spectral slope ratio (S_R) reflect the history of CDOM (i.e., source and transformation) in aquatic systems (Helms *et al.* 2008, Fichot and Benner 2012). Specific ultraviolet absorbance ($SUVA_{272}$, $SUVA_{254}$) has been used to indicate aromaticity of DOM (Traina *et al.* 1990, Weishaar *et al.* 2003).

Exposure to solar radiation reduces CDOM absorption and causes photobleaching (Whipple 1899). Breakdown of chromophoric sites and reduction in molecular weight of DOM (Lou and Xie 2006) during photobleaching is exhibited through decreasing values of a_λ, decreasing

$SUVA_{254}$ and increasing S_R (Helms *et al.* 2008, 2013). Photobleaching affects water colour-based remote sensing monitoring of CDOM fluxes (Kutser *et al.* 2005, Del Castillo and Miller 2008, Li *et al.* 2015) and enhances the penetration of biologically damaging ultraviolet-B (UV-B, 280–320 nm) radiation into surface waters (Blough and Zepp 1990, Herndl *et al.* 1993, Morris and Hargreaves 1997, Whitehead *et al.* 2000). CDOM photobleaching is closely related to DIC photoproduction (Kieber *et al.* 1990, Spencer *et al.* 2009a). Decomposition of DOM is expected to be along with photobleaching, which influences freshwater, estuarine and oceanic carbon cycling (Mopper *et al.* 1991, Moran *et al.* 2000, Raymond *et al.* 2013, Cory *et al.* 2014).

1.2.2 DIC photoproduction within inland waters

Zafiriou (1977) and Zika (1981) et al. are likely among the first few to demonstrate the importance of DOM photochemistry. These pioneering works have defined the light-induced process (Zika 1981), modelled the reaction rate, elucidated the possible mechanisms (Zafiriou 1977, Zafiriou *et al.* 1984), characterised the photoproduced reactant (Choudhry 1981, Hoigné *et al.* 1988) and bio-labile substance (Moran and Zepp 1997). Photochemistry-induced changes in DOM have been summarised, including the reduction in molecular weight, alteration in optical properties, and photochemical production of reactive oxygen species (ROS) (Blough and Zepp 1995, Zepp *et al.* 1998) and carbonyl compounds (Kieber *et al.* 1990, Valentine and Zepp 1993, Miller 1994, 1998, Zepp *et al.* 1995, Zhou and Mopper 1997).

DOC is transformed into dissolved inorganic carbon (DIC) via photochemical mineralisation (Salonen and Vähätalo 1994, Granéli *et al.* 1996). The dominant carbon photoproduct is CO_2, frequently is measured as the production of DIC. Hereby, DIC collectively describes CO_2, carbonate, bicarbonate and carbonic acid dissolved in the aqueous environment as unspecified pH-dependent speciation (Miles and Brezonik 1981, Allard *et al.* 1994, Salonen and Vähätalo 1994, Miller and Zepp 1995, Granéli *et al.* 1996, Vähätalo 2009).

Sunlight-initiated DIC production has been estimated to be responsible for 13−35 Tg C, rounded up to ~ 10 % of the total CO_2 emission from global lakes and reservoirs (Tranvik *et al.* 2009, Koehler *et al.* 2014). Mineralisation via respiration dominates CO_2 emission from lakes (Del Giorgio *et al.* 1999, Wiegner and Seitzinger 2001, Tranvik *et al.* 2009). Around 80–90 % of inland water DOC is high molecular weight (HMW) compounds that are relatively recalcitrant to direct biodegradation (Münster and Albrecht 1994, Münster and De Haan 1998). For instance, lignin derived from vascular plants is an abundant precursor of DOM (Moran and Hodson 1994, Maie *et al.* 2007). The aromatic moieties of lignin (Kögel-Knabner 2002) are refractory to biodegradation and may preserve DOM along its transport through rivers to the ocean (Ludwig and Sarkanen 1971, Ertel *et al.* 1984, Guggenberger *et al.* 1994, Hatakka 2001, Minor *et al.* 2012). Partial oxidation of HMW DOC by photochemical processes can reduce the molecular weight and modify the bioavailability of DOM (Moran *et al.* 2000,

Scully *et al.* 2004, Sulzberger and Durisch-Kaiser 2009, Remington *et al.* 2011). The complete oxidation eventually mineralises DOC to DIC photoproducts, e.g., CO_2.

Cory *et al.* (2014) demonstrated that in 73 arctic lakes and rivers photochemical oxidation exceeds respiration rates, and amounted to 70–90 % of DOC processed in the water column. It corresponds to a notable part of arctic carbon flux when scaled up to the Kuparuk River basin. They have also revealed that photochemical processes accounted for one-third of CO_2 atmospheric emission from surface water (Cory *et al.* 2014). The effort has been put to estimate UV-induced photoproduction rate and to identify alterations in the optical properties of DOM in natural waters. However, environmental factors decisive in DOM photochemistry should be taken into account when extrapolating laboratory results to *in situ* carbon fluxes, e.g., (Salonen and Vähätalo 1994, Granéli *et al.* 1996, 1998, Molot *et al.* 2005, Porcal *et al.* 2013).

1.2.3 Influence of water quality

The extent of CDOM photobleaching and DOC photomineralisation partially depends on the chemical composition of DOM. DOM comprises thousands of compounds which can be analysed using the advanced instruments e.g., Fourier-transform ion cyclotron resonance mass spectrometry, and also can be characterised with simpler techniques as absorbance and fluorescence spectroscopy (Twardowski and Donaghay 2002, Helms *et al.* 2008, Hansen *et al.* 2016). For example, absorption and fluorescence properties of DOM are similar for Suwannee River humic (SRHA) and fulvic (SRFA) acids, and solid phase extracts (C18) from Middle Atlantic Bight (Boyle *et al.* 2009). This similarity suggests that much of DOM originates from terrigenous humic substances, primarily derived from partially oxidised lignin of vascular plants origin (Boyle *et al.* 2009). A valid spectral-dependent function for CDOM photobleaching can be calibrated based on the changes in absorption spectra and incident solar energy into lakes (Osburn *et al.* 2001b). The optical properties of CDOM could be expected to be closely linked to DOM photochemistry as CDOM is a dominant light absorber in natural waters and it correlates with DOC dynamics and reactivity (Spencer *et al.* 2009a, Koehler *et al.* 2016).

DOM photochemistry also depends on the inorganic constituents in the water, e.g., Fe. Fe(III) absorbs UV-visible radiation and can interfere with photochemical reactions of DOM (Emmenegger *et al.* 2001, Weishaar *et al.* 2003). Even though Fe is the fourth most abundant chemical element in Earth's crust, it limits oceanic primary production because of its low water solubility (Geider and La Roche 1994, Jickells *et al.* 2005). Aquatic DOM may form complexes with Fe(III) or stabilise colloidal iron(oxy)hydroxides, and therefore could increase the solubility of Fe in surface waters at pH 4–9 (Gustafsson *et al.* 2000, Pullin and Cabaniss 2003, Neubauer *et al.* 2013, Chen *et al.* 2016). Light-mediated reduction of Fe(III) associated with DOM can directly oxidise DOC and release ferrous iron (Fe(II)) (Faust and Zepp 1993, Voelker *et al.* 1997). Fe(II) can be easily re-oxidised to Fe(III) under oxic circumstance by, e.g., dioxygen (O_2), or

ROS as superoxide/hydroperoxyl radicals (O_2^-/HO_2·) and hydrogen peroxides (H_2O_2) (Miles and Brezonik 1981). Reactions with ROS can further oxidise DOC. The re-oxidised Fe(III) can consequently associate with DOM and catalyse mineralisation of DOM (Miles and Brezonik 1981). During prolonged irradiation, photochemistry may decompose the Fe-binding ligands of DOM and lead to precipitation of Fe(III) (Voelker *et al.* 1997). The recent trends of increased Fe concentration in surface water emphasise the need to understand the active role of Fe in DOM photochemistry (Kritzberg and Ekström 2012).

The pH of water affects the CDOM photobleaching and photoproduction of DIC (Bertilsson and Tranvik 2000, Anesio and Granéli 2004, Porcal *et al.* 2014). Acidic pH stimulates the photobleaching and the oxidation of DOM (Gennings *et al.* 2001, Anesio and Granéli 2003, Molot *et al.* 2005). Meanwhile, pH influences Fe speciation (Neubauer *et al.* 2013) and can potentially change the optical properties of DOM (Pace *et al.* 2012). An increased pH could enhance the chromophoric properties of colloidal DOM and increases light-absorption by DOM (Baalousha *et al.* 2006, Pace *et al.* 2012). In Europe and North America, pH of freshwaters has increased as a response to the reversal of acidification (Stoddard *et al.* 1999, Skjelkvåle *et al.* 2001, Wright *et al.* 2005, Garmo *et al.* 2014), which has a potential impact on DOM photochemistry.

Other water quality could also interfere with DOM photochemical processes. For example, in the presence of nitrate and nitrite, irradiation yields hydroxyl radicals (HO·) (Zepp *et al.* 1987, Jankowski *et al.* 1999, Takeda *et al.* 2004). The HO· is a main scavenger of DOM upon irradiation to natural waters (Brezonik and Fulkerson-Brekken 1998, Vione *et al.* 2006, Minero *et al.* 2007). Survey on the combined impact caused by multiple water qualities may provide a better understanding of DOM photochemistry in the natural aquatic environment.

1.2.4 Influence of catchment property

"In every respect, the valley rules the stream", argued limnologist H.B.N. Hynes (1975). Catchment properties regulate the DOM export, influence the nature of DOM (Graeber *et al.* 2012, Autio *et al.* 2016), and affects the transport of other nutrients (e.g., N, P, Fe) into inland waters (Heikkinen 1994, Palviainen *et al.* 2016). The land use in catchments can explain a substantial part of the variance in TOC contents among freshwaters (Graeber *et al.* 2012, Palviainen *et al.* 2016). Peatlands and other wetlands are important sources of DOC (Hope *et al.* 1994, Dillon and Molot 1997, Billett *et al.* 2004). In Finland, the enhanced export of DOC from the catchment can be expected when the proportion of peatlands increases (Mattsson *et al.* 2005).

In addition to the land use, DOC concentration in freshwaters depends on the in-lake processes and hydrology in the aquatic compartment (Futter *et al.* 2007, Mattsson *et al.* 2009). Biological, chemical and physical processes remove the allochthonous TOC (von Wachenfeldt and Tranvik 2008). The TOC concentration decreases along with the hydrological residence time (Curtis and Schindler 1997, Algesten *et al.* 2004, Mattsson *et al.* 2005). For instance, the loss

of DOC via DIC photoproduction increases with the water retention time of lakes (Granéli *et al.* 1998), and likely explains the negative influence of retention time on the DOC photoreactivity (Soumis *et al.* 2007). Therefore, the DOM photochemistry in freshwaters depends both on the catchment properties regulating the TOC export to aquatic systems and on the processes taking place in the aquatic compartment which extensively remove the allochthonous TOC with prolonged hydrological residence. Photochemistry of DOM thus depends on changes in land use and hydrology that are strongly driven by anthropogenic activity (Rantakari *et al.* 2010, Drinan *et al.* 2013).

1.2.5 DIC photoproduction in marine waters

Conservatively, oceans receive ~ 50 % of terrestrial carbon discharged to inland waters (Cole *et al.* 2007). Oceanic DOM comprises one of the largest global carbon reservoirs at a level of 622 Pg C, which connects terrestrial, oceanic, and atmospheric carbon exchange (Mopper and Degens 1979, Cole *et al.* 2007, Hansell *et al.* 2009, Cai 2010). Increasing export of riverine DOC is related to the rising concentration of terrigenous DOC (tDOC) in coastal waters (De Vittor *et al.* 2008, Hoikkala *et al.* 2012). Compared to the tDOC concentration in the river waters (ca. 6 mg l^{-1}) discharged to the ocean, the concentration of DOC in the open ocean is extremely low at 34 to ~ 80 μmol kg^{-1} (Hansell *et al.* 2009). This comparison implies that tDOC is mostly mineralised in coastal waters (Opsahl and Benner 1997). Owing to the biologically refractory nature of tDOC (Hernes and Benner 2003, Fichot and Benner 2014), photochemical transformation is one of the predominant mechanisms that removes it from the sunlit ocean water (Mopper *et al.* 1991, Miller and Zepp 1995). The degradation of tDOC in marine waters leads to an offshore decrease of tDOC, along with reduced rates of tDOC photochemical transformation at both volumetric (Fichot and Benner 2014, Powers and Miller 2015) and areal (Bélanger *et al.* 2006, Aarnos *et al.* 2012) scales.

The heterogeneous coastal environment is quite distinct from the freshwaters, which sets a challenge to quantify the photochemical transformation of DOM. The estuary is a transitional region which has gradually changed chemical features, e.g., salinity pattern and optical properties. For example, increased salinity may cause changes in DOM conformation and the loss of terrigenous Fe. Thus the salinity is negatively related to the UVR absorbance and DIC photoproduction of tDOC originating from a swamp draining lower Chesapeake Bay (Kowalczuk *et al.* 2003, Minor *et al.* 2006). Terrestrial-derived CDOM typically dominates the absorption of photolytic solar radiation, particularly in coastal waters affected by the river runoff (Mobley 2001). It exposes tDOC to extensive photochemical transformation. Several initial evaluations suggested photochemical process as a major sink for biologically non-labile tDOC, by which the oceanic DOC can be photochemically oxidised to biologically labile low molecular weight (LMW) compounds (Kieber *et al.* 1989, 1990) and DIC (Miller and Zepp 1995). Defining the magnitude of the sink for the coastal tDOC may support the estimation of global carbon transit.

1.3 Apparent quantum yields

1.3.1 Modelling photochemical reactivity

A prerequisite for photochemistry is that light has to be absorbed by the reaction system, according to the Grotthnus-Draper law. In general, it can consequently cause excitation of an electron that initially occupied a low energy orbital to an unoccupied higher energy orbital. The excited transients will rapidly return to the ground states by releasing the energy in several ways, e.g., intramolecular photophysical radiative processes or chemical changes in molecular structure (Turro 1991). A conception of photochemical equivalence has been independently enunciated by Stark (1908) and Einstein (1912), which deals with the measurement issue in photochemistry. It states that one quantum of light is absorbed by one molecule of absorbing reactant. Although too simple to be practically held in some cases (see Warburg's experiment of the wavelengths' effect on photoreaction) (Allmand 1926), this law provided an effective photochemical equivalent, and the idea is applicable. Efficiency of photochemical reaction can be expressed by quantum yield (ϕ) in a general form,

$$\phi = \frac{number\ of\ events}{number\ of\ absorbed\ photons} \tag{3}$$

where *number of events* = amount of given species formed or consumed, and *number of absorbed photons* = amount of photons absorbed by the system (Turro 1991).

Extrapolating laboratory-based results to the natural condition is a difficult but meaningful question in the environmental photochemistry of DOM. One obstacle is the complexity of the reaction system, including reactants (electromagnetic radiation, heterogeneous DOC), photosensitisers (e.g. Fe) and products (LMW DOM, DIC, etc.). Photomineralisation of DOC can be measured as the photochemical production of DIC. Apparent quantum yields (AQY) can be used to describe the efficiency of this reaction in relation to the number of absorbed photons. In this type of environmental process, the term "apparent" comes from lacking knowledge of the actual compounds responsible for DIC production or light absorption. In the present thesis, AQY for DOC photomineralisation was investigated as the rate of DIC photoproduction normalised to the rate at which photons were absorbed by CDOM (Zepp 1978, Vähätalo *et al.* 2000, Johannessen and Miller 2001). Considered the spectral dependency of solar radiation, CDOM light absorption and photochemical reactivity, the spectral AQY can be expressed by an exponential decline equation,

$$\phi_\lambda = c\ e^{-d\lambda} \tag{4}$$

where ϕ_λ = spectral AQY at wavelength λ (mol C mol photons^{-1}), c = AQY at reference λ of 0 nm (mol C mol photons^{-1}), d = spectral slope coefficient of AQY (nm^{-1}) (Vähätalo *et al.* 2000, Aarnos *et al.* 2012). Another form of spectral AQY is also in use (Johannessen and Miller 2001),

$$\phi_\lambda = e^{-(m1 + m2\,(\lambda - 290))} \quad (5)$$

where $m1$ = fit parameter (dimensionless) and $m2$ = fit parameter (nm^{-1}). Transformation can be made between eq. 4 and eq. 5 (I). A brief summary was made on the reported equations fitting AQY for DIC photoproduction in natural waters (I).

1.3.2 AQY in environmental photochemistry

In both freshwater and marine water, DIC photoproduction is critical to evaluate the discrete carbon fluxes. When comparing the reactivity in different systems, AQY rather than photomineralisation rate should be used. Photomineralisation rate relies on light absorbed by reaction system, which depends on the intensity and spectral characteristics of irradiation as well as the light absorbing properties of the sample (e.g. Vähätalo *et al.* 2000). The spectrum of ϕ_λ can be adapted to model the photochemical reactions on a regional scale. For example, Vachon et al. integrated spectral AQY with the environmental irradiance and its extinction along water column, calculated the volumetric photomineralisation rate of 23.8 mg C m^{-2} d^{-1} in 3 limnologically distinct northern lakes (Vachon *et al.* 2016). In another work, Powers and Miller combined AQY spectra for carbon monoxide (CO) photoproduction and remote sensing data, estimated an annual production of 3.35 Gg C from the study area in Northern Gulf of Mexico (Powers and Miller 2015).

To understand the photochemical response of aquatic DOM pool to solar radiation, reliable underwater radiation spectra together with spectral AQY are indispensable. AQY has been determined in light fields with monochromatic (few), broadband and full spectrum irradiation (Gao and Zepp 1998, Vähätalo *et al.* 2000, Johannessen and Miller 2001). Laboratory-specific set-ups may cause variation in the determined spectral AQY values, but it's not recognised yet to which extent they are varied.

1.4 The gap: known and unknown

The loss of colour after water's direct exposure to sunlight was first described in 1899 by Whipple. Since then, a sheer volume of studies have investigated sunlight-initiated mineralisation of DOC in the aquatic systems, respectively focused on the influence of DOC characteristics (e.g. Kieber *et al.* 1990, Moran and Zepp 1997, Osburn *et al.* 2001a, Xie *et al.* 2004, Cory *et al.* 2007, Spencer *et al.* 2009b, Stubbins *et al.* 2010, Helms *et al.* 2014, Sharpless and Blough 2014) and

the surrounding environment (e.g. Mopper *et al.* 1991, Valentine and Zepp 1993, Miller and Zepp 1995, Gao and Zepp 1998, Moran *et al.* 2000, Obernosterer and Benner 2004, Bélanger *et al.* 2006, Aarnos *et al.* 2012, Koehler *et al.* 2014, Vachon *et al.* 2016). Extrinsically, some of these studies examined the source of DOC. For example, peat soil has been recognised as a significant source of DOM to the aquatic regime (Freeman *et al.* 2001). The regulation of photomineralisation is also affected by Fe because of the partial coupling of Fe redox and DOM photochemistry (Voelker *et al.* 1997). Intrinsically, change in CDOM optical properties has also been examined to understand the reactivity of DOM (e.g. Helms *et al.* 2008). Besides, regional-scale carbon flux can be predicted by AQY for the photochemical DIC production (White *et al.* 2010). However, so far we are unable to ascertain the varying carbon fluxes in DOM photomineralisation.

There is a need to understand the photoreactivity of DOM, e.g., the role of catchment land use, to what extent the water quality matter, the fate of terrestrial carbon in the marine waters, and how reliable the laboratory determination is. To reveal the unknowns about the photoreactivity of DOM, some research gaps have been identified.

At present, the trend of terrigenous DOM export shows no sign of abating, which enriches boreal lakes with terrestrial-derived DOM (Algesten *et al.* 2004, Köhler *et al.* 2013). The DOM photomineralisation is closely related to Fe concentration and pH (Gao and Zepp 1998, Bertilsson and Tranvik 2000, Anesio and Granéli 2004, Porcal *et al.* 2014), and chemical characteristics of DOM also play a role in the photoreactivity (Sulzberger and Durisch-Kaiser 2009). Nonetheless, a quantitative evaluation concerns the influence of water quality on DOM photoreactivity is missing.

The catchment and inland waters are connected when terrigenous DOM exports into lakes. Increased Fe organic colloids contents followed the peat mining industry have been noticed in the boreal region (Heikkinen 1994, Kortelainen *et al.* 2006, Palviainen *et al.* 2016). Human activities can modify the land use and hydrology in the catchment. For instance, around 60 % of the original peatlands in Finland has been drained to improve forestry (Simola *et al.* 2012). The consequent carbon loss may alter DOM flux and its photochemistry. No previous study has yet clearly addressed the photoreactivity for DIC production in relation to the catchment property of boreal zone.

Terrestrial-derived DOM transports through inland water paths and eventually merges into the ocean. Photochemical oxidation is a potentially important sink of tDOC in the ocean (Mopper *et al.* 1991, Miller and Zepp 1995) because the biological degradation of tDOC can be slow (Moran *et al.* 2000, Coble 2007, Nelson and Siegel 2013). The rates of photobleaching, DIC photoproduction and photochemical reactivity of DOC decrease along the salinity gradient (Minor *et al.* 2006, White *et al.* 2010, Aarnos *et al.* 2012). Thus, the magnitude for tDOC photomineralised in the marine waters is poorly known due to the challenges accounting for changes in photochemical reactions of tDOC along river plume.

The first AQY for DIC photoproduction has been determined almost two decades ago with monochromatic irradiation (Gao and Zepp 1998). The use of

polychromatic light sources has risen afterwards (Gao and Zepp 1998, Vähätalo *et al.* 2000, Johannessen and Miller 2001). It is still difficult to define and detect the actual radiation energy inducing photomineralisation as of today, which makes AQY spectrum a sensitive while weakly constrained model parameter to estimate aquatic DIC photoproduction. There is a dearth of probing the variability of AQYs among laboratory-specific determinations.

2 AIMS OF THE STUDY

The overall objective of this thesis is to further explore the photochemical reactivity of DOM photomineralisation in the inland waters, and the role of environmental conditions or laboratory procedures on its variability. In addition, the laboratory AQY determination was used to approximate the regional photomineralisation of terrigenous DOC in marine waters.

More specifically, following questions have been addressed in the thesis:

1) How does the water quality influence the DOM photochemical reactivity in fresh waters, with Fe and pH as the only regulators (I), or when natural water quality and DOM optical properties varied (II–III)?
2) What is the role the catchment property plays in photoreactivity of DOM within boreal lakes, particularly the combined role of land use, hydrology and water quality (II)?
3) Does the difference in methodology matter for measuring the spectral AQYs of inland waters? How much the independent determinations by 4 laboratories differed from each other (III)?
4) How to use the laboratory modelled spectral AQY to estimate DIC photoproduction from riverine DOC of terrestrial-origin in the coastal area (IV)?

3 MATERIALS AND METHODS

3.1 Overview

The present thesis surveyed the variation of photoreactivity for DIC photoproduction which was caused by changes in Fe contents and pH (I), lake water quality along with catchment property (II), and laboratory-specific procedures (III). In addition, photomineralisation of terrestrial DOC in coastal waters was estimated based on AQY modelling (IV). A technical workflow illustrating the main procedure used in each article is given in Fig. 1.

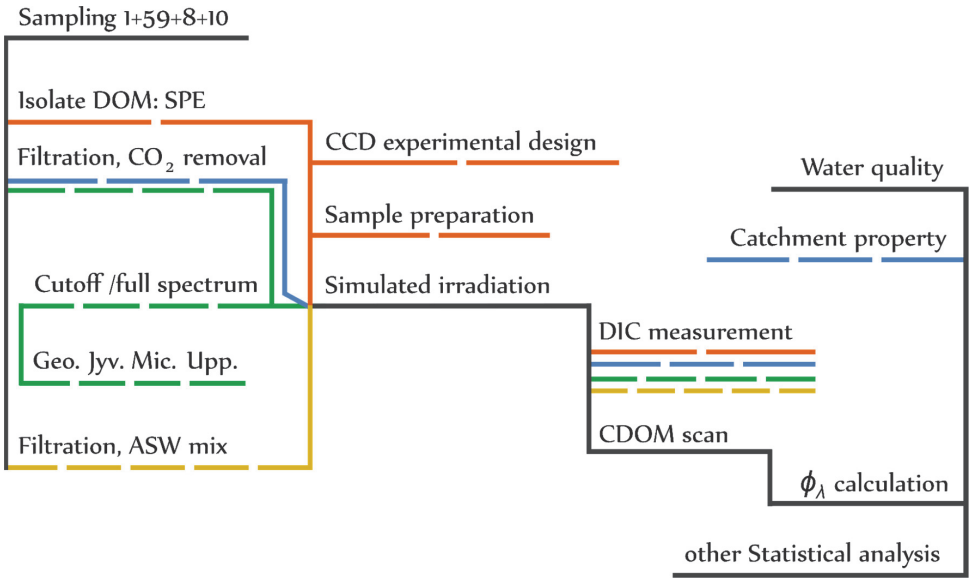

FIGURE 1 Technical workflow used in the studies. Black bars mark the common steps, and the colour and number of line breaks distinguish steps for the specific articles (I=coral, 1 break; II=blue, 2 breaks; III=green, 3 breaks; IV=yellow, 4 breaks). Dotted arrows indicate the flow directions for single article. The 1, 59, 8, 10 are the number of investigated water samples in each article.

3.2 Study sites

Surveyed lakes are situated between latitudes 60° N and 63° N in the boreal zone of southern Finland (50 lakes; I, II) and eastern middle Sweden (15 lakes; II, III). In addition, water samples from one lake and one creek in the arctic zone of Alaska were included (latitude 68° N; III). Distribution of surveyed lakes and the creek is provided in Fig. 2 and Fig. 3. The lakes and creek contained DOC with concentrations ranging from 4 to 24 mg l^{-1}, which lie along a gradient of clear to very humic waters. In addition, surface waters were collected from 10 major rivers on 5 continents, which composed one-third of freshwater discharge and DOC fluxes into the ocean (IV). Sampling map and site details for the 10 studied rivers has been described by Jaffé *et al.* (2013) and Lalonde *et al*. (2014).

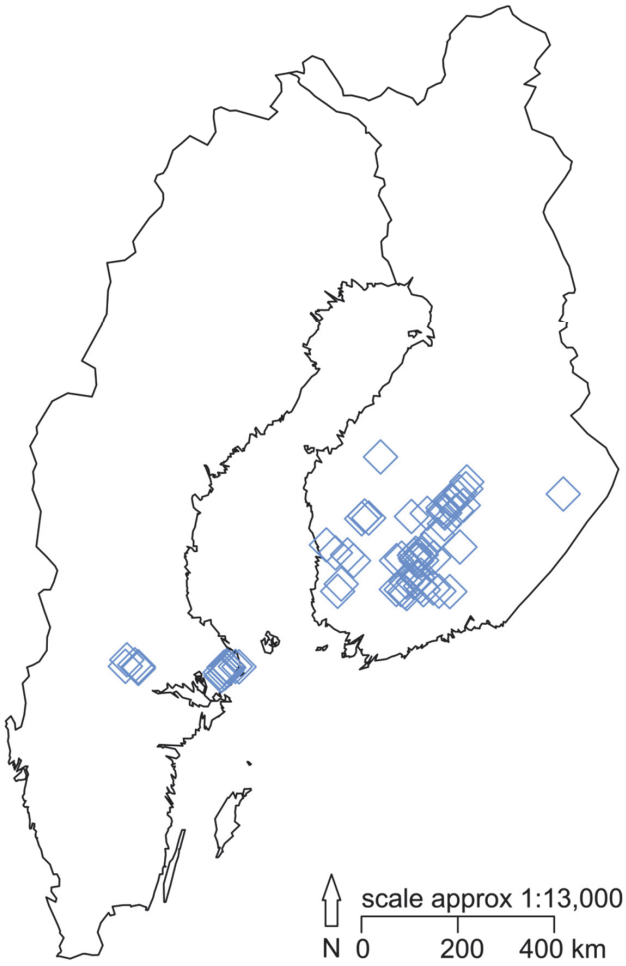

FIGURE 2 The geographic locations of the surveyed lakes in a) Finland and Sweden. The coordinates can be found in articles I–III.

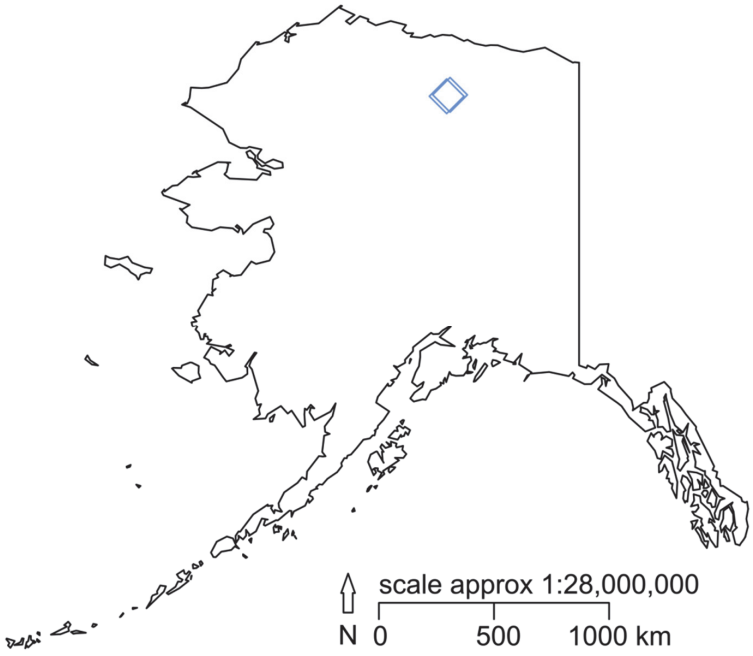

FIGURE 3 The geographic locations of the surveyed lake and creek in b) Alaska. The coordinates can be found in article III.

3.3 Sample preparation

3.3.1 Solid phase extraction (I)

Solid phase extraction (SPE) was performed to obtain Fe-free DOM isolate, using Bond Elut PPL cartridges (Agilent Technologies, United States) that retained >75 % of DOC in lake water. The procedure was according to Dittmar *et al.* (2008).

3.3.2 Filtration and background DIC removal (I−IV)

To separate DOM, raw water samples were vacuum filtered through 0.2–0.7 μm pore size filter membranes for the filtrates used in experiments. The different colour of particles left on filter papers shows the variability of the particulate matter, and suggests different water quality in the surveyed lakes (Fig. 4; samples in II). The background DIC concentration was reduced before incubation by bubbling water samples with CO_2-free air (2 ml min^{-1}) for 30−40 min in a custom-made gas exchange flask.

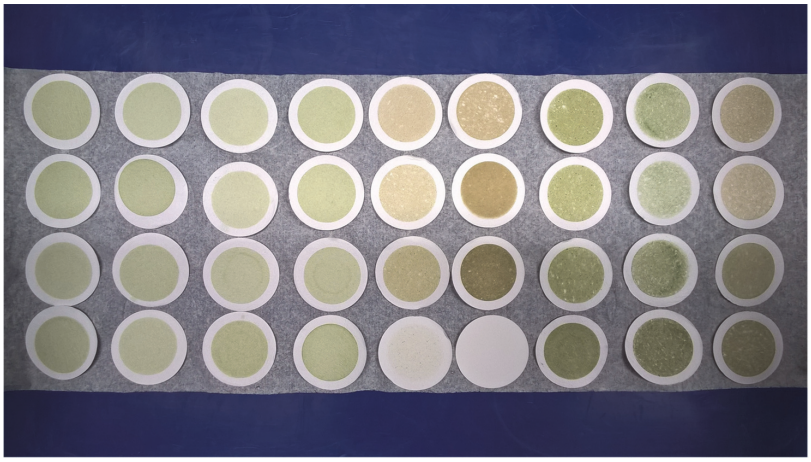

FIGURE 4 Particulate matter left on GF/C filter papers after filtration suggested the variation of water quality in the boreal lakes examined in article III. The filtrates were collected for photochemical work.

3.4 Simulated solar irradiation (I−IV)

Laboratory irradiation was conducted in a Suntest CPS+ solar simulator (Atlas Material Testing Technology, United States). For the irradiation, filtered water samples were sealed in vials with septa or ground glass stoppers (Fig. 5). The samples received simulated solar radiation at a constant temperature directly or modified with cut-off filters (Fig. 5). The intensity and spectral composition of irradiance were measured (Fig. 5). Part of samples received full polychromatic irradiation (I, II and IV). Whether the cut-off filters were applied or not was the critical difference in experimental systems of article III. The optical cut-off filters used in article III are shown in Fig. 6.

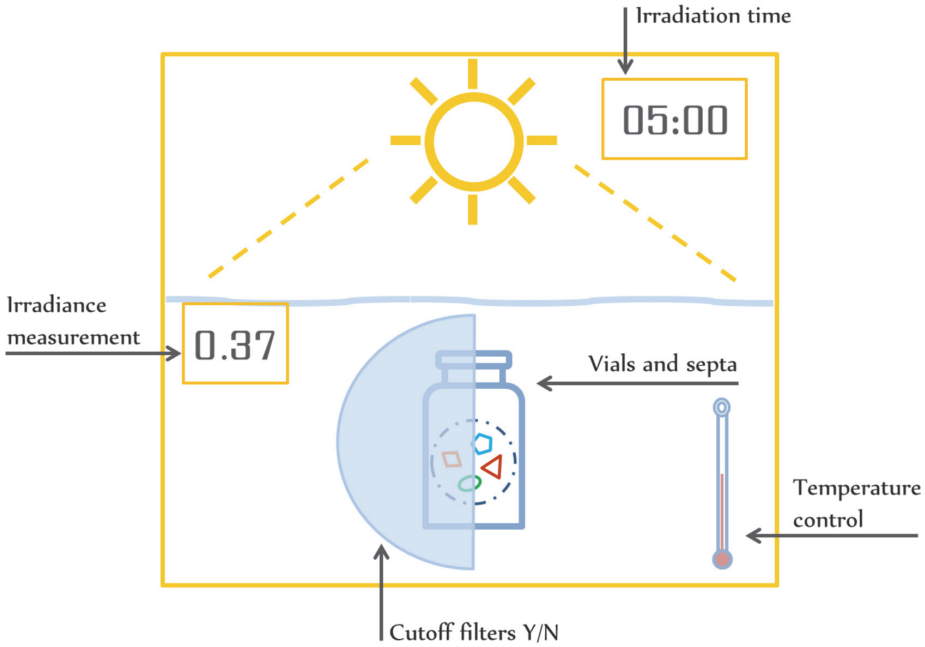

FIGURE 5 A conceptual illustration of the irradiation experiment set-up. Numbers shown for irradiance measurement and irradiation time are only examples; the actual values that were used can be found in the included articles.

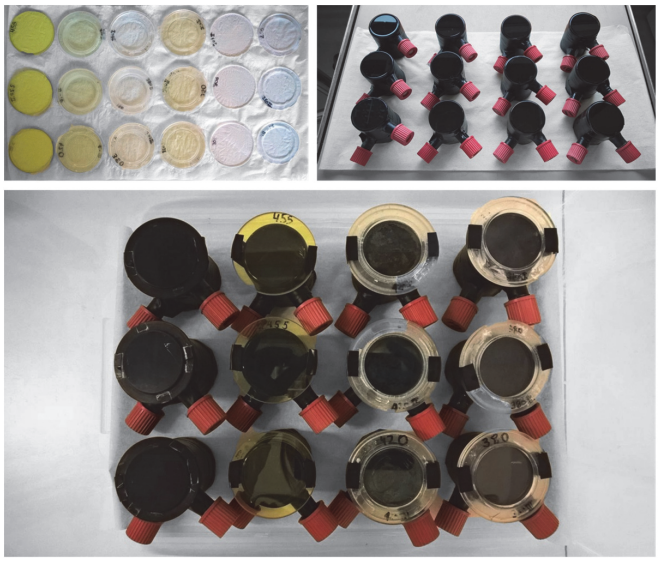

FIGURE 6 Cut-off filters (top-left, triplicates in one column, starting from left are at 250, 310, 355, 385, 420, 455 nm) and the match of glass vessels (top-right) with planar quartz top and bottom, black sides and silicon septa seal water samples. Lower photo shows the sets of cut-off filters fixed on vessels (sets used in Uppsala University).

3.5 Analytical measurement

3.5.1 DOC and DIC (I−III)

DOC and DIC in water samples were measured using a TOC analyser (TOC-L_{CPH}, Shimadzu, Japan). DOC standards were prepared using potassium hydrogen phthalate (Nacalai Tesque Inc., Japan), with six points calibrated up to 30 mg C l^{-1} for each run. For DIC determination, standards were prepared with sodium hydrogen carbonate (Nacalai Tesque Inc., Japan) right before the measurements. Five-point calibration up to 3.5 mg C l^{-1} was used throughout in each run, with the detection limit of 4 µg l^{-1}. The rate of DIC photoproduction was calculated as the difference between the DIC concentrations of the irradiated and dark control samples.

3.5.2 UV-vis absorbance (I−IV)

The absorbance of CDOM was measured by a UV-vis spectrophotometer (Lambda 850, PerkinElmer, United States) in a 1 cm quartz cuvette against an ultrapure water blank (Ultra Clear UV UF TM system; Evoqua Water Technologies, United States). The absorption coefficient of CDOM at wavelength λ was calculated according to Beer-Lambert law with following equation:

$$a_\lambda = 2.303 \left(A_{\text{solution},\lambda} - A_{\text{blank},\lambda} \right) l^{-1} \quad (6)$$

where a_λ = absorption coefficient at wavelength λ (m^{-1}), $A_{\text{solution},\lambda}$ and $A_{\text{blank},\lambda}$ = apparent absorbance of the test solution and blank, respectively, and l = the path length of the cuvette (m). Photobleaching of CDOM was defined as the change in a_λ (Δa_λ, m^{-1}) and was calculated as the difference in a_λ between the irradiated and the dark control samples. Other indicators for optical properties were calculated based on UV-vis absorbance and DOC concentration,

$$S_R = S_{275\text{–}295}\, S_{350\text{–}400}^{-1} \quad (7)$$

where S_R = slope ratio (dimensionless), $S_{275\text{–}295}$ = spectral slope coefficient at 275–295 nm wavelength region and $S_{350\text{–}400}$ = spectral slope coefficient at 350–400 nm. And

$$SUVA = a_{254}\, [DOC]^{-1} \quad (8)$$

where $SUVA$ = absorption coefficient at 254 nm (l mg C^{-1} m^{-1}), a_{254} = absorption coefficient at 254 nm (m^{-1}), and $[DOC]$ = DOC concentration (mg C l^{-1}).

3.5.3 Fe concentration (I−III)

Total Fe concentrations ([Fe]) in water samples were determined using an inductively coupled plasma optical emission spectrometer (ICP-OES) Optima 8300 with an S10 autosampler (PerkinElmer, United States). Prior to analysis, the Fe sample was acidified to contain 0.5 % nitric acid (Romil, United Kingdom). Fe was determined using axial viewing of the plasma at emission wavelength 238.204 nm, with the detection limit of 2 µg l^{-1}. Four-point calibration up to 2 mg l^{-1} was used throughout, for which the calibration standards were diluted from a standard stock solution containing 1000 mg Fe l^{-1} (Pure Grade, PerkinElmer, United States).

3.5.4 Vector photon flux density (I)

The vector photon flux densities inside the incubation chamber were determined at the 1-nm interval between 240–800 nm using a spectrophotometer (SR991, Macam Photometrics, United Kingdom), in order to quantify the downwelling and upwelling photon flux densities incident to the incubation vials.

3.5.5 Nitrite actinometry (III)

To quantify the amount of photons absorbed by the samples, nitrite actinometry was used as a reference for the irradiance measurement by spectrophotometer. Photolysis of nitrite generates HO·, which then is scavenged by benzoic acid and salicylic acid (SA) is formed. The wavelength-dependent quantum yields were determined for SA production using spectrofluorometry (Jankowski *et al.* 1999).

3.6 Main statistical analyses

3.6.1 Calculation of ϕ_λ (I–IV)

Spectral AQY for DIC photoproduction (ϕ_λ) was calculated as the rate of DIC photoproduction normalised by the CDOM absorbed photons. Details can be found from the supporting information of article I. For the full wavelength and broad band irradiation methods, separate AQY fitting techniques and uncertainty estimation methods were applied (III). Calculations were conducted with MATLAB R2013a (The MathWorks Inc., United States).

3.6.2 Areal photoproduction rate estimation (I, II, IV)

Estimation of the potential environmental photochemical production was based on the fitted spectral AQY and the typical daily solar radiation spectrum.

$$pr = \int_{\lambda_{\min}}^{\lambda_{\max}} \phi_\lambda \, Q_\lambda \, \mathrm{d}\lambda \quad (9)$$

where pr = areal rate of DIC photoproduction (mol C m^{-2} d^{-1}), ϕ_λ = spectral apparent quantum yields for DIC photoproduction at λ nm (mol C mol $photons^{-1}$) and Q_λ = mean daily solar photon flux density at the Earth's surface averaged across the latitudes (168 W m^{-2} global radiation, mol $photons^{-1}$ m^{-2} d^{-1} nm^{-1}), having the properties of ASTM G173-03 reference solar spectrum (Kiehl and Trenberth 1997). Integration was done between minimum and maximum action spectra wavelengths in each case (300–700 nm in I & II, 290–750 nm in IV).

3.6.3 Correlation and regression analyses

Spearman's rank correlation coefficient (ρ) was used to test the correlation between variables, visualised as correlation matrix (II). In the case of only two variables Fe concentration and pH and with a small sample size of 20, multiple regression analysis was carried out to quantify the dependency of DOM photochemical reactivity on the two water chemistry parameters (I). Principal component analysis (PCA) was used to diagnose the main correlations of DOM photochemistry with individual variables in water quality and catchment property (II). Partial least square (PLS) regression was further used to identify the potential of environmental factors to predict the DOM photoreactivity (II). Statistical analyses were conducted with R (version 3.4.0, R Core Team 2017). A significance level of p-value < 0.05 was applied if not specified otherwise.

4 RESULTS AND DISCUSSION

4.1 Fe and other water quality affect DOC photomineralisation (I–II)

The impact of Fe and pH on DOM photoreactivity was quantitatively evaluated with experimental irradiations using the same DOM solution (10 mg DOM l^{-1}) but varied combinations of the adjusted pH and introduced Fe concentration (I). Fe-associated photochemistry was able to explain up to 86 % of the total photoreactivity for DIC photoproduction in acidic condition, however, had no impact on DIC photoproduction at pH > 7 (I). Thus, the Fe-associated photochemical production of DIC depended on the combination of the acidity and concentration of Fe associated with DOM.

This combined impact of [Fe] and pH on the photoreactivity for DIC photoproduction was modelled by:

$$\phi_{330} = 3.76\times10^{-4} + 4.69\times10^{5}\,[Fe]\,[H^{+}] \quad (10)$$

where ϕ_{330} = AQY for DIC photoproduction at 330 nm (mol C mol photon^{-1}), *[Fe]* = total concentration of Fe complexed DOM (mol l^{-1}) and $[H^{+}] = 10^{-pH}$ (mol l^{-1}) (I).

Under acidic conditions, Fe also changed the spectral properties of AQY. This feature was examined by calculating the spectrally resolved areal DIC photoproduction rate. Compared to the corresponding Fe-free control, the presence of Fe (18 μM) shifted the median wavelength for DIC photoproduction by a 20 nm towards the long-wavelength radiation (red-shift) (Fig. 6 in I). This shift of action spectra for DIC photoproduction implied a possibility of photomineralisation at wavelengths > 500 nm, which have not been considered to induce DIC photoproduction in freshwaters, (e.g. Aarnos *et al.* 2012, Koehler *et al.* 2016).

In the laboratory study, Fe concentration and pH were important regulators of photoreactivity for DIC photoproduction. Their influence on the

photoreactivity ϕ_λ was additionally examined with water samples collected from 59 lakes, where other water qualities were varied and can also affect DIC photoproduction (II). The surveyed water quality explained around 54 % of the overall variance of the DOC photochemistry (Table 1, Fig. 3a in II). The interaction of Fe concentration and pH was a highly influential predictor to the photoreactivity for DIC production in boreal lakes (FeH; Fig. 4a in II). Secondary influence on DOC photoreactivity were optical properties such as absorption coefficient $a_{330\_initial}$ (a330) and *SUVA* (Fig. 4a in II). They also explained the main variance in the rates of CDOM photobleaching and DIC photoproduction (Fig. 3a in II). It should be noticed that Fe concentration can additionally contribute to light absorption (Voelker *et al.* 1997, Waite 2005).

The interaction of Fe and pH was strongly associated with the DOC photoreactivity (FeH; Fig. 4a in II), revealed its potential to predict the photoreactivity of DOC in boreal lakes. When applying Eq. 10 fitted based on SPE-DOM solutions to the natural lake waters, however, the interaction of Fe and pH explained only ~18 % of the variance in the ϕ_{330} values from experiments (data in II). The over 80 % residual variance may be a result of differences in other water qualities that can affect DOC photochemical reactivity. For instance, the DOM concentration (Granéli *et al.* 1998, Anesio and Granéli 2004) and optical properties (Spencer *et al.* 2009a, Koehler *et al.* 2016) affect the photomineralisation of DOC. Unlike in DOM solutions which had the same initial DOC concentrations (I), lake waters contained DOC with varying concentration from 8 to 24 mg l^{-1} and varying optical properties, e.g., a_{330} between 5–80 m^{-1} (Table 1 in II). Radicals like $HO\cdot$ can be photochemically generated from nitrate and nitrite (Mack and Bolton 1999) and mainly react with DOM in irradiated lake water (Vione *et al.* 2006), which may also differentiate the DOC photoreactivity in lake waters where the dissolved nitrogen ranged from 261 to 1 225 µg l^{-1} (Table 1 in II).

In both DOM solution and lake waters, the water qualities influential on DOC photochemistry were collinearly related, including DOC, Fe, pH and optical properties (Fig. 7). High [Fe] was significantly related to increased light absorbance ($a_{330\_initial}$), photobleaching (Δa_{330}), DIC photoproduction rate (DICpr), photoreactivity (ϕ_{330}), and declined S_R ($S_{R\_initial}$; Fig. 7). The pH was significant only in its negative relation with ϕ_{330} (Fig. 7).

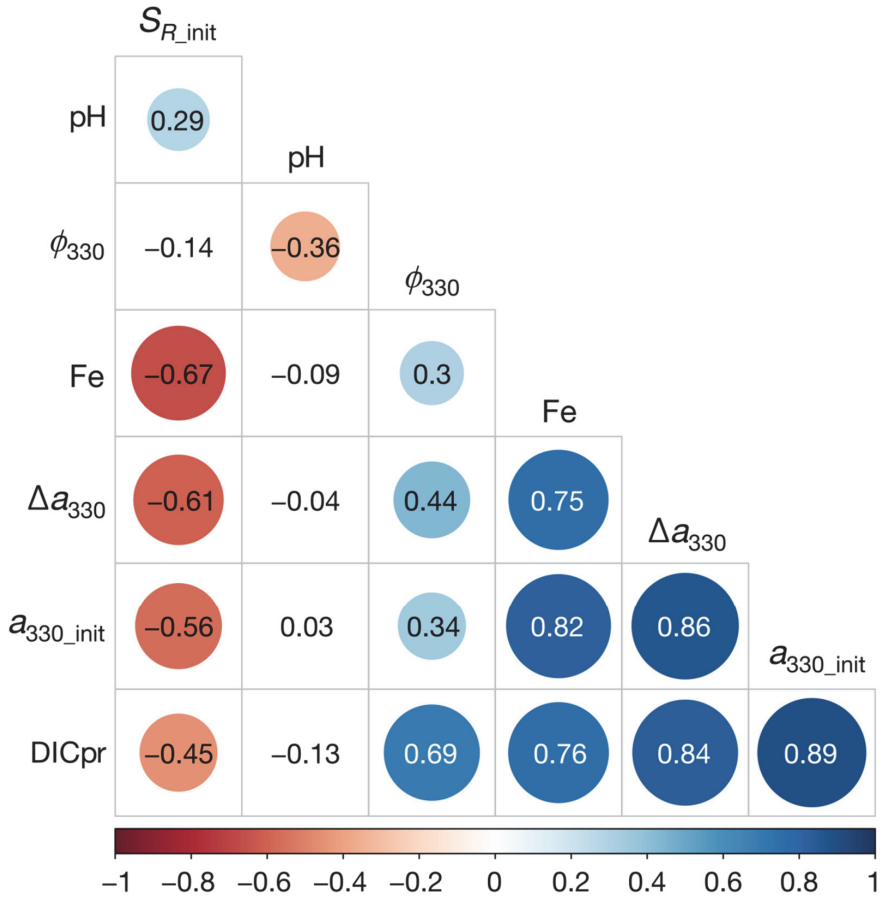

FIGURE 7 Correlation matrix contains total Fe concentration ([Fe], µmol l^{-1}), pH, optical properties, i.e., a_{330} and S_R of initial control ($a_{330\_initial}$, , m^{-1}; S_{R_init}, dimensionless) and photochemistry parameters, i.e., Δa_{330} (m^{-1}), DIC photoproduct rate (DICpr, mmol C m^{-3} h^{-1}) and photoreactivity ϕ_{330}. The size and colour of filled circle visualise the correlation coefficient presented on it, which is between the two variables given as row and column name combination. Colour key scales from red to blue represents the Spearman's ρ value between −1 and 1, and the insignificant correlation is shown without a filled circle (Data in I & II).

4.2 Combined influence of catchment property and water quality (II)

Landscape properties of the catchment can explain more than 40 % of the variation in CDOM (Arvola *et al.* 2016). Hence, the role of catchment land use and hydrology on photochemistry was also investigated. Variation of DOC photoreactivity was significantly related to catchment property (Fig. S2 in II). High percentages of peat soil/wetland (PeatWet) and small proportions of

lake/river (LakRiv) were both positively connected to photochemistry of DOC (Fig. 2b in II). One possible reason for the connection was that these two types of catchment land use are related to the export of terrigenous DOC to the aquatic regime (Freeman *et al.* 2001, Yamashita *et al.* 2010). In hydrology, water retention time is linked to the in-lake processes remove terrestrial DOC (Algesten *et al.* 2004). The mean retention time (logRT) was associated with CDOM photobleaching rate, DIC photoproduction rate and photoreactivity (Fig. 2b in II). However, the influence of retention time on DOC photoreactivity was weak when other environmental parameters were considered in the evaluation (Fig. 3b, Fig. 4b in II). This is probably due to the more direct effect of optical properties, which can explain the majority of variance in freshwater DOM photoreactivity (Koehler *et al.* 2016).

Similarly to that observed in laboratory-prepared DOM solutions, spectral features for the aquatic DIC photoproduction varied in boreal lakes. Red-shift of the median wavelength for DIC photoproduction was compared in waters from Lake Erken (370 nm) and Mouhijärvi (391 nm; Fig. S3 in II). A comparable spectral shift towards longer wavelength has been noted in DOM solutions with ~18 μmol l^{-1} higher Fe content, under acidic conditions (Fig. 6 in I). [Fe] in Mouhijärvi (pH~5.7, 16 mg DOC l^{-1}) was around 8 μmol L^{-1} higher than in Lake Erken (pH~7.7, 9 mg DOC l^{-1}), and the differences in DOC, CDOM absorption coefficient and pH, etc. additionally could affect the DIC photoproduction (Bertilsson and Tranvik 2000, Porcal *et al.* 2014). Mouhijärvi has a surface area of 7 km^2 and water residence time of 68 days, correspondingly Lake Erken has an area of 24 km^2 and 7 years residence time (Weyhenmeyer 1999). The obvious difference in catchment property suggested a higher DOC photoreactivity in Mouhijärvi (Fig. 3b in II). Small lake area and short water residence may also contribute to the red-shift of the spectra for DIC photoproduction rate.

4.3 Variability of laboratory-based AQY determination (III)

Across 4 laboratories, the spectral ϕ_λ were modelled to clarify the variability of AQY determined with different protocols, using 8 inland waters from Alaska, Finland and Sweden (Fig. 2, 3). Individual ϕ_λ spectra varied among laboratories and across freshwaters, but no pattern of consistent and pronounced divergence was identified (Fig. 2 in III). Generally, it suggested no significant bias in the examined laboratory procedures.

Since the ϕ_λ is spectral dependent, integration of ϕ_λ was used to take into account the spectral characteristic of photoreactivity for DIC production. The ϕ_λ was integrated between 300–450 nm (integral $\phi_{300–450}$) for the individual waters and each laboratory, shown in a bubble plot (Fig. 8, unpublished data in III). The height of bubbles indicated the integral $\phi_{300–450}$ values between 17.5 and 152.1 mmol DIC mol photons^{-1}, sorted by eight inland waters in each column. The diameter of bubbles indicated the integrated CDOM absorption coefficient a_λ between 280–600 nm corresponding to the integral $\phi_{300–450}$, and waters were

sorted along the axis from clean to humic inland waters and labelled with column a to h. Within one column, the discrepancy in the height of bubbles showed the laboratory-based variance of integral $\phi_{300-450}$. Light absorbance of the same inland water slightly varied among laboratories (different diameter of the bubble, Fig. 8), but the variance of integral $\phi_{300-450}$ could be small (height of the bubble in b–d, Fig. 8) or big (in e, Fig. 8). Variation of integral $\phi_{300-450}$ among laboratories (CV = 37.5 %) was over half of that among different inland waters (CV = 65.1 %). The variation is possibly caused by the difference in, e.g., defining light fields, measuring irradiation intensity, and using spectral cut-off filters or not. It suggested obvious variation may exist when comparing spectral AQYs determined with different laboratory procedures, or using the cross-laboratory AQYs as modelling parameters at present. Therefore, comparison of spectral AQY data should be taken with care when it involves data collected with different experimental techniques. As the true underlying value is unknown, the inter-laboratory systematic bias in this aggregated measure may require further concern.

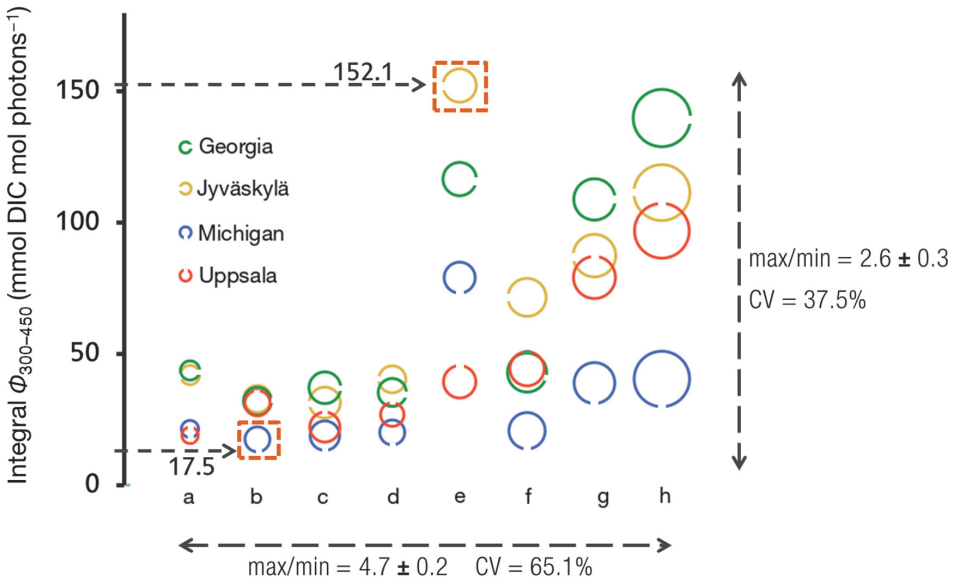

FIGURE 8 Wavelength-integrated ϕ_λ between 300 and 450 nm (integral $\phi_{300-450}$) for eight inland waters determined in 4 laboratories (marked with colour and direction of the open on the bubble). Waters are sorted in each column by ascending DOC concentrations, where a = Toolik Lake, b = Norra Bredsjön, c = Östra Skärsjön, d = Jyväsjärvi, e = Imnavait Creek, f = Gäddtjärn, g = Grästjärn, h = Svartjärn, respectively. The height of bubbles indicates integral $\phi_{300-450}$ value along the vertical axis, and the lowest (17.5) and highest (152.1) values are marked with dashed rectangles. The diameter of bubble indicates the a_λ in dark control integrated between 280–600 nm, which is corresponded to the integral $\phi_{300-450}$ values. Variation of integral $\phi_{300-450}$ across waters and laboratories are indicate, respectively, by double-headed arrows, with the ratio between maximal and minimal integrates (max/min) and CV values. Data and calculation details can be found in III.

4.4 DIC photoproducts in coastal river plume (IV)

To estimate the global and annual photomineralisation of tDOC in the coastal area, spectral AQY was determined in the laboratory using water samples collected from 10 major rivers situated on 5 continents. The value of ϕ_{330} for tDOC photomineralisation varied between 129 (μmol C mol photons^{-1}; Ganges-Brahmaputra River) and 335 (μmol C mol photons^{-1}; Mississippi River; Table 4 in IV). When integrated with the geography-specific solar irradiance, the annual rates of DIC photoproduction ranged from 52 ± 4 mmol C m^{-2} yr^{-1} in Lena River to 157 ± 2 mmol C m^{-2} yr^{-1} in Mississippi River (Table 4 in IV). Based on the linear correlation between DIC photoproduction and CDOM photobleaching (Fig. 1 in IV), the annually photoproduced DIC from known tCDOM fluxes was estimated. It was led by Amazon in an amount of 6.98 ± 1.08 Tg C yr^{-1}, which contributed to over half of the total DIC photoproduction in the examined rivers (Table 5 in IV). Assumed that tDOC dispersed uniformly around river mouth, the offshore distance required to photomineralise the riverine tCDOM were estimated. Amazon had the longest estimated distance of 1652 ± 442 km from the river mouth until tDOC was photochemically mineralised (Table 6 in IV). The dispersion areas were visualised in Fig. 5 of article IV, with the river mouth located at the centre of the area.

In global coastal waters, photochemical processes were estimated to mineralise 23–71 Tg C yr^{-1} tDOC to DIC within an area of 34 000 000 km^2. This amount of DIC photoproduction in marine waters was around 2 times of that in global lakes and reservoirs at 13–35 Tg C yr^{-1} (Koehler *et al.* 2014). It should be noted that the surface area of inland waters is 4 460 000 km^2 (Downing and Duarte 2009, Koehler *et al.* 2014), and is only one seventh of the coastal water area required for the photomineralisation of tDOC.

One explanation for this distinction can be the difference of DOC photoreactivity in coastal and inland waters. The ϕ_λ for tDOC photoreactivity of this study fell into the lower range of those observed in freshwaters (Fig. 9) (Vähätalo *et al.* 2000, Vähätalo and Wetzel 2004, Aarnos *et al.* 2012, Koehler *et al.* 2014, 2016, Groeneveld *et al.* 2016) (data in II). In article IV, the photomineralisation of tDIC was approximated from its discharge at river mouth until the complete photomineralisation in coastal waters. This range of the ϕ_λ values was expected as a result of the loss of photoreactive tDOC during inland transit, and the extended irradiation time been used (Andrews *et al.* 2000, Vähätalo and Wetzel 2004) to simulate the entire lifetime of coastal tDOC.

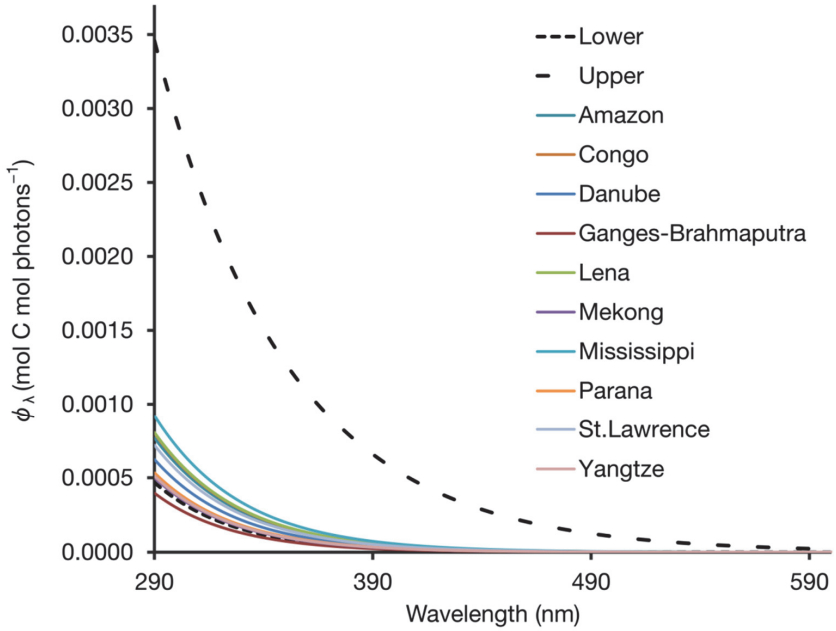

FIGURE 9 Spectral AQY for DIC photoproduction as ϕ_λ (mol C mol photons^{-1}) across 290 to 600 nm in coastal waters (10 solid lines; data in IV) and its lower and upper boundaries of the values in freshwaters as dashed lines (Vähätalo *et al.* 2000, Vähätalo and Wetzel 2004, Aarnos *et al.* 2012, Koehler *et al.* 2014, 2016, Groeneveld *et al.* 2016) (data in II).

5 REMARKS

Sunlight penetrating surface waters could transform DOM to DIC via photochemical mineralisation, which alters the aquatic carbon fluxes. Reactivity of this photochemical transformation was varied with changing water quality, catchment properties and experimental procedures.

A simple 2-factor study on the impact of Fe and pH quantified their stimulatory effect on DOM photoreactivity that can be realised with high Fe concentration and acidity. More than Fe and pH, multiple water quality and catchment conditions may adjust the content and property of DOM within boreal lakes. Hence, a survey on the multivariate influence of water chemistry, hydrology and catchment land use revealed that small lake area and a high proportion of peat soil were also relevant to a high DOM photoreactivity. Meanwhile, the variation of DOM photoreactivity can be caused by distinct protocols. Using inland waters, the across laboratory comparison established a methodology framework to measure the variance of AQY for the DOM photomineralisation, which further necessitated methodological improvement. Eventually, the terrestrial DOM passes through inland waters to the ocean. Experimental modelling of spectral AQY approximated the photomineralisation of global tDOC fluxes in the river plumes. Compared with the inland waters, a lower photoreactivity and a higher photomineralisation amount were observed for tDOC in the ocean.

Results presented in this thesis are the best possible estimates of the environmental DIC photoproduction which we could determine then. They may exemplify using spectral AQY determination to demonstrate the variability of DOM photoreactivity, to pave a way to understand the influential water quality and lake catchment properties, or to reconstruct partial carbon dynamics in the aquatic regime.

Acknowledgements

Many people had their paths crossed mine in this expedition. We shared the inspiration and worked together, or confronted the problems and saw the same vision. They are people who solidified my attachment to the places I have stayed.

First I am much obliged to thank my supervisor Dr. Anssi Vähätalo for introducing the new research area to me, guiding with patience, and listening to my idealistic thoughts and "stubborn" plans. I would like to thank my co-supervisor Prof. Jussi Kukkonen for providing me a place here to make the research and for still supporting after the research subject changed. Also, I shall thank my support group members Dr. Jarkko Akkanen and Prof. Tuula Tuhkanen for being there with the positive as usual attitude and for the sensible advice when I was unsure.

I was lucky to cooperate with and encounter some inspiring researchers in the field. A sincere thank you to all my co-authors for criticising the works and insisting on improvement, as well as for those limited but remarkable questions, discussions and presentations. I thank Prof. Andrew Rose and Dr. Amit Bhatnagar for their preliminary examination of this thesis.

It is no easy to realise how rich life is until some turning points, say now. Many people in and outside of our department helped me generously in study, teaching, and on technical support, which cannot be taken for granted. In particular, I truly thank all the people who made YMP a warm (no relevance to room temperature) and memorable place to work. Anssi L., thank you for making constructive advice on statistics and always answering my piles of questions patiently. Eeva, thank you for the spirit lift in those hard times and the most efficient duet practice in Akvaariohuone. Many thanks, Leena and Mervi, for your indispensable help both in the laboratory and in spare time, for the enormous kind cheer ups, and for filling the coffee room with delightful surprises.

I am grateful to the peer PhD students and postdoctoral researchers for their generous support and for the time we shared. Inna and Ronia, thank you for reading the long and technical thesis summary, your effort to improve it is much appreciated. Jaana and Sebastian, thank you for the best conference trip to Stockholm, ever. Hanna Aa., Hanna Ar., Anna, Anu, Elijah, Cyril and Andreas (the St. Petersburg, PhD meeting and Cyril group), thank you for saving me from lack of experience on practical issues, for those unofficial meetings and the good laughs we had. I give thanks to the friendship and companionship of Juho Rajala for his sharing the office, often commenting as a real peer reviewer, for refreshing with coffee mugs military and mysteriously missing pens, for those professional or hilarious talks and trips, and the fun of ultimate frisbee.

Though we are apart most of the time, I thank my friends. Particularly, CHEN for the brain food including a 248-min film released in 1963, and those talks on the terrace where the smell of Huangshan usually involved. Yayuan for

bringing ideas as a micro mistral wind, and those moments of "Why not? Right now". Tang for listening a lot and reminding the life outside every now and then. I shall thank my family for their support during the years of my choice from drawing and sports, to stay in the lab and live remotely. Thank you, to my grandpa for his handwriting poems and to my grandma for all those summer days at their place.

This work was financially supported by the Doctoral program in Biological and Environmental Science of the University of Jyväskylä. I would like to acknowledge the Finnish Doctoral Programme in Environmental Science and Technology (EnSTe) for the effort to connect the students and improve Environmental studies. American Geophysical Union (AGU), European Science Foundation, Institute of Oceanology Polish Academy of Sciences, Science Council of University of Jyväskylä, SETAC Europe for promoting the research visit and scientific conference. The research work was partially supported by YAD 212.1.

YHTEENVETO (RÉSUMÉ IN FINNISH)

Pintavedet auringonpaisteessa: liuenneen orgaanisen hiilen valokemiallisen reaktiivisuuden vaihtelu

Auringon valo voi valokemiallisesti mineralisoida liuennutta orgaanista hiiltä, joka kuvaa liuenneen orgaanisen aineen määrää, liuenneeksi epäorgaaniseksi hiileksi pintavesissä. Tämä prosessi on keskeinen, mutta huonosti tunnettu osa hiilen kiertoa vesistöissä. Tässä väitöskirjassa määritettiin liuenneen orgaanisen hiilen valokemiallista reaktiivisuutta spektraalisten näennäisten kvanttisaantojen avulla. Valokemiallisen reaktiivisuuden riippuvuutta veden laadusta ja valuma-alueen ominaisuuksista selvitettiin laboratoriokokein sekä tutkimalla järvivesiä. Laboratoriokokeissa määritettiin pH:n ja liuenneeseen orgaaniseen aineeseen sitoutuneen raudan vaikutusta valokemialliseen reaktiivisuuteen. Järvivesiä tutkimalla selvitettiin myös, kuinka muut veden ja valuma-alueen laatuun vaikuttavat tekijät vaikuttivat liuenneen orgaanisen hiilen valokemialliseen reaktiivisuuteen. Laboratoriossa määritettyjen näennäisten kvanttisaantojen avulla arvioitiin mantereilta tulevien jokivesien kuljettaman liuenneen orgaanisen hiilen valokemiallista mineralisaatiota rannikkovesissä. Lisäksi vertailtiin näennäisten kvanttisaantojen määritysmenetelmiä neljän laboratorion kesken.

Laboratorioiden välisessä vertailussa järvivesien näennäiset kvanttisaannot vaihtelivat enemmän kuin niiden määritykseen käytetyt menetelmät laboratorioiden välillä. Laboratoriokokeissa raudan katalysoimat valokemialliset reaktiot vastasivat enimmillään 86 % valokemiallisesti tuotetusta epäorgaanisesta hiilestä happamaksi säädetyssä vesiliuoksessa, mutta tämä vaikutus oli mitätön neutraaleissa – emäksisissä liuoksissa. Järvivesien liuenneen orgaanisen aineen reaktiivisuus riippui veden laadusta ja valuma-alueen ominaisuuksista. Valokemiallinen reaktiivisuus oli suurimmillaan järvivesissä, joissa liuenneen orgaanisen hiilen pitoisuus ja värillisen liuenneen orgaanisen aineen määrä olivat suuria. Valokemiallinen reaktiivisuus oli suuri pienissä järvissä, joiden valuma-alueella oli paljon turvemaita. Kun näennäisten kvanttisaantojen perusteella arvioitiin jokivesien mereen kuljettaman liuenneen orgaanisen valokemiallisen mineralisaation määrää rannikkovesissä, havaittiin auringonvalon mineralisoivan enemmän sisävesien liuennutta orgaanista ainetta rannikkovesissä kuin mantereilla.

REFERENCES

Aarnos H., Ylöstalo P. & Vähätalo A. V. 2012. Seasonal phototransformation of dissolved organic matter to ammonium, dissolved inorganic carbon, and labile substrates supporting bacterial biomass across the Baltic Sea. *J. Geophys. Res. Biogeosci.* 117, G01004, doi:10.1029/2010JG001633.

Algesten G., Sobek S., Bergstrom A.-K., Agren A., Tranvik L.J. & Jansson M. 2004. Role of lakes for organic carbon cycling in the boreal zone. *Glob Chang Biol* 10: 141–147.

Allard B., Borén H., Pettersson C. & Zhang G. 1994. Degradation of humic substances by UV irradiation. *Environ Int* 20: 97–101.

Allmand A.J. 1926. Part I.-Einstein's law of photochemical equivalence. Introductory address to Part I. *Trans. Faraday Soc.* 21: 438–452.

Andrews S.S., Caron S. & Zafiriou O.C. 2000. Photochemical oxygen consumption in marine waters: A major sink for colored dissolved organic matter? *Limnol. Oceanogr.* 45: 267–277.

Anesio A.M. & Granéli W. 2003. Increased photoreactivity of DOC by acidification: Implications for the carbon cycle in humic lakes. *Limnol. Oceanogr.* 48: 735–744.

Anesio A.M. & Granéli W. 2004. Photochemical mineralization of dissolved organic carbon in lakes of differing pH and humic content. *Arch. Hydrobiol.* 160: 105–116.

Arvola L., Äijälä C. & Leppäranta M. 2016. CDOM concentrations of large Finnish lakes relative to their landscape properties. *Hydrobiologia* 780: 37–46.

Autio I., Soinne H., Helin J., Asmala E. & Hoikkala L. 2016. Effect of catchment land use and soil type on the concentration, quality, and bacterial degradation of riverine dissolved organic matter. *Ambio* 45: 331–349.

Baalousha M., Motelica-Heino M. & Le Coustumer P. 2006. Conformation and size of humic substances: Effects of major cation concentration and type, pH, salinity, and residence time. *Colloids Surf A Physicochem Eng Asp* 272: 48–55.

Baña Z., Ayo B., Marrasé C., Gasol J.M. & Iriberri J. 2014. Changes in bacterial metabolism as a response to dissolved organic matter modification during protozoan grazing in coastal Cantabrian and Mediterranean waters. *Environ. Microbiol.* 16: 498–511.

Battin T.J., Luyssaert S., Kaplan L.A., Aufdenkampe A.K., Richter A. & Tranvik L.J. 2009. The boundless carbon cycle. *Nature Geosci* 2: 598–600.

Bélanger S., Xie H., Krotkov N., Larouche P., Vincent W.F. & Babin M. 2006. Photomineralization of terrigenous dissolved organic matter in Arctic coastal waters from 1979 to 2003: Interannual variability and implications of climate change. *Global Biogeochem Cycles* 20, GB4005, doi: 10.1029/2006GB002708.

Bertilsson S. & Tranvik L.J. 2000. Photochemical transformation of dissolved organic matter in lakes. *Limnol. Oceanogr.* 45: 753–762.

Billett M.F., Palmer S.M., Hope D., Deacon C., Storeton-West R., Hargreaves K.J., Flechard C. & Fowler D. 2004. Linking land-atmosphere-stream carbon fluxes in a lowland peatland system. *Global Biogeochem Cycles* 18, GB1024, doi: 10.1029/2003GB002058.

Blough N.V. & Zepp R.G. 1990. *Effects of solar ultraviolet radiation on biogeochemical dynamics in aquatic environments: report of a workshop,* Marine Biological Laboratory, Woods Hole, Massachusetts, October 23-26, 1989.

Blough N.V. & Zepp R.G. 1995. Reactive oxygen species in natural waters. In: Foote C.S., Valentine J.S., Greenberg A. & Liebman J.F. (eds), *Active oxygen in chemistry*, Springer Netherlands, Dordrecht, pp. 280–333.

Bolan N.S., Adriano D.C., Kunhikrishnan A., James T., McDowell R. & Senesi N. 2011. Chapter One – Dissolved Organic Matter: Biogeochemistry, Dynamics, and Environmental Significance in Soils. In: *Advances in agronomy*, pp. 1–75.

Boyle E.S., Guerriero N., Thiallet A., Vecchio R. Del & Blough N.V. 2009. Optical properties of humic substances and CDOM: relation to structure. *Environ. Sci. Technol.* 43: 2262–2268.

Branco A.B. & Kremer J.N. 2005. The relative importance of chlorophyll and colored dissolved organic matter (CDOM) to the prediction of the diffuse attenuation coefficient in shallow estuaries. *Estuaries* 28: 643–652.

Brezonik P.L. & Fulkerson-Brekken J. 1998. Nitrate-induced photolysis in natural waters: controls on concentrations of hydroxyl radical photo-intermediates by natural scavenging agents. *Environ. Sci. Technol.* 32: 3004–3010.

Cai W.-J. 2010. Estuarine and coastal ocean carbon paradox: CO2 sinks or sites of terrestrial carbon incineration? *Ann Rev Mar Sci* 3: 123–145.

Chen K.-Y., Chen T.-Y., Chan Y.-T., Cheng C.-Y., Tzou Y.-M., Liu Y.-T. & Teah H.-Y. 2016. Stabilization of Natural Organic Matter by Short-Range-Order Iron Hydroxides. *Environ. Sci. Technol.* 50: 12612–12620.

Choudhry G.G. 1981. Humic substances. Part II: Photophysical, photochemical and free radical characteristics. *Toxicol Environ Chem* 4: 261–295.

Coble P.G. 2007. Marine Optical Biogeochemistry: The Chemistry of Ocean Color. *Chem. Rev.* 107: 402–418.

Cole J.J., Caraco N.F., Kling G.W. & Kratz T.K. 1994. Carbon Dioxide Supersaturation in the Surface Waters of Lakes. *Science* 265: 1568–1570.

Cole J.J., Prairie Y.T., Caraco N.F., McDowell W.H., Tranvik L.J., Striegl R.G., Duarte C.M., Kortelainen P., Downing J.A., Middelburg J.J. & Melack J. 2007. Plumbing the Global Carbon Cycle: Integrating Inland Waters into the Terrestrial Carbon Budget. *Ecosystems* 10: 172–185.

Cory R.M., McKnight D.M., Chin Y.-P., Miller P. & Jaros C.L. 2007. Chemical characteristics of fulvic acids from Arctic surface waters: Microbial contributions and photochemical transformations. *J. Geophys. Res. Biogeosci.* 112, G04S51, doi: 10.1029/2006JG000343.

Cory R.M., Ward C.P., Crump B.C. & Kling G.W. 2014. Sunlight controls water column processing of carbon in arctic fresh waters. *Science* 345: 925.

Curtis P.J. & Schindler D.W. 1997. Hydrologic control of dissolved organic matter in low-order Precambrian Shield lakes. *Biogeochemistry* 36: 125–138.

Danielsson L.G. 1982. On the use of filters for distinguishing between dissolved and particulate fractions in natural waters. *Water Res.* 16: 179–182.

Del Castillo C.E. & Miller R.L. 2008. On the use of ocean color remote sensing to measure the transport of dissolved organic carbon by the Mississippi River Plume. *Remote Sens Environ* 112: 836–844.

Del Giorgio P.A., Cole J.J., Caraco N.F. & Peters R.H. 1999. Linking planktonic biomass and metabolism to net gas fluxes in northern temperate lakes. *Ecology* 80: 1422–1431.Dillon P.J. & Molot L.A. 1997. Effect of landscape form on export of dissolved organic carbon, iron, and phosphorus from forested stream catchments. *Water Resour Res* 33: 2591–2600.

Dittmar T., Koch B., Hertkorn N. & Kattner G. 2008. A simple and efficient method for the solid-phase extraction of dissolved organic matter (SPE-DOM) from seawater. *Limnol Oceanogr Methods* 6: 230–235.

Downing J.A. & Duarte C.M. 2009. Abundance and Size Distribution of Lakes, Ponds and Impoundments. In: *Encyclopedia of Inland Waters*, pp. 469–478.

Downing J.A., Cole J.J., Duarte C.M., Middelburg J.J., Melack J.M., Prairie Y.T., Kortelainen P., Striegl R.G., McDowell W.H. & Tranvik L.J. 2012. Global abundance and size distribution of streams and rivers. *Inland Waters* 2: 229–236.

Drinan T.J., Graham C.T., O'Halloran J. & Harrison S.S.C. 2013. The impact of catchment conifer plantation forestry on the hydrochemistry of peatland lakes. *Sci. Total Environ.* 443: 608–620.

Emmenegger L., Schönenberger R., Sigg L. & Sulzberger B. 2001. Light-induced redox cycling of iron in circumneutral lakes. *Limnol. Oceanogr.* 46: 49–61.

Ertel J.R., Hedges J.I. & Perdue E.M. 1984. Lignin signature of aquatic humic substances. *Science* 223: 485.

Evans C.D., Monteith D.T. & Cooper D.M. 2005. Long-term increases in surface water dissolved organic carbon: Observations, possible causes and environmental impacts. *Environ. Pollut.* 137: 55–71.

Faust B.C. & Zepp R.G. 1993. Photochemistry of aqueous iron(III)-polycarboxylate complexes: roles in the chemistry of atmospheric and surface waters. *Environ. Sci. Technol.* 27: 2517–2522.

Ferrari G.M., Dowell M.D., Grossi S. & Targa C. 1996. Relationship between the optical properties of chromophoric dissolved organic matter and total concentration of dissolved organic carbon in the southern Baltic Sea region. *Mar. Chem.* 55: 299–316.

Fichot C.G. & Benner R. 2011. A novel method to estimate DOC concentrations from CDOM absorption coefficients in coastal waters. *Geophys Res Lett* 38, L03610, doi: 10.1029/2010GL046152.

Fichot C.G. & Benner R. 2012. The spectral slope coefficient of chromophoric dissolved organic matter ($S_{275\text{-}295}$) as a tracer of terrigenous dissolved organic carbon in river-influenced ocean margins. *Limnol. Oceanogr.* 57: 1453–1466.

Fichot C.G. & Benner R. 2014. The fate of terrigenous dissolved organic carbon in a river-influenced ocean margin. *Global Biogeochem Cycles* 28: 300–318.

Finstad A.G., Helland I.P., Ugedal O., Hesthagen T. & Hessen D.O. 2014. Unimodal response of fish yield to dissolved organic carbon. *Ecol. Lett.* 17: 36–43.

Forsberg C. 1992. Will an increased greenhouse impact in Fennoscandia give rise to more humic and coloured lakes? *Hydrobiologia* 229: 51–58.

Freeman C., Evans C.D., Monteith D.T., Reynolds B. & Fenner N. 2001. Export of organic carbon from peat soils. *Nature* 412: 785.

Futter M.N., Butterfield D., Cosby B.J., Dillon P.J., Wade A.J. & Whitehead P.G. 2007. Modeling the mechanisms that control in-stream dissolved organic carbon dynamics in upland and forested catchments. *Water Resour Res* 43, doi: 10.1029/2006WR004960.

Gao H. & Zepp R.G. 1998. Factors Influencing Photoreactions of Dissolved Organic Matter in a Coastal River of the Southeastern United States. *Environ. Sci. Technol.* 32: 2940–2946.

Garmo Ø.A., Skjelkvåle B.L., de Wit H.A., Colombo L., Curtis C., Fölster J., Hoffmann A., Hruška J., Høgåsen T., Jeffries D.S., Keller W.B., Krám P., Majer V., Monteith D.T., Paterson A.M., Rogora M., Rzychon D., Steingruber S., Stoddard J.L., Vuorenmaa J. & Worsztynowicz A. 2014. Trends in Surface Water Chemistry in Acidified Areas in Europe and North America from 1990 to 2008. *Water Air Soil Pollut* 225: 1880.

Geider R.J. & La Roche J. 1994. The role of iron in phytoplankton photosynthesis, and the potential for iron-limitation of primary productivity in the sea. *Photosyn. Res.* 39: 275–301.

Gennings C., Molot L.A. & Dillon P.J. 2001. Enhanced photochemical loss of organic carbon in acidic waters. *Biogeochemistry* 52: 339–354.

Graeber D., Gelbrecht J., Pusch M.T., Anlanger C. & von Schiller D. 2012. Agriculture has changed the amount and composition of dissolved organic matter in Central European headwater streams. *Sci. Total Environ.* 438: 435–446.

Granéli W. 2012. Brownification of Lakes. In: Bengtsson L., Herschy R.W. & Fairbridge R.W. (eds), *Encyclopedia of Lakes and Reservoirs*, Springer Netherlands, Dordrecht, pp. 117–119.

Granéli W., Lindell M. & Tranvik L. 1996. Photo-oxidative production of dissolved inorganic carbon in lakes of different humic content. *Limnol. Oceanogr.* 41: 698–706.

Granéli W., Lindell M., de Faria B.M. & de Assis Esteves F. 1998. Photoproduction of dissolved inorganic carbon in temperate and tropical lakes – dependence on wavelength band and dissolved organic carbon concentration. *Biogeochemistry* 43: 175–195.

Groeneveld M., Tranvik L., Natchimuthu S. & Koehler B. 2016. Photochemical mineralisation in a boreal brown water lake: considerabletemporal variability and minor contribution to carbon dioxide production. *Biogeosciences* 13: 3931–3943.

Guggenberger G., Zech W. & Schulten H.-R. 1994. Formation and mobilization pathways of dissolved organic matter: evidence from chemical structural

studies of organic matter fractions in acid forest floor solutions. *Org. Geochem.* 21: 51–66.

Gustafsson Ö., Widerlund A., Andersson P.S., Ingri J., Roos P. & Ledin A. 2000. Colloid dynamics and transport of major elements through a boreal river — brackish bay mixing zone. *Mar. Chem.* 71: 1–21.

Hansell D.A., Carlson C.A., Repeta D.J. & Schlitzer R. 2009. Dissolved organic matter in the ocean : a controversy stimulates new insights. *Oceanography* 22: 202–211.

Hansen A.M., Kraus T.E.C., Pellerin B.A., Fleck J.A., Downing B.D. & Bergamaschi B.A. 2016. Optical properties of dissolved organic matter (DOM): Effects of biological and photolytic degradation. *Limnol. Oceanogr.* 61: 1015–1032.

Hatakka A. 2001. Biodegradation of lignin. In: Hofrichter M. & Steinbüchel A. (eds), *Biopolymers. Biology, Chemistry, Biotechnology, Applications. Vol 1. Lignin, Humic Substances and Coal*, Wiley-VCH, Weinheim, pp. 129–180.

Heikkinen K. 1990. Seasonal changes in iron transport and nature of dissolved organic matter in a humic river in northern Finland. *Earth Surf. Process. Landf.* 15: 583–596.

Heikkinen K. 1994. Organic matter, iron and nutrient transport and nature of dissolved organic matter in the drainage basin of a boreal humic river in northern Finland. *Sci. Total Environ.* 152: 81–89.

Helms J.R., Stubbins A., Ritchie J.D., Minor E.C., Kieber D.J. & Mopper K. 2008. Absorption spectral slopes and slope ratios as indicators of molecular weight, source, and photobleaching of chromophoric dissolved organic matter. *Limnol. Oceanogr.* 53: 955–969.

Helms J.R., Stubbins A., Perdue E.M., Green N.W., Chen H. & Mopper K. 2013. Photochemical bleaching of oceanic dissolved organic matter and its effect on absorption spectral slope and fluorescence. *Mar. Chem.* 155: 81–91.

Helms J.R., Mao J., Stubbins A., Schmidt-Rohr K., Spencer R.G.M., Hernes P.J. & Mopper K. 2014. Loss of optical and molecular indicators of terrigenous dissolved organic matter during long-term photobleaching. *Aquat. Sci.* 76: 353–373.

Herndl G.J., Muller-Niklas G. & Frick J. 1993. Major role of ultraviolet-B in controlling bacterioplankton growth in the surface layer of the ocean. *Nature* 361: 717–719.

Hernes P.J. & Benner R. 2003. Photochemical and microbial degradation of dissolved lignin phenols: Implications for the fate of terrigenous dissolved organic matter in marine environments. *J. Geophys. Res.* 108: 3291.

Hoge F.E., Vodacek A. & Blough N. V. 1993. Inherent optical properties of the ocean: Retrieval of the absorption coefficient of chromophoric dissolved organic matter from fluorescence measurements. *Limnol. Oceanogr.* 38: 1394–1402.

Hoigné J., Faust B.C., Haag W.R., Scully F.E. & Zepp R.G. 1988. Aquatic Humic Substances as Sources and Sinks of Photochemically Produced Transient Reactants. In: *Aquatic Humic Substances*, American Chemical Society, pp. 363–381.

Hoikkala L., Lahtinen T., Perttilä M. & Lignell R. 2012. Seasonal dynamics of dissolved organic matter on a coastal salinity gradient in the northern Baltic Sea. *Cont Shelf Res* 45: 1–14.

Hope D., Billett M.F. & Cresser M.S. 1994. A review of the export of carbon in river water: Fluxes and processes. *Environ. Pollut.* 84: 301–324.

Hopkinson C.S. & Vallino J.J. 2005. Efficient export of carbon to the deep ocean through dissolved organic matter. *Nature* 433: 142–145.

Hruška J., Krám P., McDowell W.H. & Oulehle F. 2009. Increased Dissolved Organic Carbon (DOC) in Central European Streams is Driven by Reductions in Ionic Strength Rather than Climate Change or Decreasing Acidity. *Environ. Sci. Technol.* 43: 4320–4326.

Hu C., Muller-Karger F.E. & Zepp R.G. 2002. Absorbance, absorption coefficient, and apparent quantum yield: A comment on common ambiguity in the use of these optical concepts. *Limnol. Oceanogr.* 47: 1261–1267.

Inamdar S., Finger N., Singh S., Mitchell M., Levia D., Bais H., Scott D. & McHale P. 2012. Dissolved organic matter (DOM) concentration and quality in a forested mid-Atlantic watershed, USA. *Biogeochemistry* 108: 55–76.

Jaffé R., Ding Y., Niggemann J., Vähätalo A. V, Stubbins A., Spencer R.G.M., Campbell J. & Dittmar T. 2013. Global Charcoal Mobilization from Soils via Dissolution and Riverine Transport to the Oceans. *Science* 340: 345.

Jankowski J.J., Kieber D.J. & Mopper K. 1999. Nitrate and Nitrite Ultraviolet Actinometers. *Photochem. Photobiol.* 70: 319–328.

Jickells T.D., An Z.S., Andersen K.K., Baker A.R., Bergametti G., Brooks N., Cao J.J., Boyd P.W., Duce R.A., Hunter K.A., Kawahata H., Kubilay N., La Roche J., Liss P.S., Mahowald N., Prospero J.M., Ridgwell A.J., Tegen I. & Torres R. 2005. Global Iron Connections Between Desert Dust, Ocean Biogeochemistry, and Climate. *Science* 308: 67.

Johannessen S.C. & Miller W.L. 2001. Quantum yield for the photochemical production of dissolved inorganic carbon in seawater. *Mar. Chem.* 76: 271–283.

Kamjunke N., Herzsprung P. & Neu T.R. 2015. Quality of dissolved organic matter affects planktonic but not biofilm bacterial production in streams. *Sci. Total Environ.* 506: 353–360.

Kieber D.J., McDaniel J. & Mopper K. 1989. Photochemical source of biological substrates in sea water: implications for carbon cycling. *Nature* 341: 637–639.

Kieber R.J., Zhou X. & Mopper K. 1990. Formation of carbonyl compounds from UV-induced photodegradation of humic substances in natural waters: Fate of riverine carbon in the sea. *Limnol. Oceanogr.* 35: 1503–1515.

Kiehl J.T. & Trenberth K.E. 1997. Earth's Annual Global Mean Energy Budget. *Bull. Am. Meteorol. Soc.* 78: 197–208.

Kim S.-B., Corapcioglu M.Y. & Kim D.-J. 2003. Effect of dissolved organic matter and bacteria on contaminant transport in riverbank filtration. *J. Contam. Hydrol.* 66: 1–23.

Koehler B., Landelius T., Weyhenmeyer G.A., Machida N. & Tranvik L.J. 2014. Sunlight-induced carbon dioxide emissions from inland waters. *Global Biogeochem. Cycles* 28: 696–711.

Koehler B., Broman E. & Tranvik L.J. 2016. Apparent quantum yield of photochemical dissolved organic carbon mineralization in lakes. *Limnol. Oceanogr.* 61: 2207–2221.

Kögel-Knabner I. 2002. The macromolecular organic composition of plant and microbial residues as inputs to soil organic matter. *Soil Biol. Biochem.* 34: 139–162.

Köhler S.J., Kothawala D., Futter M.N., Liungman O. & Tranvik L. 2013. In-Lake Processes Offset Increased Terrestrial Inputs of Dissolved Organic Carbon and Color to Lakes. *PLoS ONE* 8, doi: 10.1371/journal.pone.0070598.

Kononova M.M. 1966. *Soil organic matter its nature, its role in soil formation and in soil fertility*. Pergamon Press.

Kortelainen P., Mattsson T., Finér L., Ahtiainen M., Saukkonen S. & Sallantaus T. 2006. Controls on the export of C, N, P and Fe from undisturbed boreal catchments, Finland. *Aquat. Sci.* 68: 453–468.

Kowalczuk P., Cooper W.J., Whitehead R.F., Durako M.J. & Sheldon W. 2003. Characterization of CDOM in an organic-rich river and surrounding coastal ocean in the South Atlantic Bight. *Aquat. Sci.* 65: 384–401.

Kritzberg E.S. & Ekström S.M. 2012. Increasing iron concentrations in surface waters - a factor behind brownification? *Biogeosciences* 9: 1465–1478.

Kutser T., Pierson D.C., Kallio K.Y., Reinart A. & Sobek S. 2005. Mapping lake CDOM by satellite remote sensing. *Remote Sens. Environ.* 94: 535–540.

Lalonde K., Vähätalo A. V & Gélinas Y. 2014. Revisiting the disappearance of terrestrial dissolved organic matter in the ocean: a $\delta^{13}C$ study. *Biogeosciences* 11: 3707–3719.

Lapierre J.-F., Guillemette F., Berggren M. & Giorgio P.A. del. 2013. Increases in terrestrially derived carbon stimulate organic carbon processing and CO2 emissions in boreal aquatic ecosystems. *Nat. Commun.* 4: 2972.

Li L., Li L. & Song K. 2015. Remote sensing of freshwater cyanobacteria: An extended IOP Inversion Model of Inland Waters (IIMIW) for partitioning absorption coefficient and estimating phycocyanin. *Remote Sens. Environ.* 157: 9–23.

Löfgren S. & Zetterberg T. 2011. Decreased DOC concentrations in soil water in forested areas in southern Sweden during 1987–2008. *Sci. Total Environ.* 409: 1916–1926.

Lou T. & Xie H. 2006. Photochemical alteration of the molecular weight of dissolved organic matter. *Chemosphere* 65: 2333–2342.

Ludwig C.H. & Sarkanen K.V. 1971. *Lignins: occurrence, formation, structure and reactions*. Wiley-Interscience, New York.

Mack J. & Bolton J.R. 1999. Photochemistry of nitrite and nitrate in aqueous solution: a review. *J. Photochem. Photobiol. A Chem.* 128: 1–13.

Maie N., Scully N.M., Pisani O. & Jaffé R. 2007. Composition of a protein-like fluorophore of dissolved organic matter in coastal wetland and estuarine ecosystems. *Water Res.* 41: 563–570.

Mattsson T., Kortelainen P. & Räike A. 2005. Export of DOM from Boreal Catchments: Impacts of Land Use Cover and Climate. *Biogeochemistry* 76: 373–394.

Mattsson T., Kortelainen P., Laubel A., Evans D., Pujo-Pay M., Räike A. & Conan P. 2009. Export of dissolved organic matter in relation to land use along a European climatic gradient. *Sci. Total Environ.* 407: 1967–1976.

Mayorga E., Aufdenkampe A.K., Masiello C.A., Krusche A. V, Hedges J.I., Quay P.D., Richey J.E. & Brown T.A. 2005. Young organic matter as a source of carbon dioxide outgassing from Amazonian rivers. *Nature* 436: 538–541.

McDowell W.H. & Likens G.E. 1988. Origin, Composition, and Flux of Dissolved Organic Carbon in the Hubbard Brook Valley. *Ecol. Monogr.* 58: 177–195.

McNaught A.D. & Wilkinson A. 1997. *Compendium of Chemical Terminology*. Blackwell Scientific Publications, Oxford.

Miles C.J. & Brezonik P.L. 1981. Oxygen consumption in humic-colored waters by a photochemical ferrous-ferric catalytic cycle. *Environ. Sci. Technol.* 15: 1089–1095.

Miller W.L. 1994. Recent advances in the photochemistry of natural dissolved organic matter. In: Helz G.R., Zepp R.G. & Crosby D.G. (eds), *Aquatic and surface photochemistry*, Lewis Publishers, Boca Raton, pp. 111–127.

Miller W.L. 1998. Effects of UV radiation on aquatic humus: photochemical principles and experimental considerations. In: Hessen D.O. & Tranvik L.J. (eds), *Aquatic humic substances: ecology and biogeochemistry*, Springer Berlin Heidelberg, Berlin, Heidelberg, pp. 125–143.

Miller W.L. & Zepp R.G. 1995. Photochemical production of dissolved inorganic carbon from terrestrial organic matter: Significance to the oceanic organic carbon cycle. *Geophys. Res. Lett.* 22: 417–420.

Minero C., Chiron S., Falletti G., Maurino V., Pelizzetti E., Ajassa R., Carlotti M.E. & Vione D. 2007. Photochemincal processes involving nitrite in surface water samples. *Aquat. Sci.* 69: 71–85.

Minor E.C., Pothen J., Dalzell B.J., Abdulla H. & Mopper K. 2006. Effects of salinity changes on the photodegradation and ultraviolet-visible absorbance of terrestrial dissolved organic matter. *Limnol. Oceanogr.* 51: 2181–2186.

Minor E.C., Steinbring C.J., Longnecker K. & Kujawinski E.B. 2012. Characterization of dissolved organic matter in Lake Superior and its watershed using ultrahigh resolution mass spectrometry. *Org. Geochem.* 43: 1–11.

Mobley C.D. 2001. Radiative Transfer in the Ocean. In: Steele J.H., Turekian K.K. & Thorpe S.A. (eds), *Encyclopedia of Ocean Sciences*, pp. 619–628.

Molot L.A., Hudson J.J., Dillon P.J. & Miller S.A. 2005. Effect of pH on photo-oxidation of dissolved organic carbon by hydroxyl radicals in a coloured, softwater stream. *Aquat. Sci.* 67: 189–195.

Monteith D.T., Stoddard J.L., Evans C.D., Wit H.A. de, Forsius M., Hogasen T., Wilander A., Skjelkvale B.L., Jeffries D.S., Vuorenmaa J., Keller B., Kopacek

J. & Vesely J. 2007. Dissolved organic carbon trends resulting from changes in atmospheric deposition chemistry. *Nature* 450: 537–540.

Mopper K. & Degens E.T. 1979. Organic carbon in the ocean: nature and cycling. In: Bolin B., Degens E.T., Kempe S. & Ketner P. (eds), *The global carbon cycle*, John Wiley & Sons, Chichester, New York, Brisbane, Toronto, pp. 1–491.

Mopper K., Zhou X., Kieber R.J., Kieber D.J., Sikorski R.J. & Jones R.D. 1991. Photochemical degradation of dissolved organic carbon and its impact on the oceanic carbon cycle. *Nature* 353: 60–62.

Moran M.A. & Hodson R.E. 1994. Dissolved humic substances of vascular plant origin in a coastal marine environment. *Limnol. Oceanogr.* 39: 762–771.

Moran M.A. & Zepp R.G. 1997. Role of photoreactions in the formation of biologically labile compounds from dissolved organic matter. *Limnol. Oceanogr.* 42: 1307–1316.

Moran M.A., Sheldon W.M. & Zepp R.G. 2000. Carbon loss and optical property changes during long-term photochemical and biological degradation of estuarine dissolved organic matter. *Limnol. Oceanogr.* 45: 1254–1264.

Morris D.P. & Hargreaves B.R. 1997. The role of photochemical degradation of dissolved organic carbon in regulating the UV transparency of three lakes on the Pocono Plateau. *Limnol. Oceanogr.* 42: 239–249.

Morris D.P., Zagarese H., Williamson C.E., Balseiro E.G., Hargreaves B.R., Modenutti B., Moeller R. & Queimalinos C. 1995. The attenuation of solar UV radiation in lakes and the role of dissolved organic carbon. *Limnol. Oceanogr.* 40: 1381–1391.

Mostofa K.M.G., Liu C., Mottaleb M.A., Wan G., Ogawa H., Vione D., Yoshioka T. & Wu F. 2013. Dissolved Organic Matter in Natural Waters. In: Mostofa K.M.G., Yoshioka T., Mottaleb A. & Vione D. (eds), *Photobiogeochemistry of Organic Matter: Principles and Practices in Water Environments*, Springer Berlin Heidelberg, Berlin, Heidelberg, pp. 1–137.

Münster U. & Albrecht D. 1994. Dissolved organic matter: analysis of composition and function by a molecular-biochemical approach. In: *Microbial Ecology of Lake Plußsee*, Springer, New York, pp. 24–62.

Münster U. & De Haan H. 1998. The role of microbial extracellular enzymes in the transformation of dissolved organic matter in humic waters. In: Hessen D.O. & Tranvik L.J. (eds), *Aquatic Humic Substances: Ecology and Biogeochemistry*, Springer Berlin Heidelberg, Berlin, Heidelberg, pp. 199–257.

Neal C., Lofts S., Evans C.D., Reynolds B., Tipping E. & Neal M. 2008. Increasing Iron Concentrations in UK Upland Waters. *Aquat. Geochem.* 14: 263–288.

Nelson N.B. & Siegel D.A. 2013. The Global Distribution and Dynamics of Chromophoric Dissolved Organic Matter. *Ann. Rev. Mar. Sci.* 5: 447–476.

Neubauer E., Köhler S.J., Kammer F. von der, Laudon H. & Hofmann T. 2013. Effect of pH and Stream Order on Iron and Arsenic Speciation in Boreal Catchments. *Environ. Sci. Technol.* 47: 7120–7128.

Obernosterer I. & Benner R. 2004. Competition between biological and photochemical processes in the mineralization of dissolved organic carbon. *Limnol. Oceanogr.* 49: 117–124.

Opsahl S. & Benner R. 1997. Distribution and cycling of terrigenous dissolved organic matter in the ocean. *Nature* 386: 480–482.

Osburn C.L., Morris D.P., Thorn K.A. & Moeller R.E. 2001a. Chemical and optical changes in freshwater dissolved organic matter exposed to solar radiation. *Biogeochemistry* 54: 251–278.

Osburn C.L., Zagarese H.E., Morris D.P., Hargreaves B.R. & Cravero W.E. 2001b. Calculation of spectral weighting functions for the solar photobleaching of chromophoric dissolved organic matter in temperate lakes. *Limnol. Oceanogr.* 46: 1455–1467.

Pace M., Reche I., Cole J., Fernández-Barbero A., Mazuecos I. & Prairie Y. 2012. pH change induces shifts in the size and light absorption of dissolved organic matter. *Biogeochemistry* 108: 109–118.

Palviainen M., Laurén A., Launiainen S. & Piirainen S. 2016. Predicting the export and concentrations of organic carbon, nitrogen and phosphorus in boreal lakes by catchment characteristics and land use: A practical approach. *Ambio* 45: 933–945.

Philippe A. & Schaumann G.E. 2014. Interactions of Dissolved Organic Matter with Natural and Engineered Inorganic Colloids: A Review. *Environ. Sci. Technol.* 48: 8946–8962.

Porcal P., Dillon P.J. & Molot L.A. 2013. Seasonal changes in photochemical properties of dissolved organic matter in small boreal streams. *Biogeosciences* 10: 5533–5543.

Porcal P., Dillon P.J. & Molot L.A. 2014. Interaction of extrinsic chemical factors affecting photodegradation of dissolved organic matter in aquatic ecosystems. *Photochem. Photobiol. Sci.* 13: 799–812.

Potter B.B. & Wimsatt J.C. 2005. *Measurement of total organic carbon, dissolved organic carbon and specific UV absorbance at 254 nm in source water and drinking water*. U.S. Environmental Protection Agency, Washington, DC.

Poulin B.A., Ryan J.N. & Aiken G.R. 2014. Effects of Iron on Optical Properties of Dissolved Organic Matter. *Environ. Sci. Technol.* 48: 10098–10106.

Powers L.C. & Miller W.L. 2015. Photochemical production of CO and CO2 in the Northern Gulf of Mexico: Estimates and challenges for quantifying the impact of photochemistry on carbon cycles. *Mar. Chem.* 171: 21–35.

Pullin M.J. & Cabaniss S.E. 2003. The effects of pH, ionic strength, and iron–fulvic acid interactions on the kinetics of non-photochemical iron transformations. I. Iron(II) oxidation and iron(III) colloid formation. *Geochim. Cosmochim. Acta* 67: 4067–4077.

Qualls R.G. & Haines B.L. 1991. Geochemistry of Dissolved Organic Nutrients in Water Percolating through a Forest Ecosystem. *Soil Sci. Soc. Am. J.* 55: 1112–1123.

Rantakari M., Mattsson T., Kortelainen P., Piirainen S., Finér L. & Ahtiainen M. 2010. Organic and inorganic carbon concentrations and fluxes from managed and unmanaged boreal first-order catchments. *Sci. Total Environ.* 408: 1649–1658.

Raymond P.A., Hartmann J., Lauerwald R., Sobek S., McDonald C., Hoover M., Butman D., Striegl R., Mayorga E., Humborg C., Kortelainen P., Durr H.,

Meybeck M., Ciais P. & Guth P. 2013. Global carbon dioxide emissions from inland waters. *Nature* 503: 355–359.

Remington S., Krusche A. & Richey J. 2011. Effects of DOM photochemistry on bacterial metabolism and CO2 evasion during falling water in a humic and a whitewater river in the Brazilian Amazon. *Biogeochemistry* 105: 185–200.

Salonen K. & Vähätalo A. 1994. Photochemical mineralisation of dissolved organic matter in lake Skjervatjern. *Environ. Int.* 20: 307–312.

Sarkkola S., Nieminen M., Koivusalo H., Laurén A., Kortelainen P., Mattsson T., Palviainen M., Piirainen S., Starr M. & Finér L. 2013. Iron concentrations are increasing in surface waters from forested headwater catchments in eastern Finland. *Sci. Total Environ.* 463: 683–689.

Scully N.M., Maie N., Dailey S.K., Boyer J.N., Jones R.D. & Jaffé R. 2004. Early diagenesis of plant-derived dissolved organic matter along a wetland, mangrove, estuary ecotone. *Limnol. Oceanogr.* 49: 1667–1678.

Shapiro J. 1964. Effect of Yellow Organic Acids on Iron and Other Metals in Water. *J. Am. Water Works Assoc.* 56: 1062–1082.

Sharpless C.M. & Blough N. V. 2014. The importance of charge-transfer interactions in determining chromophoric dissolved organic matter (CDOM) optical and photochemical properties. *Environ. Sci. Process Impacts* 16: 654–671.

Simola H., Pitkänen A. & Turunen J. 2012. Carbon loss in drained forestry peatlands in Finland, estimated by re-sampling peatlands surveyed in the 1980s. *Eur. J. Soil Sci.* 63: 798–807.

Skjelkvåle B.L., Stoddard J.L. & Andersen T. 2001. Trends in Surface Water Acidification in Europe and North America (1989–1998). *Water Air Soil Pollut.* 130: 787–792.

Skjelkvåle B.L., Stoddard J.L., Jeffries D.S., Tørseth K., Høgåsen T., Bowman J., Mannio J., Monteith D.T., Mosello R., Rogora M., Rzychon D., Vesely J., Wieting J., Wilander A. & Worsztynowicz A. 2005. Regional scale evidence for improvements in surface water chemistry 1990–2001. *Environ. Pollut.* 137: 165–176.

Soumis N., Lucotte M., Larose C., Veillette F. & Canuel R. 2007. Photominealization in a Boreal Hydroelectric Reservoir: A Comparison with Natural Aquatic Ecosystems. *Biogeochemistry* 86: 123–135.

Spencer R.G.M., Aiken G.R., Butler K.D., Dornblaser M.M., Striegl R.G. & Hernes P.J. 2009a. Utilizing chromophoric dissolved organic matter measurements to derive export and reactivity of dissolved organic carbon exported to the Arctic Ocean: A case study of the Yukon River, Alaska. *Geophys. Res. Lett.* 36, L06401, doi: 10.1029/2008GL036831.

Spencer R.G.M., Stubbins A., Hernes P.J., Baker A., Mopper K., Aufdenkampe A.K., Dyda R.Y., Mwamba V.L., Mangangu A.M., Wabakanghanzi J.N. & Six J. 2009b. Photochemical degradation of dissolved organic matter and dissolved lignin phenols from the Congo River. *J. Geophys. Res.* 114, G03010, doi: 10.1029/2009JG000968.

Stoddard J.L., Jeffries D.S., Lukewille A., Clair T.A., Dillon P.J., Driscoll C.T., Forsius M., Johannessen M., Kahl J.S., Kellogg J.H., Kemp A., Mannio J.,

Monteith D.T., Murdoch P.S., Patrick S., Rebsdorf A., Skjelkvale B.L., Stainton M.P., Traaen T., Dam H. van, Webster K.E., Wieting J. & Wilander A. 1999. Regional trends in aquatic recovery from acidification in North Americaand Europe. *Nature* 401: 575–578.

Stubbins A., Spencer R.G.M., Chen H., Hatcher P.G., Mopper K., Hernes P.J., Mwamba V.L., Mangangu A.M., Wabakanghanzi J.N. & Six J. 2010. Illuminated darkness: Molecular signatures of Congo River dissolved organic matter and its photochemical alteration as revealed by ultrahigh precision mass spectrometry. *Limnol. Oceanogr.* 55: 1467–1477.

Sulzberger B. & Durisch-Kaiser E. 2009. Chemical characterization of dissolved organic matter (DOM): A prerequisite for understanding UV-induced changes of DOM absorption properties and bioavailability. *Aquat. Sci.* 71: 104–126.

Takeda K., Takedoi H., Yamaji S., Ohta K. & Sakugawa H. 2004. Determination of Hydroxyl Radical Photoproduction Rates in Natural Waters. *Anal. Sci.* 20: 153–158.

Traina S.J., Novak J. & Smeck N.E. 1990. An Ultraviolet Absorbance Method of Estimating the Percent Aromatic Carbon Content of Humic Acids. *J. Environ. Qual.* 19: 151–153.

Tranvik L.J., Downing J.A., Cotner J.B., Loiselle S.A., Striegl R.G., Ballatore T.J., Dillon P., Finlay K., Fortino K., Knoll L.B., Kortelainen P.L., Kutser T., Larsen S., Laurion I., Leech D.M., McCallister S.L., McKnight D.M., Melack J.M., Overholt E., Porter J.A., Prairie Y., Renwick W.H., Roland F., Sherman B.S., Schindler D.W., Sobek S., Tremblay A., Vanni M.J., Verschoor A.M., von Wachenfeldt E. & Weyhenmeyer G.A. 2009. Lakes and reservoirs as regulators of carbon cycling and climate. *Limnol. Oceanogr.* 54: 2298–2314.

Turro N.J. 1991. *Modern molecular photochemistry*. University Science Books.

Twardowski M.S. & Donaghay P.L. 2002. Photobleaching of aquatic dissolved materials: Absorption removal, spectral alteration, and their interrelationship. *J. Geophys. Res.* 107, 3091, doi: 10.1029/1999JC000281.

Vachon D., Lapierre J.-F. & del Giorgio P.A. 2016. Seasonality of photochemical dissolved organic carbon mineralization and its relative contribution to pelagic CO_2 production in northern lakes. *J. Geophys. Res. Biogeosci.* 121: 864–878.

Vähätalo A.V. 2009. Light, Photolytic Reactivity and Chemical Products. In: Likens G.E. (ed.), *Encyclopedia of Inland Waters*, pp. 761–773.

Vähätalo A. V & Wetzel R.G. 2004. Photochemical and microbial decomposition of chromophoric dissolved organic matter during long (months-years) exposures. *Mar. Chem.* 89: 313–326.

Vähätalo A. V., Salkinoja-Salonen M., Taalas P. & Salonen K. 2000. Spectrum of the quantum yield for photochemical mineralization of dissolved organic carbon in a humic lake. *Limnol. Oceanogr.* 45: 664–676.

Valentine R.L. & Zepp R.G. 1993. Formation of carbon monoxide from the photodegradation of terrestrial dissolved organic carbon in natural waters. *Environ. Sci. Technol.* 27: 409–412.

Vione D., Falletti G., Maurino V., Minero C., Pelizzetti E., Malandrino M., Ajassa R., Olariu R.-I. & Arsene C. 2006. Sources and Sinks of Hydroxyl Radicals upon Irradiation of Natural Water Samples. *Environ. Sci. Technol.* 40: 3775–3781.

Vittor C. De, Paoli A. & Fonda Umani S. 2008. Dissolved organic carbon variability in a shallow coastal marine system (Gulf of Trieste, northern Adriatic Sea). *Estuar. Coast Shelf Sci.* 78: 280–290.

Voelker B.M., Morel F.M.M. & Sulzberger B. 1997. Iron redox cycling in surface waters: effects of humic substances and light. *Environ. Sci. Technol.* 31: 1004–1011.

von Wachenfeldt E. & Tranvik L.J. 2008. Sedimentation in Boreal Lakes—The Role of Flocculation of Allochthonous Dissolved Organic Matter in the Water Column. *Ecosystems* 11: 803–814.

Vuorenmaa J., Forsius M. & Mannio J. 2006. Increasing trends of total organic carbon concentrations in small forest lakes in Finland from 1987 to 2003. *Sci. Total Environ.* 365: 47–65.

Waite T.D. 2005. Role of iron in light-induced environmental processes. In: Boule P., Bahnemann D.W. & Robertson P.K.J. (eds), *Environmental Photochemistry Part II*, Springer Berlin Heidelberg, Berlin, Heidelberg, pp. 255–298.

Weishaar J.L., Aiken G.R., Bergamaschi B.A., Fram M.S., Fujii R. & Mopper K. 2003. Evaluation of specific ultraviolet absorbance as an indicator of the chemical composition and reactivity of dissolved organic carbon. *Environ. Sci. Technol.* 37: 4702–4708.

Weyhenmeyer G. 1999. *Lake Erken: Meteorological, physical, chemical and biological data and a list of publications from 1933 to 1998*. Uppsala.

Whipple G.C. 1899. *The microscopy of drinking-water*. Wiley, New York.

White E.M., Kieber D.J., Sherrard J., Miller W.L. & Mopper K. 2010. Carbon dioxide and carbon monoxide photoproduction quantum yields in the Delaware Estuary. *Mar. Chem.* 118: 11–21.

Whitehead R.F., Mora S. de, Demers S., Gosselin M., Monfort P. & Mostajir B. 2000. Interactions of ultraviolet-B radiation, mixing, and biological activity on photobleaching of natural chromophoric dissolved organic matter: A mesocosm study. *Limnol. Oceanogr.* 45: 278–291.

Wiegner T.N. & Seitzinger S.P. 2001. Photochemical and microbial degradation of external dissolved organic matter inputs to rivers. *Aquat. Microb. Ecol.* 24: 27–40.

Wright R.F., Larssen T., Camarero L., Cosby B.J., Ferrier R.C., Helliwell R., Forsius M., Jenkins A., Kopáček J., Majer V., Moldan F., Posch M., Rogora M. & Schöpp W. 2005. Recovery of Acidified European Surface Waters. *Environ. Sci. Technol.* 39: 64A–72A.

Xiao Y.-H., Sara-Aho T., Hartikainen H. & Vähätalo A. V. 2013. Contribution of ferric iron to light absorption by chromophoric dissolved organic matter. *Limnol. Oceanogr.* 58: 653–662.

Xiao Y.-H., Räike A., Hartikainen H. & Vähätalo A. V. 2015. Iron as a source of color in river waters. *Sci. Total Environ.* 536: 914–923.

Xie H., Zafiriou O.C., Cai W.-J., Zepp R.G. & Wang Y. 2004. Photooxidation and Its Effects on the Carboxyl Content of Dissolved Organic Matter in Two Coastal Rivers in the Southeastern United States. *Environ. Sci. Technol.* 38: 4113–4119.

Yamashita Y., Scinto L.J., Maie N. & Jaffé R. 2010. Dissolved Organic Matter Characteristics Across a Subtropical Wetland's Landscape: Application of Optical Properties in the Assessment of Environmental Dynamics. *Ecosystems* 13: 1006–1019.

Zafiriou O.C. 1977. Marine organic photochemistry previewed. *Mar. Chem.* 5: 497–522.

Zafiriou O.C., Joussot-Dubien J., Zepp R.G. & Zika R.G. 1984. Photochemistry of natural waters. *Environ. Sci. Technol.* 18: 358A–371A.

Zepp R.G. 1978. Quantum yields for reaction of pollutants in dilute aqueous solution. *Environ. Sci. Technol.* 12: 327–329.

Zepp R.G., Hoigne J. & Bader H. 1987. Nitrate-induced photooxidation of trace organic chemicals in water. *Environ. Sci. Technol.* 21: 443–450.

Zepp R.G., Callaghan T. V & Erickson D.J. 1995. Effects of increased solar ultraviolet radiation on biogeochemical cycles. *Ambio* 24: 181–187.

Zepp R.G., Callaghan T.V. & Erickson D.J. 1998. Effects of enhanced solar ultraviolet radiation on biogeochemical cycles. *J. Photochem. Photobiol. B, Biol.* 46: 69–82.

Zhou X. & Mopper K. 1997. Photochemical production of low-molecular-weight carbonyl compounds in seawater and surface microlayer and their air-sea exchange. *Mar. Chem.* 56: 201–213.

Zika R.G. 1981. Chapter 10 Marine Organic Photochemistry. In: Duursma E.K. & Dawson R. (eds), *Marine Organic Chemistry: Evolution, Composition, Interactions and Chemistry of Organic Matter in Seawater*, Elsevier B.V., Amsterdam, pp. 299–325.

Zsolnay Á. 1996. Dissolved humus in soil waters. In: Piccolo A. (ed.), *Humic substances in terrestrial ecosystems*, Elsevier B.V., Amsterdam, pp. 171–223.

Zsolnay Á. 2003. Dissolved organic matter: artefacts, definitions, and functions. *Geoderma* 113: 187–209.

ORIGINAL PAPERS

I

IRON AND PH REGULATING THE PHOTOCHEMICAL MINERALIZATION OF DISSOLVED ORGANIC CARBON

by

Gu Y., Lensu A., Perämäki, S., Ojala A. & Vähätalo A.V. 2017.

ACS Omega 2: 1905–1914.

ACS OMEGA

Article

http://pubs.acs.org/journal/acsodf

Iron and pH Regulating the Photochemical Mineralization of Dissolved Organic Carbon

Yufei Gu,*[,†] Anssi Lensu,[†] Siiri Perämäki,[‡] Anne Ojala,[§,∥] and Anssi V. Vähätalo[†]

[†]Department of Biological and Environmental Science and [‡]Department of Chemistry, University of Jyväskylä, P.O. Box 35, FI-40014 Jyväskylä, Finland

[§]Department of Forest Sciences, University of Helsinki, P.O. Box 27, FI-00014 Helsinki, Finland

[∥]Department of Environmental Sciences, University of Helsinki, P.O. Box 65, FI-00014 Helsinki, Finland

Supporting Information

ABSTRACT: Solar radiation mineralizes dissolved organic matter (DOM) to dissolved inorganic carbon through photochemical reactions (DIC photoproduction) that are influenced by iron (Fe) and pH. This study addressed as to what extent Fe contributes to the optical properties of the chromophoric DOM (CDOM) and DIC photoproduction at different pH values. We created the associations of Fe and DOM (Fe-DOM) that cover the range of loadings of Fe on DOM and pH values found in freshwaters. The introduced Fe enhanced the light absorption by CDOM independent of pH. Simulated solar irradiation decreased the light absorption by CDOM (i.e., caused photobleaching). Fe raised the rate of photobleaching and steepened the spectral slopes of CDOM in low pH but resisted the slope steepening in neutral to alkaline pH. The combination of a low pH (down to pH 4) and high Fe loading on DOM (up to 3.5 μmol mg DOM^{-1}) increased the DIC photoproduction rate and the apparent quantum yields for DIC photoproduction up to 7-fold compared to the corresponding experiments at pH >6 or without Fe. The action spectrum for DIC photoproduction shifted toward the visible spectrum range at low pH in the presence of Fe. Our results demonstrated that Fe can contribute to DIC photoproduction by up to 86% and produce DIC even at the visible spectrum range in acidic waters. However, the stimulatory effect of Fe is negligible at pH >7.

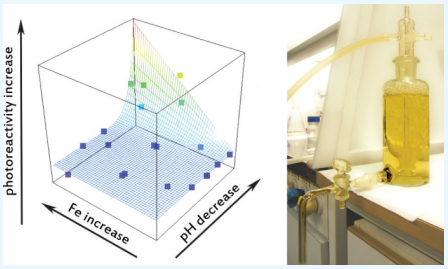

INTRODUCTION

Solar radiation photochemically mineralizes 13−35 Tg C yr^{-1} of dissolved organic carbon (DOC) to dissolved inorganic carbon (DIC) in lakes and reservoirs.[1] Iron (Fe) increases the light absorption by chromophoric dissolved organic matter (CDOM), and therefore influences DIC photoproduction indirectly through changes in the optical properties of CDOM. Solar radiation can mineralize Fe(III)-polycarboxylate complexes of DOM to DIC (Figure S1).[2] Irradiation of Fe can generate reactive oxygen species that mineralize DOC (Figure S1).[3] Low pH enhances Fe-stimulated DIC photoproduction (Figure S1, red circles).[4−6] The recent increases in Fe concentration ([Fe]) and DOC as well as in pH[7−14] emphasize the need to understand the impact of pH and [Fe] on the optical properties of CDOM and DIC photoproduction in freshwaters.

In many surface waters with pH 4−9, ferric iron exists primarily as complexes with DOM and as colloids of iron(oxy)hydroxide stabilized by DOM.[15−19] The colloids stabilized by DOM resist gravitoidal settling, pass filters (e.g., 0.45 μm), and are difficult to separate from Fe complexed by DOM.[15,19,20] In this study, the Fe associated with DOM is abbreviated to Fe-DOM, which includes both the Fe complexes of DOM and the iron(oxy)hydroxide colloids stabilized by DOM.

The importance of Fe stimulus for DIC photoproduction in natural waters has been examined mostly with two approaches: (1) relating DIC photoproduction to water quality parameters and (2) introducing strong complexing ligands for Fe into natural water samples. The first approach has shown that [Fe] and acidity correlate positively with DIC photoproduction.[21−23] According to the second approach, the complexing ligands for Fe reduce DIC photoproduction rates (DICprs).[4,5,23] Both approaches show that [Fe] and acidity play important roles in DIC photoproduction. The quantitative role of Fe on DIC photoproduction remains unclear because the photoreactivity of DOM in natural waters can vary[24] even without Fe and the introduced complexing ligands may potentially interfere with DIC photoproduction.

The DICpr depends on the intensity of irradiation and optical properties of natural waters. Fe(III) enhances light absorption of CDOM, particularly at the longer wavelengths of

Received: April 13, 2017
Accepted: April 21, 2017
Published: May 9, 2017

DOI: 10.1021/acsomega.7b00453
ACS Omega 2017, 2, 1905−1914

the visible spectrum range.[25,26] DIC photoproduction and the photoreduction of Fe(III) to Fe(II) increase exponentially with shorter wavelengths of irradiance,[4,27−29] indicating that Fe-stimulated DIC photoproduction has strong spectral dependence. Photon flux densities of solar radiation increase from low values at the UV range to the maximum of the visible spectrum range. The light absorption by CDOM and the photochemical reactivity of DOM are all spectrally dependent due to solar radiation, and spectral dependence should be accounted for the Fe-stimulated DIC photoproduction.

This study quantified the impact of [Fe] and pH on the optical properties of CDOM, the light-induced changes in optical properties, DICprs, and the spectral-apparent quantum yields for DIC photoproduction (ϕ_λ). To generate the associations between Fe(III) and DOM (Fe-DOM), the same concentration (10 mg DOM L^{-1}) of Fe-free DOM isolate from lake water received Fe(III) at different concentrations. Our experiments covered 20 combinations of pH and [Fe], where the pH ranged from 4 to 9.4 and the Fe loadings on DOM were from 0.004 to 3.5 μmol Fe mg DOM^{-1}. Competing multiple regression models were used to find the most parsimonious model that was able to explain the effect of pH and [Fe] on the optical properties of CDOM and DIC photoproduction. On the basis of the modeling, we estimated the magnitude of the Fe-stimulated DIC photoproduction. Determination of ϕ_λ allowed us to evaluate the spectral dependence of DIC photoproduction and showed that Fe shifted the action spectrum of DIC photoproduction towards the visible spectrum range.

RESULTS

Dependence of Optical Properties on pH and [Fe]. When the same DOM concentration (10 mg DOM L^{-1}) was associated with the different Fe concentrations and adjusted to pH values ranging from 4 to 9.4 (Table S2), the absorption coefficient of CDOM at 330 nm (a_{330}) increased with the rising [Fe] (a_{330_Dark} in Figure 1a; "Init." in Table S5). The dependence of a_{330} on [Fe] and pH (expressed as the concentration of hydrogen ion, $[H^+] = 10^{-pH}$ in the models) was analyzed with eight competing regression models (Table S8). The a_{330_Dark} was significantly dependent on [Fe] in all models that included [Fe] as a separate predictor variable (shown as bold regression coefficients $b1$ for the models 2, 4, 6, and 8 in Table S8). In the model 7 without [Fe] as a separate predictor variable, a_{330_Dark} was significantly dependent on pH (term $[H^+]$, coefficient $b2$) and the interaction between pH and [Fe] (term [Fe] $[H^+]$, coefficient $b3$; Table S8). Among the models containing only significant terms (models 1, 2, and 7 in Table S8), the model 2 had the lowest value of AICc (110 in Table S8). Therefore, the model 2 (marked with * in Table S8) was selected to explain the simplest significant dependence of a_{330_Dark} on the predictor variables. According to the best model 2 (Table S8), a_{330_Dark} was significantly dependent on [Fe] alone. The model 2 (Table S8) is illustrated as a surface in Figure 1a together with color-coded dots that show a_{330_Dark} in the 20 experiments (Table S5). In a similar manner, text in the later results section refers to the significant dependencies of the most parsimonious models marked with * in Tables S8−S18, which are also illustrated as surfaces in Figures 1−3.

The Fe associated with DOM increased the absorption coefficient of CDOM at different wavelengths unequally because the spectral slope coefficients ($S_{275-295}$, $S_{350-400}$) decreased with increasing [Fe] associated to DOM (Table S6). The value of $S_{275-295}$ decreased more than that of $S_{350-400}$, which was seen as a decrease in the slope ratio (S_R) (Figure 1b, Table S6). The changes in $S_{275-295}$ (model 2 in Table S9) and S_R (model 2 in Table S10) depended only on [Fe], as illustrated for S_R (Figure 1b). Therefore, the changes in optical properties of CDOM depended only on the introduced [Fe] and not on pH adjustment (Tables S9−S11, Figure 1).

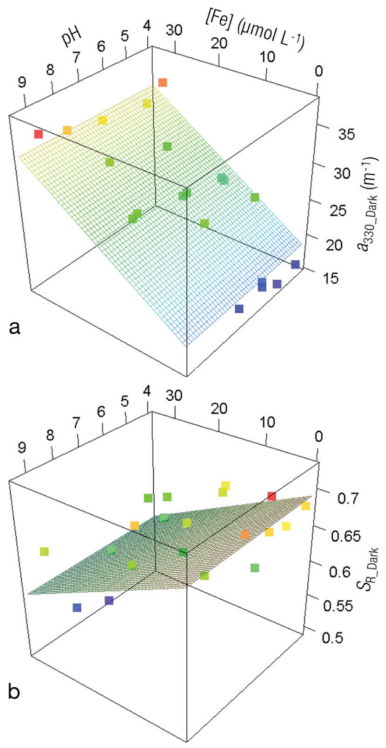

Figure 1. Impact of [Fe] and pH on the optical properties of CDOM represented as (a) the absorption coefficient of CDOM at 330 nm (a_{330_Dark}) and (b) the spectral slope ratio (S_{R_Dark}) in the dark control samples. Dots show the experimental data (Tables S5 and S6), and the surfaces show the fit of the best model on the data (model 2 in both Tables S8 and S10). The color of dots and the surfaces follows the value of the vertical axis. The lowest values are shown in violet, intermediate values with cyan, blue, green, yellow, and orange, and the highest values in red.

Simulated solar irradiation decreased a_{330} (i.e., caused photobleaching) and increased $S_{275-295}$ and S_R values (Tables S5 and S6). The photobleaching of a_{330} (Δa_{330}) and photochemistry-induced change in $S_{275-295}$ ($\Delta S_{275-295}$) and in S_R (ΔS_R) depended positively on the interaction between [Fe] and acidity (Figure 2a,b; model 5 in Table S11, models 6 in Tables S12 and S13). $\Delta S_{275-295}$ and ΔS_R were additionally negatively dependent on [Fe] (Figure 2b; models 6 in Tables S12 and S13).

Rate of DIC Photoproduction at Different pH and [Fe]. Irradiation produced DIC at rates ranging from 1.72 to 12.08

DOI: 10.1021/acsomega.7b00453
ACS Omega 2017, 2, 1905−1914

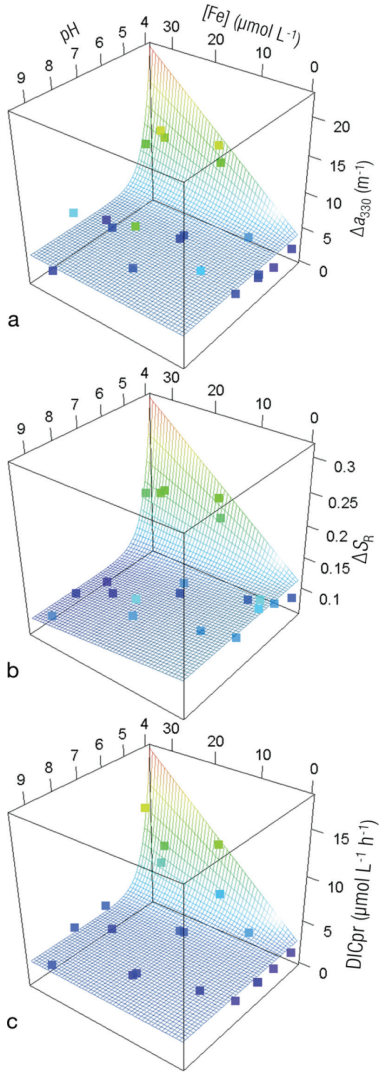

Figure 2. Impact of [Fe] and pH on (a) the photobleaching of a_{330} (Δa_{330}), (b) the photochemistry-induced change in S_R (ΔS_R), and (c) DICpr. Dots show experimental data (Tables S5–S7) and the surfaces show the fit of the best models on data (model 5 in Table S11, model 6 in Table S13 and model 5 in Table S14). Note that the highest values in the surface exceed the experimental data and should be treated with caution. Color-coding is the same as in Figure 1.

μmol C L^{-1} h^{-1} (Table S7). Because each experiment contained an identical concentration (10 mg DOM L^{-1}) of the same solid-phase extracted DOM (SPE-DOM), the up to 7-fold differences in the rate of DIC photoproduction were caused by the experimental adjustments of pH and [Fe]. According to the best model, DICpr was dependent on the interaction between pH and [Fe] (Figure 2c; model 5 in Table S14).

Influence of Fe and pH on ϕ_λ. The calculations of ϕ_λ (details in Supporting Information) accounted for the light absorption by the introduced Fe (Figure 1) and photobleaching of CDOM during the irradiations (Figure 2). The ϕ_λ values are reported in Table S7 with two parameters: c, the apparent quantum yields at wavelength 0 nm ($=\phi_0$) and d, the spectral slope coefficient of ϕ_λ (eq 2). These two parameters allow the calculation of ϕ_λ spectrally, as shown in Figure S5 or at a specific wavelength (e.g., 330 nm; ϕ_{330}, Table S7), which approximates the median wavelength ($\lambda_{50\%}$) that induced DIC photoproduction during the irradiations.

Both ϕ_{330} and c were positively dependent on the interaction between [Fe] and acidity (Figure 3a,b; models 5 in Tables S15 and S16) similar to that found for the rate of DIC photoproduction (Figure 2c; model 5 Table S14). The spectral slope coefficient of ϕ_λ, d, had a similar but negative dependence on the interaction between [Fe] and acidity (Figure 3c, model 5 in Table S17). The rise in c indicated a general increase in ϕ_λ at any wavelength, but the decrease in d meant that ϕ_λ increased relatively more at longer wavelengths.

To demonstrate the role of [Fe] on DIC photoproduction at different pH values, we calculated the relative contribution of Fe-stimulated ϕ_{330} ($\phi_{330,Fe}$) to the total ϕ_{330} ($\phi_{330,total}$) for a few selected [Fe] (Figure 4). When [Fe] was >10 μM, Fe-stimulated reactions dominated DIC photoproduction at pH 4, but their contribution fell to a few percent at pH 6 and was negligible at pH >7 (Figure 4).

Figure 5 compares the largest ϕ_λ at pH 4 with 18 μM [Fe] (experiment #11) to the ϕ_λ without the introduced Fe at a similar pH (#1; Table S7). The Fe-stimulated ϕ_λ is calculated as the difference in ϕ_λs between experiment #11 and #1 (#11–#1, Figure 5, red dotted line). The spectral slope coefficient for ϕ_λ was smaller for the Fe-stimulated DIC photoproduction (d = 0.020 nm^{-1}, Figure 5, red dotted line) than for the corresponding experiment without the introduced Fe (d = 0.025 nm^{-1} in #1, Figure 5, blue dotted line).

To illustrate the potential environmental impact of Fe on DIC photoproduction in acidic waters (pH ≈ 4), we calculated the action spectra for DIC photoproduction per m^2 using a typical daily solar radiation spectrum and the ϕ_λ values reported in Figure 5 (Figure 6). The rate of DIC photoproduction calculated as an integral over 300–700 nm was 2456 μmol C m^{-2} day^{-1} in the presence of 18 μM [Fe] and 5.8 times larger than 424 μmol C m^{-2} day^{-1} in the presence of negligible 0.04 μM [Fe] (Figure 6). Fe shifted the action spectrum toward the visible spectrum range and caused Fe-stimulated DIC photoproduction even at wavelengths >500 nm (Figure 6). At wavelengths >500 nm, Fe stimulus is nearly entirely responsible for DIC photoproduction (Figure 6). The median wavelength for DIC photoproduction ($\lambda_{50\%}$) shifted by 20 nm from 378 (#1) to 398 nm (#11; Figure 6).

DISCUSSION

This study systematically examined the combined impact of pH and introduced Fe(III) onto the optical properties of CDOM, the rates of photoreactions (photobleaching, DIC photoproduction), and the spectral photochemical reactivity (ϕ_λ) of a natural Fe-free isolate of aquatic DOM. Our major findings (summarized in Table 1) imply that Fe can have a strong effect

DOI: 10.1021/acsomega.7b00453
ACS Omega 2017, 2, 1905–1914

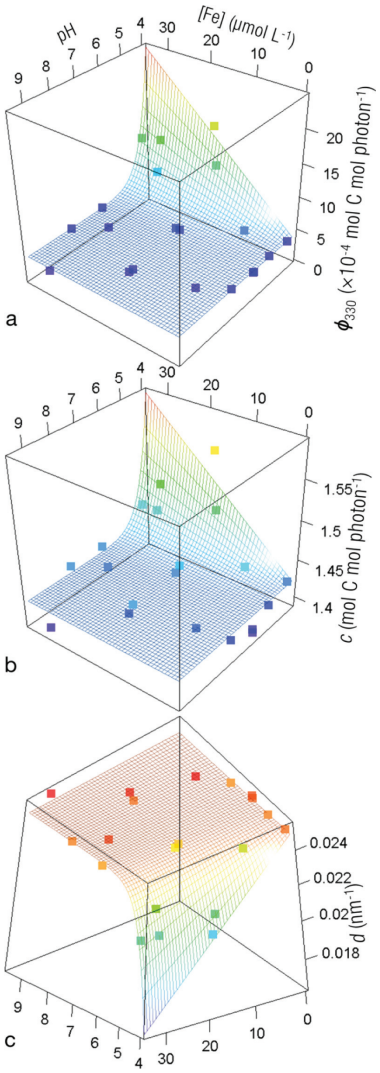

Figure 3. Impact of [Fe] and pH on the apparent quantum yields spectra for DIC photoproduction, ϕ_λ values (a) at 330 nm, ϕ_{330}; (b) c of eq 2; and (c) spectral slope coefficient of ϕ_λ (=d of eq 2). Dots indicate experimental data (Table S7), and the surfaces show the fit of the best model on data (models 5 in Tables S14–S16). Please note that in (c) the orientation of the three-dimensional cube is different.

on the optical properties and photochemistry of DOM, but the effect is often regulated by pH.

Impact of Fe and pH on Optical Properties. As expected for the DOM isolated from a humic lake, its low S_R (≈0.7) is a characteristic of a terrestrial DOM that has entered the aquatic

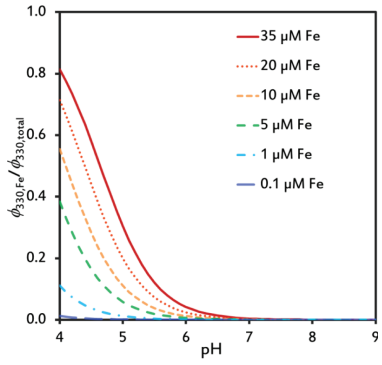

Figure 4. Contribution of Fe to the apparent quantum yields for DIC photoproduction at 330 nm ($\phi_{330,Fe}/\phi_{330,total}$) at the selected [Fe], along a pH gradient. The ratio $\phi_{330,Fe}/\phi_{330,total}$ is calculated from model 5 in Table S15 (also shown as a surface in Figure 3a). According to model 5, $\phi_{330,Fe} = \phi_{330,total} - 3.76 \times 10^{-4}$ (mol C mol photons^{-1}), where the intercept refers to a pH-independent ϕ_{330} without Fe. The concentration of DOM was always 10 mg DOM L^{-1}, therefore, e.g., 35 μM Fe refers to a loading of 3.5 μmol Fe mg DOM^{-1}.

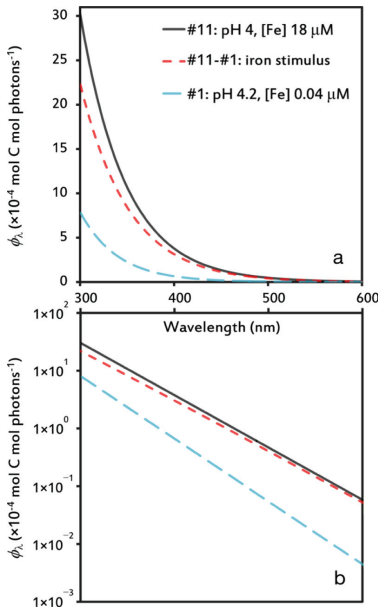

Figure 5. ϕ_λs in acidic (pH ≈ 4) experiments #1 (0.04 μM [Fe]) and #11 (18 μM [Fe]) as well as the Fe-stimulated ϕ_λ calculated as a difference in ϕ_λ values between #11 and #1. c and d are reported in Table S7 for #1 and #11. For the Fe-stimulated ϕ_λ (#11–#1), c = 0.934 mol C mol photons^{-1} and d = 0.0200 nm^{-1}. The same ϕ_λs are shown in (a) linear and (b) in logarithmic scales.

DOI: 10.1021/acsomega.7b00453
ACS Omega 2017, 2, 1905–1914

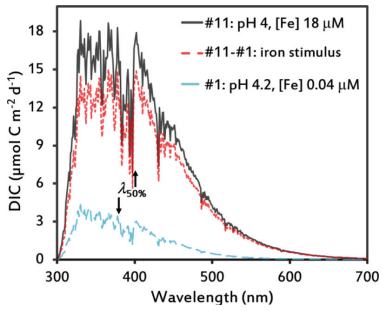

Figure 6. Calculated action spectrum for areal DIC photoproduction at pH 4. DIC photoproduction is calculated as $\int_{\lambda_{300}}^{\lambda_{700}} \phi_\lambda Q_\lambda \, d\lambda$, where ϕ_λ (mol C mol photons^{-1} nm^{-1}) is from experiments #1, #11, or #11−#1 (Figure 5) and Q_λ (mol photons^{-1} m^{-2} day^{-1} nm^{-1}) is the mean daily solar photon flux density at the earth surface averaged across the latitudes (168 W m^{-2} global radiation), having the properties of ASTM G173-03 reference solar spectrum.[41] The arrows show the median wavelength inducing areal DIC photoproduction ($\lambda_{50\%}$), which is 378 nm in #1 without Fe and 398 nm in #11 with 18 μM Fe.

Table 1. Summary of Major Findings in this Study

no.	finding	figure and table
1	Fe stimulates photobleaching of CDOM and increases $S_{275-295}$ and S_R in acidic waters but resists an increase in $S_{275-295}$ and S_R in neutral−alkaline water	Figure 2a,b; Tables S6, S11, and S12
2	DIC photoproduction in Fe-free DOM is pH-independent (pH 4−7)	Figures 2c and S7; Table S7
3	the association of Fe with DOM can enhance the photochemical mineralization rate of DOC 7-fold	Figure 2c
4	Fe contributes 0−86% to DIC photoproduction depending on pH and [Fe]	Figure 4; Table S7
5	the association of Fe with DOM can increase the ϕ_λ for DIC photoproduction by 5-fold	Figure 3a; Table S7
6	the spectral slope coefficient of ϕ_λ for Fe-stimulated DIC photoproduction is low and similar to the corresponding slopes for Fe(III) photoreduction	Figures 5 and S8
7	in acidic water, the association of Fe with DOM shifts the action spectrum of DIC photoproduction toward the visible spectrum range	Figure 6
8	solar radiation >500 nm can potentially mineralize DOC in acidic Fe-rich waters photochemically	Figure 6

regime recently.[38] Our experimental Fe introduction demonstrated that the association of Fe(III) with DOM decreases $S_{275-295}$ more than $S_{350-400}$ when independent of pH and causes a decline in S_R in agreement with earlier studies.[25,26] These observations suggest that Fe(III) associated with DOM contributes to a high a_λ and low S_R that is related to the fresh input of terrestrial CDOM into the aquatic regime.[25,38]

In this study, a_λ increases linearly along the concentration of Fe(III) associated with DOM, consistent with the previous findings.[25,26,42] The rise in a_λ caused by Fe(III) is pH-independent according to this (pH 4−9.4) and an earlier study (pH 2−7).[26] Some studies have reported an increase in a_λ with pH,[42−44] but for waters rich in Fe, this pH effect is smaller than the contribution of Fe(III) to a_λ (this study).[26,42] For instance, 35 μM Fe doubled a_λ and contributed about 50% to the light absorption by Fe(III)-DOM (Table S5). Similar or even higher contributions of Fe to the light absorption by CDOM have been reported in rivers[33] or springs fed by groundwater.[25]

Irradiation decreases (i.e., photobleaches) a_λ and increases S_R according to this and earlier studies.[6,38] In our experiments, these changes in the optical properties of CDOM took place both in the presence and absence of Fe, although to a different degree, depending on the combination of [Fe] and pH. In this study, Fe-stimulated photobleaching increased S_R and $S_{275-295}$ at low pH but resisted these changes in the spectral slopes at high pH (Figure 2a,b; Tables S12 and S13). The stimulatory effect of [Fe] and acidity may be partly related to photoproduced Fe(II), which absorbs light weakly and oxidizes slowly to highly absorbing Fe(III) at low pH.[26,45] Additionally, the same combination (high Fe(III) and low pH) stimulates photoproduction of HO$^\bullet$, which can attack organic chromophores and enhance their photobleaching.[46−48] At high pH, photoproduced Fe(II) is oxidized rapidly back to highly absorbing Fe(III) and the photobleaching of Fe-DOM likely primarily concerns the organic chromophores of CDOM. The chromophores of Fe(III) in nonacidic waters seem to withstand photobleaching similar to iron oxides that are commonly used as weather-resistant outdoor pigments in neutral−alkaline conditions.[49]

Impact of Fe and pH on DIC Photoproduction. According to our irradiation experiments, pH (4−9.4) alone has a nonsignificant impact on DICpr when [Fe] is low (Table S7). Similarly, an earlier study showed that an experimental acidification by one pH unit had a nonsignificant effect on DIC photoproduction in lake waters (pH 4.2−7.2) with low [Fe].[50] Our study showed that Fe stimulates DIC photoproduction in acidic but not in neutral to alkaline conditions. In agreement with our findings, DIC photoproduction was dependent on [Fe] in 38 Swedish lakes, including acidic lakes (pH 4.5−9.5) but the dependence was absent in a subset of 27 lakes having pH >6 (Figure S6).[21] Likewise, in six lakes and two reservoirs (Québec, Canada), the broadband-apparent quantum yields for DIC photoproduction showed a nonsignificant relationship with ambient pH 6.4−8.2.[51] Fe introduction to circumneutral Brandy Lake inflow did not give rise to photochemical loss of DOC.[23] Thus, pH has a minor role on DIC photoproduction in the absence of Fe (ref S0, this study) or in neutral to alkaline waters even in the presence of Fe (refs 21, 23, 51, this study).

Our experiments showed that Fe stimulates DIC photoproduction only in acidic conditions similar to those found earlier in natural water samples.[3−5,21,44,48,50,52] According to our volumetric DICprs (Figure 2c), $\phi_{\lambda s}$ (Figures 3 and 4), or the areal rates calculated from $\phi_{\lambda s}$ (Figure 6), the Fe-stimulated DIC photoproduction is responsible for up to 86% of the total DIC photoproduction at pH ≈ 4 with up to 3.5 μmol Fe mg DOM^{-1}. In the example illustrated in Figure 6 (pH ≈ 4, 1.8 μmol Fe mg DOM^{-1}), Fe contributed 83% to the total DIC photoproduction. The calculated contribution (Figure 5) would fall to 56% at pH 4, with 1 μmol Fe mg DOM^{-1}, which is the highest reported amount of Fe complexed by DOM in natural waters.[18] In typical boreal wetlands and forested streams (pH 4−5; 0.3−0.4 μmol complexed Fe mg DOM^{-1}),[18] the calculated (Figure 5) contribution of Fe to DIC photoproduction is between 4 and 33%. In a strict sense, these calculations apply to our experimental conditions, but they suggest that Fe can contribute up to ≈50% to DIC photoproduction in acidic surface waters.

How Does Iron Stimulate DIC Photoproduction at Low pH? Our study was not designed to address the

DOI: 10.1021/acsomega.7b00453
ACS Omega 2017, 2, 1905−1914

mechanistic details of Fe-stimulated DIC photoproduction, but here, we discuss how our observations fit to the mechanistic understanding gained by earlier studies.[2,3] Fe can contribute to DIC photoproduction through two principal mechanisms: (1) the photochemical decarboxylation of Fe(III)−carboxylate complexes and (2) the photo-Fenton reactions (Figure S1). DOM can bind Fe(III) into Fe(III)−carboxylate complexes ([1], Figure S1). In the first mechanism, a light-induced ligand-to-metal-charge-transfer (LMCT; [2], Figure S1) can decarboxylate the Fe(III)−carboxylate complexes and produce DIC ([3], Figure S1). In the second mechanism, photoproduced ferrous iron (Fe(II)) can reduce dioxygen (O_2) to superoxide/hydroperoxyl radicals ($HO_2^{\bullet}/O_2^{-}$; [4], Figure S1). Dismutation of $HO_2^{\bullet}/O_2^{-}$ produces hydrogen peroxide (H_2O_2), which can oxidize Fe(II) and generate hydroxyl radicals ($HO^{\bullet}$) through photo-Fenton reactions ([5] and [9], Figure S1). $HO^{\bullet}$ can oxidize DOM and produce DIC ([6], Figure S1). A single reaction between DOM and $HO^{\bullet}$ can release CO_2 ([6], Figure S1), but approximately three moles $HO^{\bullet}$ are typically needed to produce 1 mol CO_2 from DOM.[53]

Fe-stimulated DIC photoproduction benefits from acidic conditions (refs 23, 50, this study), as indicated with red circles in Figure S1: (i) acidity facilitates complexation of Fe(III) with DOM instead of formation of insoluble Fe(III)(hydr)oxides;[18] (ii) at low pH, O_2^{-} equilibrates to $HO_2^{\bullet}$;[54] (iii) acidity promotes the dismutation of $HO_2^{\bullet}/O_2^{-}$ to H_2O_2;[54] and (iv) acidity promotes the formation of $HO^{\bullet}$ instead of a weaker oxidant Fe(IV).[55] Fe-stimulated DIC photoproduction through the photochemical decarboxylation of Fe(III)−carboxylate complexes can be efficient (quantum yields up to 1 in Fe(III)-oxalate),[2] but requires re-formation of Fe(III)−carboxylate complexes that is favored by low pH. Photo-Fenton mechanisms do not necessarily require physical association between DOM and Fe, because numerous species of Fe(III),[56] simple ions ($[Fe(III)\ OH\ (H_2O)_5]^{2+}$),[27] inorganic colloids or solids,[57] or organic complexes[46,58] can efficiently yield Fe(II) and $HO^{\bullet}$. Our study cannot evaluate the relative importance of the two principal mechanisms for Fe-stimulated DIC production, but both of these mechanisms require photochemical reduction of Fe(III) and benefit from low pH.

ϕ_λs and Spectral Dependence of Fe-Stimulated DIC Photoproduction. The ϕ_{330}s determined in this study have a similar range reported earlier for freshwater, in which the magnitude of the reported ϕ_{330}s depend mostly on the optical properties of DOM but decrease with pH (Figure S7).[1,24,28,37,59,60] The pH dependence of ϕ_{330}s in freshwater (Figure S7) is possibly related to their indigenous Fe because the magnitude of ϕ_{330} depends on the interaction of pH and Fe.

In this study, the spectral slope coefficient of ϕ_λ for Fe-stimulated DIC photoproduction was lower compared to that of the corresponding slope without Fe stimulation (Figure 5). This indicates that the contribution of Fe to DIC photoproduction changes with wavelength. This phenomenon depends in part on the effect of Fe(III) on the optical properties of CDOM (a reduction of spectral slope of CDOM, Table S6)[25,26] but also suggests that Fe is photochemically active at long wavelengths.

All mechanisms for Fe-assisted DIC photoproduction (Figure S1) require the photochemical reduction of Fe(III) to Fe(II). The photoreduction of Fe(III) is involved in the $HO^{\bullet}$ production from $[Fe(III)\ OH\ (H_2O)_5]^{2+}$[27] and in the photochemical dissolution of lepidocrocite.[29] The apparent quantum yields for these reactions decrease exponentially with wavelength and have spectral slopes similar to those of Fe-stimulated DIC photoproduction (Figure S8). This similarity suggests that the apparent quantum yields for the photochemical reduction of Fe(III) to Fe(II) decreases exponentially with wavelength and determines the spectral dependence of associated reactions (e.g., the photoproduction of $HO^{\bullet}$,[27] dissolved Fe(II),[29] or DIC (this study)).

Our calculated action spectrum for Fe-stimulated DIC photoproduction at pH 4 was shifted toward the visible spectrum range compared to that for DIC photoproduction without Fe (Figure 6). Although the UV and the short-wavelength visible spectrum range dominate the calculated DIC photoproduction, Fe is almost entirely responsible for DIC photoproduction at the wavelengths >500 nm (Figure 6). Irradiation at 590−630 or 577 nm can photoreduce Fe(III) in lepidocrocite or in Fe(III)-phenolate (quantum yields approximately 10^{-4}), respectively.[29,61] These observations indicate that the light absorption by Fe in the visible spectrum range even at >500 nm can reduce Fe(III)-DOM to Fe(II) and stimulate DIC photoproduction in acidic waters.

Environmental Significance. During the past two to three decades, the export of Fe from land to inland waters has increased and enhanced the role of Fe in water color.[10,12,14,62] Since the 1980s, a reduction in sulfate deposition has raised pH[7,63] and mobilized soil-derived organic matter to aquatic systems.[64,65] This study suggests that these trends may reduce photobleaching of color (or CDOM) and DIC photoproduction in some instances because the chromophores of Fe(III) photobleach poorly and cannot efficiently mediate DIC photoproduction at pH >∼7. In naturally and anthropogenically acidic surfaces or atmospheric waters instead, Fe stimulates the photobleaching of CDOM and can enhance DIC photoproduction remarkably at wavelengths >500 nm.

MATERIALS AND METHODS

Sampling, Extraction of DOM, and Chemicals. Approximately 200 L lake water was collected from the humic Lake Kuivajärvi (0.61 km^2; DOC ≈ 12 mg L^{-1}; total nitrogen ≈ 0.4 mg L^{-1}, total phosphorus ≈ 15 μg L^{-1}; 61°50.743′N, 24°17.134′E; Finland)[30] on October 8, 2013. Water was collected into acid-washed polyethylene containers and filtered through 0.2 μm (Sartobran 300 Sterile Capsule; Sartorius Stedim, Germany) for solid phase extraction (SPE) with Bond Elut PPL cartridges (Agilent Technologies), which previously retained 76% of DOC in humic lake water.[31,32] Prior to SPE, water was acidified to pH ≈ 2 with hydrochloric acid (HCl; Merck, Germany) and equilibrated overnight with 0.01 M fluoride (NaF; Merck, Germany), which was added as a ligand to complex Fe.[4] These complexes and the unbound F^{-} passed the SPE cartridge during extraction. To evaluate the retention of Fe in the SPE-DOM, we collected water before and after SPE cartridge and preserved the water samples with super-pure nitric acid (Romil, U.K.) for Fe determination. (Total iron measurement is described in the Supporting Information.) The concentration of Fe was 3.42 ± 0.034 and 3.45 ± 0.044 μmol L^{-1} (mean ± SD) in triplicated water samples before and after the SPE cartridge, respectively. The negligible difference indicates that the SPE-DOM was free of Fe within the analytical accuracy (≤0.04 μmol L^{-1}) of determination. In agreement with this finding, the measured concentration of total Fe was 0.04 ± 0.002 μmol L^{-1} in the aqueous solutions of SPE-DOM (10 mg DOM L^{-1}) used for the experiments.

DOI: 10.1021/acsomega.7b00453
ACS Omega 2017, 2, 1905−1914

Ultrapure water (Ultra Clear UV UF TM system; Evoqua Water Technologies) was used in all experiments. The Fe solutions were prepared by dissolving iron (III) sulfate hydrate (AnalaR, VWR International Ltd., U.K.) in 0.1 M HCl. All the quartz- and glassware used in the experiments were soaked in 2% nitric acid (Merck, Germany) for >24 h, rinsed throughout with ultrapure water, and pre-combusted at 450 °C for 4 h.

Experimental Design. To examine the combined impact of pH and concentration of total iron (denoted [Fe]) on the spectral properties of CDOM, the rates of photoreactions (photobleaching, DIC photoproduction), and ϕ_λs, we generated the associations between Fe and DOM (Fe-DOM) using the same concentration of SPE-DOM (10 mg DOM L^{-1}) but different loadings of Fe on DOM at pH values ranging from 4 to 9.4 (Figure S2b, Table S2). The selected Fe loadings on DOM ranged from 0.004 (no introduced Fe) to 3.5 μmol Fe mg DOM^{-1} (the highest amount of introduced Fe; Table S2, Figure S2b). The lowest loading represented the small amount of Fe that was associated to SPE-DOM despite our attempts to isolate entirely Fe-free DOM using a Fe-complexing ligand (F^-) during the extraction. Our lowest loading was substantially smaller than the median (0.357 μmol Fe mg DOM^{-1}) found in large Swedish and Canadian lakes among 58 888 water samples examined.[1] The largest loading was representative of the upper 10% of loadings (2.0−12.8 μmol Fe mg DOM^{-1}) observed in 6128 Finnish river water samples.[33] Our lowest experimental pH (pH 4) corresponded to that found in naturally acidic boreal streams[18] or acidified atmospheric waters.[34] The highest experimental pH (pH 9.4) represented pH values found in alkaline soda lakes or even in circumneutral lakes during algal blooms.[35]

To find the optimal combinations of [Fe] and pH values across the anticipated range of loadings and pH, we selected nine combinations according to a central-composite design and replicated five of them (Figure S2, Tables S1 and S2). To highlight the effect of pH with high [Fe] and without Fe, we introduced five additional combinations from pH 4 to 9.4 and from 0.004 to 3.5 μmol Fe mg DOM^{-1}, which resulted in a total of 20 experiments (Table S2, Figure S2). The Pearson correlation coefficient between [Fe] and pH was 0.09 (p value >0.1), showing that the selected combinations of pH and [Fe] were not correlated and that pH and [Fe] were independent predictor variables in the statistical analyses.

To evaluate the changes in optical properties and to measure DIC photoproduction, the selected 20 combinations of Fe-DOM were exposed to simulated solar radiation. The optical properties were measured prior to irradiation, from the irradiated Fe-DOM and their corresponding dark controls. For the determination of ϕ_λs, the DIC photoproduction was related to the number of absorbed photons by CDOM.

Preparation of Fe-DOM. The acidic (pH ≈ 1.2) solutions for experiments were prepared as a 1:1 mixture of SPE-DOM solution and Fe(III) solution in a 500 mL gas exchange flask (see the graphical abstract) to final concentrations of 10 mg DOM L^{-1} and [Fe] between 0 and 35 μmol of the introduced Fe(III) L^{-1} (Table S2). The solutions were adjusted to pH 2 with NaOH and bubbled with CO_2-free air (2 L min^{-1}) for 30−45 min to reduce the background DIC concentration. To associate Fe(III) with DOM, the pH of solutions inside the gas exchange flasks were raised slowly with NaOH to the selected pH values (Table S2, Figure S2b). This type of titration leads to the mononuclear binding of Fe on DOM[36] or to the colloids of Fe(III)(oxy)hydroxide stabilized by DOM.[19,20] According to a chemical equilibrium modeling described in the Supporting Information, Fe(III) was bound entirely on DOM in the experiments #1−13 at ≤1.8 μmol Fe mg DOM^{-1} but in the experiments #14−20 up to 28% of Fe(III) existed as iron(oxy)hydroxides (Table S2). No visual precipitates were observed at any stage of the experiments. The absence of precipitates suggested that Fe(III)(oxy)hydroxide colloids were stabilized by DOM.[19,20] For the statistical analyses, we used the total concentration of Fe in the experiments because both Fe complexed by DOM and iron(oxy)hydrodixes affect optical properties[25,26] and can induce DIC photoproduction.[2,3]

Each Fe-DOM solution was tapped in a set of one quartz and two glass vials overflowing with a volume of the vial (∼12 mL) more than three times and sealed without headspace using ground glass stoppers. The quartz vial was exposed to simulated solar radiation (labeled "irradiated"). One glass vial was placed in an ice water bath (0 °C; "initial"). The other glass vial was wrapped in aluminum foil ("dark control") but otherwise treated identically as the quartz vial.

Simulated Solar Irradiation. Solutions in quartz vials were irradiated for 5 h (765 W m^{-2}) using an Atlas Suntest CPS+ solar simulator (Atlas Material Testing Technology), as described previously[37] and in the Supporting Information. For the irradiation at +20 °C, the quartz vials were placed on a stainless steel grid immersed in a water bath, along with the dark controls. The spectral photon flux densities (mol photons m^{-2} s^{-1} nm^{-1}) incident to the quartz vials from above and below were measured from 240 to 800 nm at 1 nm intervals with a spectroradiometer (SR991; Macam Photometrics, Scotland, U.K.). These measurements, together with characterization of downwelling and upwelling light fields, allowed us to calculate the spectral absorption of photons by CDOM in the irradiated samples, accounting for vial dimension, inner filtering effects, and CDOM photobleaching during irradiation (Supporting Information).

Analytical Measurements. After the irradiation, the DIC concentration and the spectral absorption by CDOM was measured from the irradiated, dark control, and initial samples. The DIC concentration was determined as a median of multiple (n = 3) injections into an inorganic carbon reaction vessel of a TOC analyzer (TOC-L_{CPH}; Shimadzu, Japan; detection limit 0.3 μmol C L^{-1}). The analyzer was 6-point calibrated with sodium hydrogen carbonate (Nacalai Tesque Inc., Japan) standard solutions on each measurement day. The analytical precision ranged from 0.18 to 2 μmol C L^{-1} for individual DIC determination, with a median of 0.28 μmol C L^{-1} for all determinations. The concentration of DIC was identical in the initial and dark control samples (95% confidence intervals for the difference were between −0.51 and 0.18 μmol C L^{-1}). This lack of difference indicated that all vials received initially the same DIC concentration and that any dark processes modifying the DIC concentration were negligible. DIC photoproduction was calculated as the difference in the DIC concentration between the irradiated and the corresponding dark control sample.

The spectral absorption by CDOM was measured with a UV−vis spectrophotometer (Lambda 850; PerkinElmer) in a 1 cm quartz cuvette. The apparent absorbance of CDOM and blanks (ultrapure water) was first measured from 190 to 700 nm at 1 nm steps against air (i.e., an empty reference cell holder). The absorption coefficient of CDOM at wavelength λ (a_λ; m^{-1}) was calculated from eq 1

DOI: 10.1021/acsomega.7b00453
ACS Omega 2017, 2, 1905−1914

$$a_\lambda = 2.303(A_{\text{solution},\lambda} - A_{\text{blank},\lambda})l^{-1} \quad (1)$$

where $A_{\text{solution},\lambda}$ and $A_{\text{blank},\lambda}$ are the apparent absorbance of DOM solution and blank, respectively, and l is the path length of the cuvette (m).

The CDOM spectral slope coefficients were calculated as a linear fit to ln-transformed a_λ for two spectral regions: 275−295 nm ($S_{275-295}$; nm^{-1}) and 350−400 nm ($S_{350-400}$; nm^{-1}). The slope ratio (S_R; dimensionless) was expressed as $S_R = S_{275-295}(S_{350-400})^{-1}$, according to Helms et al.[38]

The initial and its corresponding dark control samples had identical a_λ, $S_{275-295}$, $S_{350-400}$, and S_R (Tables S5, S6), indicating negligible changes in the optical properties of CDOM due to the sample treatment without the irradiation. The photochemistry-induced changes in optical properties were calculated by subtracting the values of dark controls from those of irradiated solutions.

Calculation of AQY Spectrum. The ϕ_λ (mol C mol photons^{-1} at wavelength λ) was calculated by dividing the amount of photoproduced DIC with the number of photons absorbed by CDOM in the Fe-DOM solutions during the irradiations as in Aarnos et al.[37] but now with a Monte Carlo approach (details in Supporting Information). In these calculations, it was assumed that ϕ_λ decreases exponentially with increasing wavelength.

$$\phi_\lambda = c\, e^{-d\lambda} \quad (2)$$

where c represents AQY (mol C mol photons^{-1}) at the reference wavelength (0 nm) and d is spectral slope coefficient for ϕ_λ (nm^{-1}). This assumption was adapted from the earlier determinations of ϕ_λ for DIC photoproduction (Supporting Information) and for Fe(III) photoreduction.[27,29]

Statistical Analyses. The dependencies of the optical properties of CDOM and the photochemical transformations of DOM on [Fe] and pH were explored with eight competing regression models (Supporting Information, Tables S8−S18). The models tested the explanatory power of [Fe] and pH separately, together, or through the interaction of [Fe] and pH (Tables S8−S18). For the statistical analyses, pH was expressed as the concentration of hydrogen ion ($[H^+] = 10^{-pH}$) using the same unit (mol L^{-1}) as for [Fe]. For the visualization of models in Figures 1−4, $[H^+]$ was transformed back to pH. To identify the simplest statistically significant dependence between the response and the predictor variables, we sought for the most parsimonious model among those candidate models that included only significant terms. From those models, the best one was selected on the basis of the corrected Akaike Information Criterion (AICc)[39,40] to provide the simplest significant dependence of the optical properties or photochemical transformation of DOM on pH and [Fe]. Statistical analyses were performed using MATLAB R2013a (The MathWorks Inc.) and R (version 3.3.3, R Core Team 2017).

■ ASSOCIATED CONTENT

Supporting Information

The Supporting Information is available free of charge on the ACS Publications website at DOI: 10.1021/acsomega.7b00453.

Scheme for the major reactions involved in the Fe-stimulated DIC photoproduction; the method for the determination of Fe; details of the experimental design; the speciation of Fe(III) in the experiments; details of the method for the determination of ϕ_λ and the uncertainty estimates for ϕ_λs; the data for the optical properties, the DICprs and ϕ_λs from the individual experiments; the regression analyses with the competing models; three figures supporting the discussion; and accompanying references (PDF)

■ AUTHOR INFORMATION

Corresponding Author

*E-mail: yufei.y.gu@jyu.fi. Tel: +358 40 480 2691.

ORCID

Yufei Gu: 0000-0002-6606-2592

Notes

The authors declare no competing financial interest.

■ ACKNOWLEDGMENTS

This study was funded by the University of Jyväskylä and Academy of Finland Centre of Excellence (grant 272041). We thank Jaana Bäck for financial support, Derek K. Ho for linguistic corrections, Veli-Mikko S. Puupponen for technique support concerning AQY fitting, Ari Väisänen for advice on iron determination, and Yihua Xiao for help in sampling and preparation.

■ REFERENCES

(1) Koehler, B.; Landelius, T.; Weyhenmeyer, G. A.; Machida, N.; Tranvik, L. J. Sunlight-induced carbon dioxide emissions from inland waters. *Global Biogeochem. Cycles* **2014**, *28*, 696−711.

(2) Faust, B. C.; Zepp, R. G. Photochemistry of aqueous iron(III)-polycarboxylate complexes: roles in the chemistry of atmospheric and surface waters. *Environ. Sci. Technol.* **1993**, *27*, 2517−2522.

(3) Voelker, B. M.; Morel, F. M. M.; Sulzberger, B. Iron redox cycling in surface waters: effects of humic substances and light. *Environ. Sci. Technol.* **1997**, *31*, 1004−1011.

(4) Gao, H.; Zepp, R. G. Factors influencing photoreactions of dissolved organic matter in a coastal river of the southeastern United States. *Environ. Sci. Technol.* **1998**, *32*, 2940−2946.

(5) Wu, F. C.; Mills, R. B.; Cai, Y. R.; Evans, R. D.; Dillon, P. J. Photodegradation-induced changes in dissolved organic matter in acidic waters. *Can. J. Fish. Aquat. Sci.* **2005**, *62*, 1019−1027.

(6) Helms, J. R.; Mao, J.; Schmidt-Rohr, K.; Abdulla, H.; Mopper, K. Photochemical flocculation of terrestrial dissolved organic matter and iron. *Geochim. Cosmochim. Acta* **2013**, *121*, 398−413.

(7) Vuorenmaa, J.; Forsius, M.; Mannio, J. Increasing trends of total organic carbon concentrations in small forest lakes in Finland from 1987 to 2003. *Sci. Total Environ.* **2006**, *365*, 47−65.

(8) Monteith, D. T.; Stoddard, J. L.; Evans, C. D.; de Wit, H. A.; Forsius, M.; Hogasen, T.; Wilander, A.; Skjelkvale, B. L.; Jeffries, D. S.; Vuorenmaa, J.; Keller, B.; Kopacek, J.; Vesely, J. Dissolved organic carbon trends resulting from changes in atmospheric deposition chemistry. *Nature* **2007**, *450*, 537−540.

(9) Keller, W.; Paterson, A. M.; Somers, K. M.; Dillon, P. J.; Heneberry, J.; Ford, A. Relationships between dissolved organic carbon concentrations, weather, and acidification in small Boreal Shield lakes. *Can. J. Fish. Aquat. Sci.* **2008**, *65*, 786−795.

(10) Neal, C.; Lofts, S.; Evans, C. D.; Reynolds, B.; Tipping, E.; Neal, M. Increasing iron concentrations in UK upland waters. *Aquat. Geochem.* **2008**, *14*, 263−288.

(11) Haaland, S.; Hongve, D.; Laudon, H.; Riise, G.; Vogt, R. D. Quantifying the drivers of the increasing colored organic matter in boreal surface waters. *Environ. Sci. Technol.* **2010**, *44*, 2975−2980.

(12) Kritzberg, E. S.; Ekström, S. M. Increasing iron concentrations in surface waters − a factor behind brownification? *Biogeosciences* **2012**, *9*, 1465−1478.

(13) Oni, S. K.; Futter, M. N.; Bishop, K.; Köhler, S. J.; Ottosson-Löfvenius, M.; Laudon, H. Long-term patterns in dissolved organic

DOI: 10.1021/acsomega.7b00453
ACS Omega 2017, 2, 1905−1914

carbon, major elements and trace metals in boreal headwater catchments: trends, mechanisms and heterogeneity. *Biogeosciences* **2013**, *10*, 2315−2330.
(14) Kritzberg, E. S.; Villanueva, A. B.; Jung, M.; Reader, H. E. Importance of boreal rivers in providing iron to marine waters. *PLoS One* **2014**, *9*, No. e107500.
(15) Gustafsson, C.; Gschwend, P. M. Aquatic colloids: Concepts, definitions, and current challenges. *Limnol. Oceanogr.* **1997**, *42*, 519−528.
(16) Gustafsson, Ö.; Widerlund, A.; Andersson, P. S.; Ingri, J.; Roos, P.; Ledin, A. Colloid dynamics and transport of major elements through a boreal river — brackish bay mixing zone. *Mar. Chem.* **2000**, *71*, 1−21.
(17) Ingri, J.; Widerlund, A.; Land, M.; Gustafsson, Ö.; Andersson, P.; Öhlander, B. Temporal variations in the fractionation of the rare earth elements in a boreal river; the role of colloidal particles. *Chem. Geol.* **2000**, *166*, 23−45.
(18) Neubauer, E.; Köhler, S. J.; von der Kammer, F.; Laudon, H.; Hofmann, T. Effect of pH and stream order on iron and arsenic speciation in boreal catchments. *Environ. Sci. Technol.* **2013**, *47*, 7120−7128.
(19) Chen, K.-Y.; Chen, T.-Y.; Chan, Y.-T.; Cheng, C.-Y.; Tzou, Y.-M.; Liu, Y.-T.; Teah, H.-Y. Stabilization of natural organic matter by short-range-order iron hydroxides. *Environ. Sci. Technol.* **2016**, *50*, 12612−12620.
(20) Philippe, A.; Schaumann, G. E. Interactions of dissolved organic matter with natural and engineered inorganic colloids: a review. *Environ. Sci. Technol.* **2014**, *48*, 8946−8962.
(21) Bertilsson, S.; Tranvik, L. J. Photochemical transformation of dissolved organic matter in lakes. *Limnol. Oceanogr.* **2000**, *45*, 753−762.
(22) Anesio, A. M.; Granéli, W. Increased photoreactivity of DOC by acidification: Implications for the carbon cycle in humic lakes. *Limnol. Oceanogr.* **2003**, *48*, 735−744.
(23) Porcal, P.; Dillon, P. J.; Molot, L. A. Interaction of extrinsic chemical factors affecting photodegradation of dissolved organic matter in aquatic ecosystems. *Photochem. Photobiol. Sci.* **2014**, *13*, 799−812.
(24) Koehler, B.; Broman, E.; Tranvik, L. J. Apparent quantum yield of photochemical dissolved organic carbon mineralization in lakes. *Limnol. Oceanogr.* **2016**, *61*, 2207−2221.
(25) Xiao, Y.; Sara-Aho, T.; Hartikainen, H.; Vähätalo, A. V. Contribution of ferric iron to light absorption by chromophoric dissolved organic matter. *Limnol. Oceanogr.* **2013**, *58*, 653−662.
(26) Poulin, B. A.; Ryan, J. N.; Aiken, G. R. Effects of iron on optical properties of dissolved organic matter. *Environ. Sci. Technol.* **2014**, *48*, 10098−10106.
(27) Benkelberg, H.; Warneck, P. Photodecomposition of iron (III) hydroxo and sulfato complexes in aqueous solution: wavelength dependence of OH and SO_4^- quantum yields. *J. Phys. Chem.* **1995**, *99*, 5214−5221.
(28) Vähätalo, A. V.; Salkinoja-Salonen, M.; Taalas, P.; Salonen, K. Spectrum of the quantum yield for photochemical mineralization of dissolved organic carbon in a humic lake. *Limnol. Oceanogr.* **2000**, *45*, 664−676.
(29) Borer, P.; Sulzberger, B.; Hug, S. J.; Kraemer, S. M.; Kretzschmar, R. Wavelength-dependence of photoreductive dissolution of lepidocrocite (γ-FeOOH) in the absence and presence of the siderophore DFOB. *Environ. Sci. Technol.* **2009**, *43*, 1871−1876.
(30) Miettinen, H.; Pumpanen, J.; Heiskanen, J. J.; Aaltonen, H.; Mammarella, I.; Ojala, A.; Levula, J.; Rantakari, M. M. Towards a more comprehensive understanding of lacustrine greenhouse gas dynamics - two -year measurements of concentrations and fluxes of CO_2, CH_4 and N_2O in a typical boreal lake surrounded by managed forests. *Boreal Environ. Res.* **2015**, *20*, 75−89.
(31) Dittmar, T.; Koch, B.; Hertkorn, N.; Kattner, G. A simple and efficient method for the solid-phase extraction of dissolved organic matter (SPE-DOM) from seawater. *Limnol. Oceanogr.: Methods* **2008**, *6*, 230−235.
(32) Xiao, Y.; Hoikkala, L.; Kasurinen, V.; Tiirola, M.; Kortelainen, P.; Vähätalo, A. V. The effect of iron on the biodegradation of natural dissolved organic matter. *J. Geophys. Res.: Biogeosci.* **2016**, *121*, 2544−2561.
(33) Xiao, Y.-H.; Räike, A.; Hartikainen, H.; Vähätalo, A. V. Iron as a source of color in river waters. *Sci. Total Environ.* **2015**, *536*, 914−923.
(34) Amato, P.; Ménager, M.; Sancelme, M.; Laj, P.; Mailhot, G.; Delort, A. Microbial population in cloud water at the Puy de Dôme: Implications for the chemistry of clouds. *Atmos. Environ.* **2005**, *39*, 4143−4153.
(35) López-Archilla, A. I.; Moreira, D.; López-García, P.; Guerrero, C. Phytoplankton diversity and cyanobacterial dominance in a hypereutrophic shallow lake with biologically produced alkaline pH. *Extremophiles* **2004**, *8*, 109−115.
(36) Karlsson, T.; Persson, P. Complexes with aquatic organic matter suppress hydrolysis and precipitation of Fe(III). *Chem. Geol.* **2012**, *322*−323, 19−27.
(37) Aarnos, H.; Ylöstalo, P.; Vähätalo, A. V. Seasonal photo-transformation of dissolved organic matter to ammonium, dissolved inorganic carbon, and labile substrates supporting bacterial biomass across the Baltic Sea. *J. Geophys. Res.: Biogeosci.* **2012**, *117* 10.1029/2010JG001633.
(38) Helms, J. R.; Stubbins, A.; Ritchie, J. D.; Minor, E. C.; Kieber, D. J.; Mopper, K. Absorption spectral slopes and slope ratios as indicators of molecular weight, source, and photobleaching of chromophoric dissolved organic matter. *Limnol. Oceanogr.* **2008**, *53*, 955−969.
(39) Anderson, D. R.; Burnham, K. P.; White, G. C. AIC model selection in overdispersed capture-recapture data. *Ecology* **1994**, *75*, 1780−1793.
(40) Burnham, K. P.; Anderson, D. R. Multimodel inference: understanding AIC and BIC in model selection. *Sociol. Methods Res.* **2004**, *33*, 261−304.
(41) Kiehl, J. T.; Trenberth, K. E. Earth's annual global mean energy budget. *Bull. Am. Meteorol. Soc.* **1997**, *78*, 197−208.
(42) Weishaar, J. L.; Aiken, G. R.; Bergamaschi, B. A.; Fram, M. S.; Fujii, R.; Mopper, K. Evaluation of specific ultraviolet absorbance as an indicator of the chemical composition and reactivity of dissolved organic carbon. *Environ. Sci. Technol.* **2003**, *37*, 4702−4708.
(43) Baes, A. U.; Bloom, P. R. Fulvic acid ultraviolet-visible spectra: influence of solvent and pH. *Soil Sci. Soc. Am. J.* **1990**, *54*, 1248−1254.
(44) Porcal, P.; Dillon, P. J.; Molot, L. A. Seasonal changes in photochemical properties of dissolved organic matter in small boreal streams. *Biogeosciences* **2013**, *10*, 5533−5543.
(45) Collienne, R. H. Photoreduction of iron in the epilimnion of acidic lakes. *Limnol. Oceanogr.* **1983**, *28*, 83−100.
(46) Southworth, B. A.; Voelker, B. M. Hydroxyl radical production via the photo-Fenton reaction in the presence of fulvic acid. *Environ. Sci. Technol.* **2003**, *37*, 1130−1136.
(47) White, E. M.; Vaughan, P. P.; Zepp, R. G. Role of the photo-Fenton reaction in the production of hydroxyl radicals and photobleaching of colored dissolved organic matter in a coastal river of the southeastern United States. *Aquat. Sci.* **2003**, *65*, 402−414.
(48) Molot, L.; Hudson, J.; Dillon, P.; Miller, S. Effect of pH on photo-oxidation of dissolved organic carbon by hydroxyl radicals in a coloured, softwater stream. *Aquat. Sci.* **2005**, *67*, 189−195.
(49) Cornell, R. M.; Schwertmann, U. *The Iron Oxides: Structure, Properties, Reactions, Occurrences and Uses*; John Wiley & Sons, 2003.
(50) Anesio, A. M.; Granéli, W. Photochemical mineralization of dissolved organic carbon in lakes of differing pH and humic content. *Arch. Hydrobiol.* **2004**, *160*, 105−116.
(51) Soumis, N.; Lucotte, M.; Larose, C.; Veillette, F.; Canuel, R. Photomineralization in a boreal hydroelectric reservoir: a comparison with natural aquatic ecosystems. *Biogeochemistry* **2007**, *86*, 123−135.
(52) Miles, C. J.; Brezonik, P. L. Oxygen consumption in humic-colored waters by a photochemical ferrous-ferric catalytic cycle. *Environ. Sci. Technol.* **1981**, *15*, 1089−1095.
(53) Goldstone, J. V.; Pullin, M. J.; Bertilsson, S.; Voelker, B. M. Reactions of hydroxyl radical with humic substances: bleaching,

DOI: 10.1021/acsomega.7b00453
ACS Omega 2017, 2, 1905−1914

mineralization, and production of bioavailable carbon substrates. *Environ. Sci. Technol.* **2002**, *36*, 364−372.
(54) Bielski, B. H. J.; Cabelli, D. E.; Arudi, R. L.; Ross, A. B. Reactivity of HO_2/O^-_2 radicals in aqueous solution. *J Phys. Chem. Ref. Data* **1985**, *14*, 1041−1100.
(55) Hug, S. J.; Leupin, O. Iron-catalyzed oxidation of arsenic(III) by oxygen and by hydrogen peroxide: pH-dependent formation of oxidants in the Fenton reaction. *Environ. Sci. Technol.* **2003**, *37*, 2734−2742.
(56) Mcknight, D. M.; Kimball, B. A.; Bencala, K. E. Iron photoreduction and oxidation in an acidic mountain stream. *Science* **1988**, *240*, 637−640.
(57) Vermilyea, A. W.; Voelker, B. M. Photo-Fenton reaction at near neutral pH. *Environ. Sci. Technol.* **2009**, *43*, 6927−6933.
(58) Zepp, R. G.; Faust, B. C.; Hoigne, J. Hydroxyl radical formation in aqueous reactions (pH 3−8) of iron(II) with hydrogen peroxide: the photo-Fenton reaction. *Environ. Sci. Technol.* **1992**, *26*, 313−319.
(59) Vähätalo, A. V.; Wetzel, R. G. Photochemical and microbial decomposition of chromophoric dissolved organic matter during long (months−years) exposures. *Mar. Chem.* **2004**, *89*, 313−326.
(60) Groeneveld, M.; Tranvik, L.; Natchimuthu, S.; Koehler, B. Photochemical mineralisation in a boreal brown water lake: considerable temporal variability and minor contribution to carbon dioxide production. *Biogeosciences* **2016**, *13*, 3931−3943.
(61) Kunkely, H.; Vogler, A. Photoredox reactivity of iron (III) phenolates in aqueous solution induced by ligand-to-metal charge transfer excitation. *Inorg. Chem. Commun.* **2003**, *6*, 1335−1337.
(62) Knorr, K.-H. DOC-dynamics in a small headwater catchment as driven by redox fluctuations and hydrological flow paths – are DOC exports mediated by iron reduction/oxidation cycles? *Biogeosciences* **2013**, *10*, 891−904.
(63) Battarbee, R. W.; Shilland, E. M.; Kernan, M.; Monteith, D. T.; Curtis, C. J. Recovery of acidified surface waters from acidification in the United Kingdom after twenty years of chemical and biological monitoring (1988−2008). *Ecol. Indic.* **2014**, *37*, 267−273.
(64) Evans, C. D.; Monteith, D. T.; Cooper, D. M. Long-term increases in surface water dissolved organic carbon: Observations, possible causes and environmental impacts. *Environ. Pollut.* **2005**, *137*, 55−71.
(65) Ekström, S. M.; Sandahl, M.; Nilsson, P. A.; Kleja, D. B.; Kritzberg, E. S. Reactivity of dissolved organic matter in response to acid deposition. *Aquat. Sci.* **2016**, *78*, 463−475.

DOI: 10.1021/acsomega.7b00453
ACS Omega 2017, 2, 1905−1914

SUPPORTING INFORMATION

Iron and pH regulating the photochemical mineralization of dissolved organic carbon

Yufei Gu,[*,†] Anssi Lensu,[†] Siiri Perämäki,[‡] Anne Ojala,[§∓] Anssi V. Vähätalo[†]

[†] University of Jyväskylä, Department of Biological and Environmental Science, P.O. Box 35, FI-40014 University of Jyväskylä, Finland

[‡] University of Jyväskylä, Department of Chemistry, P.O. Box 35, FI-40014 University of Jyväskylä, Finland

[§] University of Helsinki, Department of Forest Sciences, P.O. Box 27, FI-00014 University of Helsinki, Finland

[∓] University of Helsinki, Department of Environmental Sciences, P.O. Box 65, FI-00014 University of Helsinki, Finland

* Corresponding author: Yufei Gu. E-mail: yufei.y.gu@jyu.fi. Tel: +358 40 480 2691.

CONTENTS

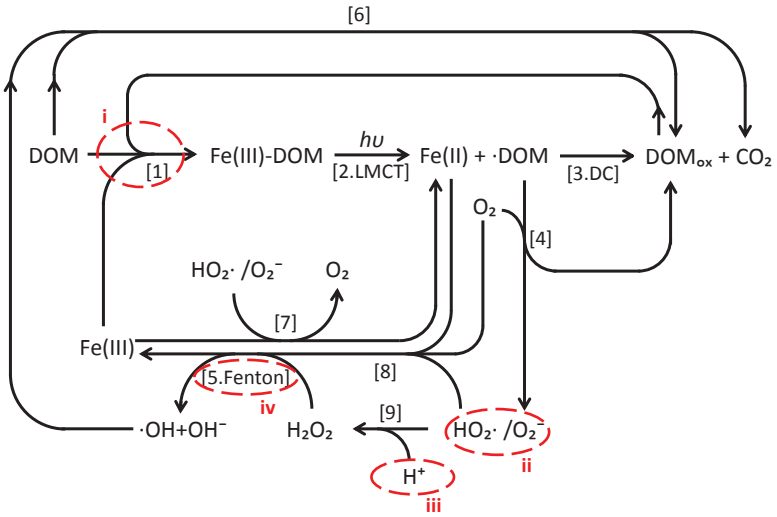

Figure S1. Conceptual scheme of the major reactions involved in DIC photoproduction of Fe-DOM associates. [1] Complexation of Fe(III) and DOM; [2] ligand-to-metal charge transfer (LMCT); [3] decarboxylation of Fe(III)-polycarboxylate complexes; [4] reduction of O_2 by Fe(II) or DOM radicals; [5] Fenton-like reactions; [6] DOM oxidation by HO·; [7] Fe(III) reduction by $HO_2\cdot/O_2^-$; [8] Fe(II) oxidation by O_2 and $HO_2\cdot/O_2^-$; [9] dismutation of $HO_2\cdot/O_2^-$; [10] Fe(III) precipitation. Red circles show the reactions that stimulate DIC photoproduction under acidic conditions: the formation of Fe(III)-DOM (i) and the reactions related to photo-Fenton reaction (ii–iv). Modified from Faust et al. 1993 and Voelker et al. 1997.[1, 2]

Total iron measurement

Total iron concentration ([Fe]) was determined using an inductively coupled plasma optical emission spectrometer (ICP-OES) Optima 8300 with an S10 autosampler (PerkinElmer, USA). Prior to analysis, the sample was acidified to contain 0.5% nitric acid. The acidified sample was introduced with a flow rate of 1.5 mL min^{-1} into a GemCone Low-Flow nebulizer, operating at nebulizer gas flow rate of 0.6 L min^{-1}. A glass cyclonic spray chamber was used. The auxiliary gas flow rate was 0.2 L min^{-1}, plasma gas flow rate 8 L min^{-1}, and plasma power 1500 W. Fe was determined using axial viewing of the plasma at emission wavelength 238.204 nm, with the detection limit of 2.0 µg L^{-1}. Four-point calibration up to 2.0 mg L^{-1} was used throughout, for which the calibration standards were diluted from a standard stock solution containing 1000 mg L^{-1} Fe (Pure Grade, PerkinElmer, United States).

Experimental design

Central-composite design (CCD) was used to choose most of the combinations of pH and [Fe] for the experiment (Table S1, Figure S2a). CCD is one of the techniques developed within Response Surface Methodology (RSM). It is widely used in optimization for photocatalysis of organic chemicals.[3-5] CCD was used to identify optimal combinations of [Fe] and pH in experiments, in order to describe the dependency of DOM photoreactivity across the range of environmental variability by a nonlinear approximation. The function `ccd.pick` was used to choose preliminary [Fe]-pH pairs in a fractional factorial design done with rsm package[6] in R (version 3.3.3, R Core Team 2017),[6] with coded levels −1.41, −1, 0, 1, and 1.41 (Table S1, Figure S2a). Five points close to (pH, [Fe]) combinations (6, 0), (4, 18), (6, 18), (8, 18), and (4, 30) were replicated to estimate the variance of responses (Figure S2b). To examine the effect of pH without any introduced Fe and with high [Fe], additional combinations were added into the pH-[Fe] space (Figure S2b). Altogether, the experiments consisted of 20 solutions as combinations of pH and [Fe] (Table S2).

Table S1. Experimental design with CCD for initial photomineralization using isolated DOM.

Experiment	pH		[Fe]	
	Value	code level	Value (μmol L^{-1})	code level
1	4.59	−1	5	−1
2	7.41	1	5	−1
3	7.41	1	30	1
4	4.59	−1	30	1
5	6.00	0	18	0
6	6.00	0	18	0
7	6.00	0	35	1.41
8	7.99	1.41	18	0
9	4.01	−1.41	18	0
10	6.00	0	0	−1.41

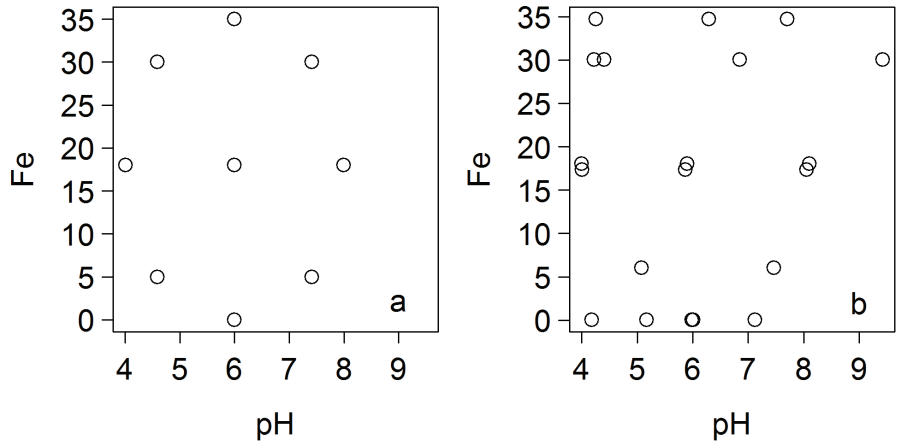

Figure S2. Values of controllable variables for the experiments. (a) pH and [Fe] combinations suggested by central-composite design. (b) Actual pH and [Fe] values used in the experiments (Table S2).

Speciation of Fe(III) in the experimental associations between Fe(III) and DOM

Although Fe can exist in numerous inorganic complexes and mineral species, in freshwater with typical pH ranges (pH 4–9) ferric iron frequently associates with DOM as true dissolved complexes and as colloids stabilized by DOM.[7-11] The aim of our experiments was to simulate these associations of Fe with DOM, which are collectively denoted Fe-DOM without any precise reference for the speciation of Fe. Similar to Karlsson and Persson,[12] our Fe-DOM was prepared by titrating an acidic solution of ferric iron and DOM with sodium hydroxide. During the titration, the binding sites of DOM will suppress the hydrolysis of ferric iron and bind the ferric iron cations into mononuclear complexes of DOM.[12] If the concentration of ferric iron exceeds the concentration of binding sites in DOM, DOM directs the speciation of Fe(III) towards poorly crystalline mineral species such as ferrihydrate.[11] DOM stabilizes ferrihydrate into colloidal forms that resist gravitoidal settling.[7, 13] In freshwaters, a large fraction of Fe(III) exists in colloids.[8-10]

The speciation of ferric iron in the experimental treatments was estimated with chemical equilibrium modeling (Visual Minteq, version 3.1) into the concentrations in dissolved inorganic forms, bound on DOM, and iron(oxy)hydroxide. Similar to Neubauer et al.,[10] Fe was entered to the model as Fe(III) and was allowed to precipitate when its concentration exceeded the solubility product of ferrihydrite ($Fe(OH)_3$, log Ks of 3.2). DOM was described as the NICA-Donnan model at 20 °C.[14] According to the modeling, Fe was entirely bound on DOM in the experiments #1–13 (Table S2). In experiments #14–20, with the highest concentrations of Fe, the majority of Fe (≥72%) was bound by DOM, but up to 28% was bound on ferrihydrate (Table S2). Visual precipitates were absent in all phases of experiments, including those with the highest concentrations of Fe, which indicated that ferrihydrate existed as colloidal forms stabilized by DOM.[13]

Table S2. The pH and Fe concentration in total, dissolved inorganic, bound to DOM, and ferrihydrate forms across the 20 experiments calculated based on a chemical equilibrium modeling (Visual Minteq 3.1). The concentration of SPE-DOM extracted from Lake Kuivajärvi was 10 mg DOM L^{-1} in all experiments.

Expr.	pH	Distribution of Fe (μmol L^{-1})				Distribution of Fe (%)		
		total	dissolved inorganic	bound to DOM	ferrihydrate	dissolved inorganic	bound to DOM	ferrihydrate
1	4.18	0.04	0.00	0.04	0.00	0.00	100.00	0.00
2	5.17	0.04	0.00	0.04	0.00	0.00	100.00	0.00
3	5.98	0.04	0.00	0.04	0.00	0.00	100.00	0.00
4	6.01	0.04	0.00	0.04	0.00	0.00	100.00	0.00
5	7.12	0.04	0.00	0.04	0.00	0.00	100.00	0.00
6	5.08	6.04	0.00	6.04	0.00	0.00	100.00	0.00
7	7.46	6.04	0.00	6.04	0.00	0.00	100.00	0.00
8	4.01	17.37	0.01	17.36	0.00	0.05	99.95	0.00
9	5.87	17.37	0.00	17.37	0.00	0.00	100.00	0.00
10	8.05	17.37	0.00	17.37	0.00	0.00	100.00	0.00
11	4	18.04	0.01	18.03	0.00	0.07	99.93	0.00
12	5.9	18.04	0.00	18.04	0.00	0.00	100.00	0.00
13	8.1	18.04	0.00	18.04	0.00	0.00	100.00	0.00
14	4.22	30.04	0.36	25.07	4.60	1.21	83.47	15.32
15	4.41	30.04	0.21	25.01	4.82	0.70	83.25	16.04
16	6.85	30.04	0.00	24.87	5.17	0.00	82.79	17.21
17	9.42	30.04	0.00	24.94	5.10	0.00	83.02	16.98
18	4.26	34.71	0.32	25.13	9.25	0.93	72.41	26.66
19	6.29	34.71	0.00	24.97	9.73	0.01	71.95	28.04
20	7.7	34.71	0.00	24.97	9.74	0.00	71.95	28.05

AQY determination

Overview on the determination of AQYs for DIC photoproduction

Apparent quantum yields (AQY) relate the rate of photoreaction to the rate of photons absorbed by the sample. Traditionally and prior to the year 2000, AQY determinations have been performed by irradiating the samples with monochromatic irradiation (often created as narrow spectral bands separated from polychromatic source of irradiation) and quantifying the photon fluxes with e.g., actinometers.[16, 17] The monochromatic AQY demonstrated that AQYs for DIC photoproduction decrease exponentially with wavelength.[16, 17] The same exponential decrease in AQY also applies to the photochemical reduction of ferric iron when measured as a photoproduction of hydroxyl radicals from $Fe(III)OH^{2+}$ and photoreductive dissolution of lepidocrocite irradiated with narrow spectral bands.[18, 19] The determination of AQY with separate narrow bands of irradiation is a relatively simple and well-established technique, but it has also some limitations. If one wishes to estimate the environmental rates of photoreactions based on monochromatic AQYs, one needs to carry out several separate determinations of monochromatic AQY across the photochemically active range of solar radiation. Monochromatic irradiation cannot reproduce potential interactions among different spectral regions, which can be present e.g., in polychromatic solar irradiance.[20]

Since the publication of Vähätalo et al. 2000,[17] the photochemical reactivity of DOM has also been described as spectral AQY (Table S3). The apparent quantum yield spectrum for a photoreaction (ϕ_λ) is a convenient and powerful modeling parameter for the prediction of environmental photoreaction rates as demonstrated in this study (e.g., Figure 6). The determinations of ϕ_λ for DIC photoproduction have been carried out with two types of methods: 1) a "Vähätalo"-method[7] and 2) a "cut-off filter" method (Johannessen and Miller 2001; Table S3).[21] In the Vähätalo-method, samples are irradiated once with full polychromatic irradiation, the equation for ϕ_λ is defined *a priori*, and the values of parameters for ϕ_λ are iterated. In the "cut-off filter"-method, several aliquots of sample are irradiated with polychromatic irradiation modified by 5–8 cut-off filters and a statistical fit determines the values of parameters for ϕ_λ.[20]

In the "cut-off filter" method, a statistical fit can evaluate how well the mathematical equations used to describe ϕ_λ explain the rates of DIC photoproduction under separate cut-off filters (called "Internal validation of ϕ_λ" in Table S3). In nearly all cases, the expression for ϕ_λ has been:

$$\phi_\lambda = e^{(-m1 + m2(\lambda - 290))} \quad \text{(S1)}$$

where 290 is wavelength (nm), and *m1* and *m2* are fitting parameters (Table S3). Only once has a small difference (R^2 0.98 ± 0.02 vs. 0.99 ± 0.01) in *a posteriori* statistics suggested another slightly modified formulation for ϕ_λ (Bélanger et al. 2006, Table S3).[8] In the "Vähätalo" method, *a priori* formulation of ϕ_λ has been:

$$\phi_\lambda = c\, e^{(-d\,\lambda)} \quad \text{(S2)}$$

where *c* and *d* are fitting parameters (Table S3). The eq. S1 and S2 can both be re-formulated into the same simple exponential equation:

$$\phi_\lambda = \phi_{\lambda ref}\, e^{-S(\lambda - \lambda ref)} \quad \text{(S3)}$$

where the pre-exponential parameter ($\phi_{\lambda ref}$) refers to the apparent quantum yield (mol C mol photons^{-1}) at the reference wavelength λ, *S* is the spectral slope coefficient of AQY (nm^{-1}), and λref is the reference wavelength (nm). The eq. S2 can be converted to eq. S3 by noticing that $\lambda ref = 0$ nm, $\phi_{\lambda ref} = \phi_0 = c$, and $S = d$. Correspondingly, eq. S1 can be expressed as eq. S3 when $\lambda ref = 290$ nm, $\phi_{\lambda ref} = \phi_{290} = e^{-m1}$, and $S = -m2$.

In the "cut-off filter" method, the internal validation of ϕ_λ with *a posteriori* statistic is a valuable feature for photochemical reactions with unknown spectral dependence of AQY. Earlier studies that

have determined the ϕ_λ for DIC photoproduction with the "cut-off filter" method have nearly always selected a simple exponential equation to describe ϕ_λ (Table S3). Therefore, *a priori* selection of ϕ_λ for DIC photoproduction in the "Vähätalo" method (eq. S2) is supported by both monochromatic AQYs[16, 17] and the ϕ_λ values derived through "cut-off filter" method.[21-26]

The external validation of ϕ_λ for DIC photoproduction has been conducted for both polychromatic methods through *in situ* experiments (Table S3).[17, 24, 25, 27] In these validations, the DIC photoproduction predicted with ϕ_λ was compared to those measured in lakes; good matches were found for both methods.[17, 24, 25, 27] In the case of the "Vähätalo" method, ϕ_λ for DIC photoproduction agreed with the determinations done with monochromatic irradiation at a few separate wavelengths.[17] Thus, the external validations suggest that both methods describe DIC photoproduction well in surface waters[17, 24, 25, 27] and that, at least, the "Vähätalo" method provides AQYs comparable with the monochromatic method.[17]

The methods for the determination of AQYs face analytical challenges differently (Table S3). In the "Vähätalo" method, samples receive the full spectrum of polychromatic irradiance, which yields the maximal rate of DIC photoproduction with the available source of irradiation. This feature of the "Vähätalo" method has several benefits. The rates of DIC photoproduction can be detected with the highest possible accuracy, with the shortest irradiation times, and with the lowest interference of unwanted dark abiotic or biotic reactions. In the other methods, only a fraction of polychromatic irradiance passes monochromators and cut-off filters. In less-intense irradiation, the rates of photoreactions are low and their detection becomes challenging particularly in the visible spectrum range, where both the absorption by CDOM and AQY decrease to negligible. Thus, the "Vähätalo" method is more robust than the "cut-off filter" method. For one ϕ_λ, the "cut-off filter" method requires five to eight determinations of DIC from the irradiated samples, while only one is needed for the "Vähätalo" method. Thus, the "Vähätalo" method requires the least amount of analytic determinations.

Table S3. Comparison of features among the methods used for the determinations of AQYs for DIC photoproduction.

Feature	Method		
	Monochromatic[a]	Vähätalo[b]	Cut-off[c]
Irradiation	Monochromatic	Polychromatic	Polychromatic
Filters	Monochromator	None	Cut-off filters
Calculation of AQY	A ratio	Iteration	Statistical fit
Spectral description	No	$\phi_\lambda = c\ e^{(-d\,\lambda)}$	$\phi_\lambda = e^{(-m1\,+\,m2(\lambda-290))}$ $\phi_\lambda = k1\ e^{k2\,/(\lambda+k3))}$ [d] $\phi_\lambda = e^{-\,(m1+m2(\lambda-m3))}$ [e]
Internal validation of ϕ_λ		No	Yes[g]
External validation with:			
monochromatic AQY		Done[h]	
in situ experiments		Done[i]	Done[j,k]
n for one ϕ_λ [l]		1	5–8
Analytical challenges [m]	low–high	Low	low–high
References[16, 17, 21-32]	[a]Gao and Zepp 1998; [a]Vähätalo et al. 2000.	[b,h]Vähätalo et al. 2000; [b]Vähätalo and Wetzel 2004; [b,i]Aarnos et al. 2012; [b]Cory et al. 2014; [b]Vachon et al. 2016.	[c]Johannessen and Miller 2001 (n = 6); [c,d]Bélanger et al. 2006 (n = 8); [c]White et al. 2010 (n = 8); [c,e]Reader and Miller 2012 (n = 7), equation for ϕ_λ defined *a priori*; [c,j]Koehler et al. 2014 (n = 5); [c]Powers and Miller 2015 (n = 7); [c,k]Groeneveld et al. 2016 (n = 7); [c]Koehler et al. 2016 (n = 6).

[g]A possibility to evaluate the mathematical formulation of ϕ_λ with statistical fit from the data collected during each determination of AQY. [l]The number of irradiated aliquots required for one ϕ_λ. The n = 5–8 refers to the number of cut-off filters used, which is detailed separately for each publication. [m]Analytical challenges are low when the sample receives intense simulated solar radiation or monochromatic radiation at shortest wavelengths (e.g. ≈300 nm) and the rate of DIC photoproduction is high. The rates of DIC photoproduction are low and difficult to detect at the long wavelengths of monochromatic irradiation or when the ultraviolet radiation has been cut off with filters.

Compared to the monochromatic determination of AQY, both the "cut-off filter" and "Vähätalo" methods include numerous technical details for obtaining the primary data and for computing the values of the parameters that describe ϕ_λ. In the following sections, we describe the details of "Vähätalo" method used in the present study.

Details of irradiation experiments

Experimental irradiations and irradiation measurements were performed in a water bath (Figures S3,S4). The bath replaced a metal plate at the bottom of irradiation chamber of Suntest CPS+. The stainless steel water bath received cooling water from a thermostat (Lauda RE 112, Germany). The water bath contained a stainless steel grid, which held 12 cylindrical quartz-glass vials (with an inner diameter of 13.4 mm) located 57 mm below the surface of cooling water during irradiations. The quartz-glass vials were irradiated close to the center of irradiation chamber (Figures S3–S4). The cooling water prevented light focusing into the irradiated samples[17] and enabled controlling of irradiation temperature. Dark controls were wrapped into aluminum foil and kept on the bottom of water bath during irradiations to ensure that their temperature was identical to irradiated samples (Figures S3,S4).

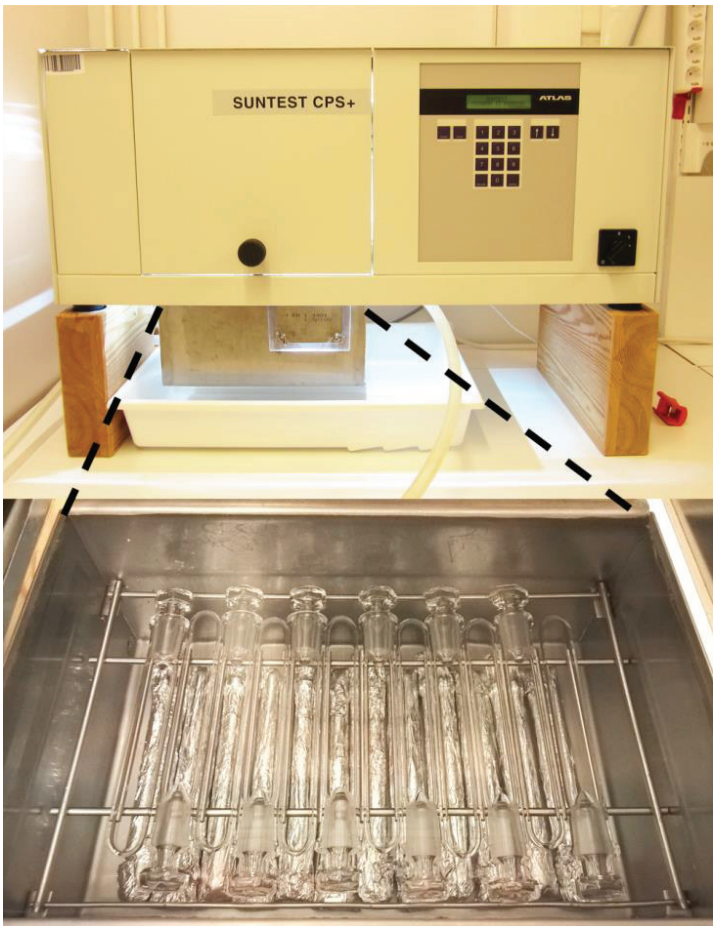

Figure S3.The upper photo shows Suntest CPS+ in operation. The water bath received cooling water from the tubing visible on the left and circulated cooling water to a thermostat from the tubing visible on the right. The lower photo shows the water bath below the xenon lamp with 12 samples to be irradiated in quartz-glass vials on the grid. The corresponding 12 aluminum foil-wrapped dark control vials are barely visible below quartz tubes on the bottom of water bath.

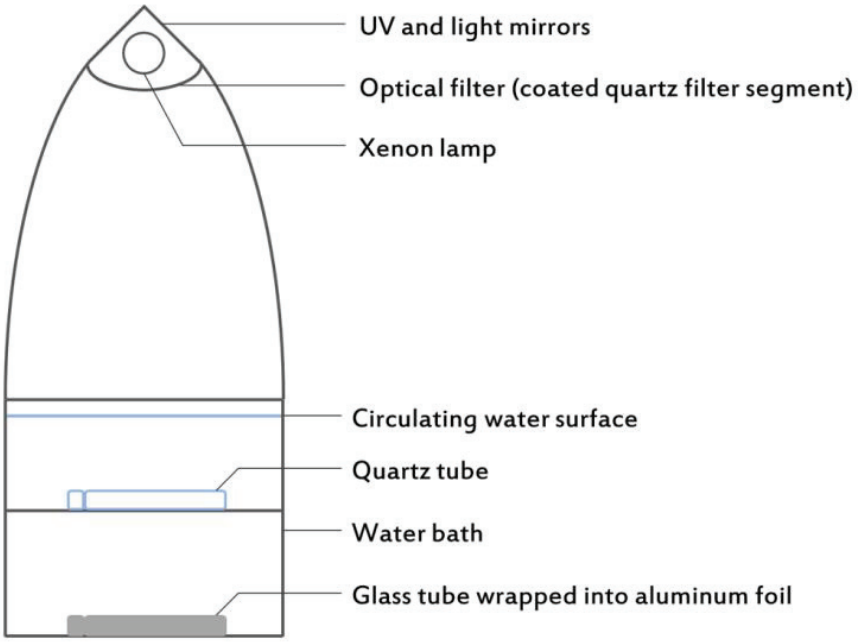

Figure S4. A schematic cross-section of the irradiation chamber and the water bath below. The cylindrical xenon lamp is in the focal point of parabolic reflector. An optical filter below the lamp cuts off short wavelength (< ≈290 nm) ultraviolet radiation. The water bath below the xenon lamp has a quartz-glass vial on the grid 57 mm below the surface of circulating water, and a dark control vial on the bottom of water bath.

Vector photon flux densities

Downwelling and upwelling vector photon flux densities ($Q_{v,d,\lambda}$ and $Q_{v,u,\lambda}$, respectively, mol photons m^{-2} nm^{-1} s^{-1}) of Suntest CPS+ were measured with a Macam SR991 spectroradiometer inside the water bath filled with cooling water. The front wall of water bath has an opening for the irradiation measurement (Figure S2). During irradiation experiments, the opening was covered by a stainless steel plate (Figure S2), the opening held a black rubber gasket (waterproofed with Blu-tack), which allowed entrance of an optical fiber and a cosine collector inside the water bath in circumstances that were identical to those in irradiation experiments. Since the dark control and irradiated sample vials modified the light field inside the water bath, the vials were kept inside the water bath also during irradiation measurements. The irradiation level of Suntest CPS+ was set to 250 W m^{-2} during irradiation measurements to avoid damage to Macam SR991 by high intensity irradiance at 765 W m^{-2} as used in experiments. The measured irradiation was later calculated to match the intensity of 765 W m^{-2}. The irradiance spectra were scanned from 240 nm to 800 nm at 1-nm steps and 200 analog-to-digital converted samples at each wavelength. The bandwidth of each wavelength was 2 nm, a default value of Macam SR991. Prior to the measurements, the Macam SR991 was calibrated in air at Irradian Ltd, Tranent, Scotland, the current representative of Macam spectroradiometers. The measured values were multiplied with an immersion correction factor for the cosine collector (1.34), which was experimentally determined by following a change in the level of downwelling irradiation with mean cosine μ_d = 1 (from Suntest CPS+) upon an immersion of cosine collector by a thin (approximately 2 mm) layer of tap water.

For $Q_{v,d,\lambda}$, the upward-facing cosine collector of Macam SR991 was mounted on a stainless steel holder placed on the grid inside the water bath through the opening. For $Q_{v,u,\lambda}$, the cosine collector was

turned such that the diffuser of cosine collector faced downward and received only upward irradiance. The diffuser was fitted between two bars of the grid with a piece of black tape. The position of the cosine collector well represents the site where the irradiated samples received upwelling irradiance. However, the cosine collector itself caused self-shading. During irradiation experiments, the quartz-glass vials filled with sample water were relatively transparent and attenuated the downwelling irradiance only slightly. Thus, $Q_{v,u,\lambda}$ received by irradiated samples was larger than the self-shading biased-measured $Q_{v,u,\lambda}$ values. This bias was corrected by accounting for the mean cosine of upwelling irradiance (μ_u) measured separately (see scalar irradiance measurements below).

Mean cosines for irradiances incident to the samples

To determine the mean cosines for down and upwelling irradiance (μ_d and μ_u, respectively), scalar photon flux densities for downwelling ($Q_{s,d,\lambda}$) and upwelling irradiance ($Q_{s,u,\lambda}$) at the range 400–700 nm were measured at the same locations as $Q_{v,d,\lambda}$ and $Q_{v,u,\lambda}$ with a spherical scalar irradiance sensor (QSL 2101, Biospherical Instruments, United States). To measure the scalar photon flux density from one hemisphere, the other hemisphere of spherical sensor was covered with black tape. Prior to measurements, the QSL 2011 was cross-calibrated with Macam SR991 using downwelling irradiation from Suntest CPS+ as a source. A cross calibration correction factor (*ccf*) was calculated as:

$$ccf = Q_{v,d,400–700}\ \ Q_{s,d,400–700}^{-1} \tag{S4}$$

where $Q_{v,d,400–700}$ is the downwelling vertical photon flux density integrated over 400–700 nm spectral range measured with Macam SR901 spectroradiometer, and $Q_{s,d,400–700}$ is the downwelling scalar photon flux density for photosynthetically active radiation (from 400–700 nm) measured with the QSL 2101. The *ccf* was 1.6.

The mean cosine of downwelling irradiance (μ_d) was calculated as:

$$\mu_d = Q_{v,d,400–700}\ \ (1.6\ Q_{s,d,400–700})^{-1} \tag{S5}$$

where $Q_{v,d,400–700}$ is the measured (Macam SR991) immersion-corrected downwelling vector photon flux density integrated from 400–700 nm, 1.6 is the *ccf*, and $Q_{s,d,400–700}$ is the measured (QSL 2101) immersion-corrected downwelling scalar photon flux density between 400–700 nm. The immersion correction for the QSL 2101 was obtained by selecting the measurement mode for the submerged spherical sensor (provided by manufacturer). The measured μ_d was 0.988, which indicated that the downwelling irradiance incident to samples was more or less vertical (i.e., came from the zenith). This value agreed well with the manufacturer's aim to generate vertical downward irradiance from the Xenon arch by using a parabolic reflector (Figure S4). Additionally, a refraction of light at the air-water interface directs it towards the nadir.

The mean cosine of upwelling irradiance (μ_u) was calculated as:

$$\mu_u = Q_{v,u,400–700}\ (1.6\ Q_{s,u,400–700})^{-1} \tag{S6}$$

where the measurements were performed as described above, but the sensors were turned upside down such that they measured only upwelling irradiance. The measured μ_u was 0.172, which indicated that the upwelling irradiance incident to the samples was rather horizontal. This simple interpretation of upwelling light field is likely incorrect, because the self-shading of cosine collector (Macam SR991) biased $Q_{v,u,400–700}$ towards too low values. The sensor of QSL 2101 used for the scalar irradiance measurements was a white Teflon sphere (13 mm), which also caused some self-shading but much less than the larger (approximately 35 mm) cosine collector of Macam SR991. In practice, the measured μ_u did not account only for the shape of upwelling light field but also corrected for the self-shading of measured $Q_{v,u,\lambda}$.

The photon flux density incident to the sample

The doses of downwelling and upwelling photon flux densities incident to samples ($Q_{i,d,\lambda}$ and $Q_{i,u,\lambda}$, respectively) during experimental irradiations (mol photons m^{-2} nm^{-1} irradiation $time^{-1}$) were calculated from vector photon flux densities and their mean cosines for irradiance accounting irradiation time, t (s):

$$Q_{i,d,\lambda} = Q_{v,d,\lambda}\ t\ \mu_d^{-1} \quad \text{(S7)}$$

$$Q_{i,u,\lambda} = Q_{v,u,\lambda}\ t\ \mu_u^{-1} \quad \text{(S8)}$$

Mean optical path length inside the sample vials

For our cylindrical vials (Figure S1), the geometric path length of light ranged from the inner diameter (D = 13.4 mm at the center of vial) to zero (minimum at the side of vial). The mean optical path length of vials (L) was calculated according to:

$$L = D^{-1}\int_0^D f(x)dx \quad \text{(S9)}$$

where D is the inner diameter ($D = 2r$) and $f(x)$ is the length of a segment at the distance x across the inner diameter (according to Pythagoras $f(x) = (r^2 - (r-x)^2)^{0.5}$). The solution for the integral above divided by D is $L = 0.5\pi r$. For our vials L was 10.52 mm.

Mean spectral absorption coefficient of CDOM during the experimental irradiation

The experimental irradiations photobleached CDOM (a_λ) in irradiated samples (a_{330}, Table S5). To account for this photobleaching in the determinations of apparent quantum yields, we calculated the mean a_λ of irradiated samples during experimental irradiations. For the mean a_λ, the CDOM measurements were carried out after irradiations for the irradiated and the dark control samples. In these measurements, the lower detection limit was defined as 3 × SD (standard deviation) of replicated measurements. The values of a_λ that were below the detection limit were calculated according to a spectral slope coefficient of CDOM determined for an approximately 100 nm wavelength band towards the shorter wavelengths from the wavelength of the lowest level of detection. Finally, the spectrum of a_λ from 190 nm to 700 nm was compiled using the measured values directly for the UV and short-wavelength visible part of spectrum and the calculated values at the long-wavelength and infrared part of the spectrum. This extrapolation was done only for the determination of AQY, and the spectral slope coefficients reported in Table S6 are based on spectral regions, where a_λ was above the limit of detection.

The mean a_λ of irradiated samples during irradiation was calculated from the measured post-irradiation a_λ of irradiated and dark control samples based on first order kinetics reaction rate coefficients defined for every λ. First, the first order rate constant for photobleaching for every λ (k_λ) was calculated as:

$$k_\lambda = \ln(a_{\lambda\_Dark}) - \ln(a_{\lambda\_Irra}) \quad \text{(S10)}$$

from a_λ in the irradiated (a_{λ_Irra}) and the dark control (a_{λ_Dark}) samples. For mathematical convenience, the experimental irradiation time was set to 1 and is not shown in eqs. S10 and S11. Then the mean a_λ was calculated as a definite integral of a_λ in the irradiated sample from the beginning to the end of irradiation:

$$\text{mean } a_\lambda = a_{\lambda\_Dark}\, k_\lambda^{-1}\, (1-e^{-k_\lambda}) \quad \text{(S11)}$$

The number of photons absorbed by CDOM of sample

The number of downwelling ($Q_{abs,d,\lambda}$) and upwelling ($Q_{abs,u,\lambda}$) photons absorbed by CDOM (mol photons m^{-2} irradiation $time^{-1}$ nm^{-1}) were calculated as:

$$Q_{abs,d,\lambda} = Q_{i,d,\lambda} \ (1-e^{(-a_\lambda L)}) \tag{S12}$$

$$Q_{abs,u,\lambda} = Q_{i,u,\lambda} \ (1-e^{(-a_\lambda L)}) \tag{S13}$$

where the parameters refer to those described in eqs. S7, S8, S9, and S11. The total number of absorbed photons ($Q_{abs,\lambda}$; mol photons m^{-2} irradiation $time^{-1}$ nm^{-1}) was calculated as:

$$Q_{abs,\lambda} = Q_{abs,d,\lambda} + Q_{abs,u,\lambda} \tag{S14}$$

Defining apparent quantum yield

Apparent quantum yields (AQY) for photoproduction of DIC were defined as a simple ratio:

$$\phi = \text{photoproduction of DIC } Q_{abs}^{-1} \tag{S15}$$

where photochemical production of DIC expresses the amount of photoproduced DIC (mol C m^{-2} irradiation $time^{-1}$) and Q_{abs} is the number of photons absorbed by CDOM of sample expressed per area (mol photons m^{-2} irradiation $time^{-1}$). The measured rate of photoproduced DIC per area was calculated as:

$$\text{photoproduction of DIC (areal)} = \text{photoproduction of DIC (volumetric)} \ L \tag{S16}$$

where the volumetric photoproduction of DIC (mol C m^{-3} irradiation $time^{-1}$) is multiplied by the mean optical pathlength (L = 0.01052 m; eq. S9). After this conversion, the unit of ϕ (eq. S15) is mol C mol $photons^{-1}$.

The AQY for DIC photoproduction has a strong spectral dependence; AQY decreases exponentially with increasing wavelength.[16] The spectral AQY was described in this study as [17]:

$$\phi_\lambda = ce^{-d\lambda} \tag{S17}$$

where c is the AQY at reference wavelength λ (mol C mol $photons^{-1}$), and d is spectral slope coefficient (nm^{-1}) of AQY. The reference wavelength λ in eq. S17 is 0 nm.

The ϕ_λ (eq. S17) was determined as:

$$\phi_\lambda = \text{photoproduction of DIC } Q_{abs,\lambda}^{-1} \tag{S18}$$

where $Q_{abs,\lambda}$ is the spectrum of photons absorbed by the CDOM of sample from 268 to 700 nm at 1-nm steps (mol photons m^{-2} nm^{-1} irradiation $time^{-1}$). The photon fluxes were nearly negligible at wavelengths below approximately 290 nm because of the optical filter in front of Xenon lamp (Figure S4). While ϕ of eq. S15 has a unique mathematical solution, the values of c and d defining ϕ_λ of eq. S18 cannot be arithmetically calculated directly.

Iteration of the spectral apparent quantum yield with MATLAB

The values of c and d were iterated from given starting values using the Nelder-Mead algorithm embedded in `fminsearch` function of MATLAB. Here we explain the concept of iteration; the *funBaltic.m* and *fitBaltic.m* scripts below show the actual code used in the iteration. During the first round of iteration, the rate of DIC photoproduction was calculated based on $Q_{abs,\lambda}$ (eq. S14) and ϕ_λ, which are defined by the starting values of c and d (eq. S17) and compared to the measured rate of DIC photoproduction:

$$\text{DIC photoproduction (measured)} = \phi_\lambda \, Q_{abs,\lambda} \tag{S19}$$

The calculated photoproduction of DIC ($\phi_\lambda \, Q_{abs,\lambda}$ of eq. S19) was subtracted from the measured photoproduction of DIC (eq. S16) to evaluate the difference between the measured and calculated values. For the following round of iteration, the `fminsearch` function changed the values of c and d. The photoproduction of DIC was then calculated again to evaluate any changes in the difference between the measured and the calculated values. The `fminsearch` function performed several rounds of iterations to find the optimized values of c and d that minimize the difference between the measured and the calculated values (i.e., residual). The *funBaltic.m* script (listed in full below) executed the calculation of residuals.

During the iteration, the values of c and d defining ϕ_λ (eq. S17) are interdependent. Large values of c are compensated by large values of d. In the other way around, low values of c are compensated by low values of d. To minimize this interdependence, the starting value for c was set to 1, which is a mathematically neutral pre-exponential factor in eq. S17. This starting value also assumes that the apparent quantum yield remains ≤1 even at the shortest wavelengths of electromagnetic spectrum (i.e., at the reference wavelength 0 nm ($\phi_0 = c$) with infinitely high energies of photons). The starting values for d were selected randomly between 0.011 nm^{-1} and 0.084 nm^{-1} to approximate the extremes of spectral slope coefficients for AQY reported in literature (e.g. Powers et al. 2015).[32] During the actual iteration, the values for c or d are not constrained. For instance, the iteration can assign values >1 for c or values outside the range of starting values for d. However, if the iteration results in negative values of ϕ_λ, the parameters c and d are re-iterated, because ϕ_λ for DIC photoproduction cannot be negative.

The spectral region selected for iteration (268–700 nm) entirely covers the region that contributes to the photochemical transformation of DOM or photoreduction of Fe(III), but also includes long wavelengths (red part of spectrum) that are not known to mineralize DOC to DIC or to cause photoreduction of ferric iron. The iteration process does not set any constrains for the longest wavelength inducing photochemical transformation. Instead, it is assumed that the measured DIC photoproduction become spectrally negligible when the AQY and the light absorbed by CDOM decreased exponentially with increasing wavelength to give a negligible product ($\phi_\lambda \, Q_{abs,\lambda}$ of eq. S19). Those wavelengths where $\phi_\lambda \, Q_{abs,\lambda}$ of eq. S19 becomes negligible also approximate the longest wavelengths that contribute to DIC photoproduction.

To obtain consistent optimized values for c and d as well as to evaluate the error associated with the iteration, we adapted a Monte Carlo approach for the iteration. The *fitBaltic.m* script (listed in full below) determined the values of c and d 1000 times. The 1000 spectra of AQY defined by c and d were arranged into a matrix, which was used for the selection of best estimate for c and d as well as to evaluate the error associated with the iteration. One of the iterated combinations of c and d, which defined ϕ_λ closest to the median AQY among the 1000 determinations, was selected as the best estimate for c and d. After ranking the 1000 wavelength-specific AQY in ascending order, the AQY with a rank 25 and 975 were considered to present the lower and upper 95% confidence interval, respectively, for the fitting.

An example of MATLAB code used in the iteration for ϕ_λ.

funBaltic.m

```
% This file defines the function for the apparent quantum yield.

function [ress,pmzest,fiil] = funBaltic(cd, absp, pmzmes, l)
% Where pmzest is estimated photochemical mineralization at depth z (mol C m-2 h-1),
% ress sums the squared relative difference between estimated (pmzest) and measured (pmzmes)
% photomineralization, absp is the amount of spectral photon absorption and
% l is the range of wavelengths (268-700 nm) in 1-nm steps.

% Gets the optimized c and d values from the argument vector (cd).
c = cd(1);
d = cd(2);
% Defines the theoretical equation for the apparent quantum yields over the spectral range
% defined in l.
fiil = c*exp(-d*l);

% Calculates an estimate of the photochemical mineralization at depth z for each wavelength
% based on the suggested apparent quantum yields (fiil) and absQ.
pmzestl = absp.*fiil';

% Sums the estimated values over the wavelength range l (268-700 nm).
pmzest = sum(pmzestl);

% Calculates (diff) the difference between estimated and the measured photomineralization,
% the relative difference (relative_diff) and the squared relative difference (ress).
diff = pmzmes - pmzest;
relative_diff = diff./pmzmes;
ress = (relative_diff).^2;
```

fitBaltic.m

```
% This file performs iteration to select the best c and d for the apparent quantum yield.
% The optimization is based on minimization of the residual between the measured and the
% estimated photomineralization.

% Initializes vectors for the temporary c and d values (cd), for the optimized c, d values
% (cd_opt) and a variable for the squared relative difference between the measured and the
% estimated photomineralization with the optimized c and d values (residual).
cd = zeros(1,2);
cd_opt = zeros(1,2);
residual = 0.0;

% Defines the wavelength range, 268-700 nm with 1 nm step interval.
l = 268:1:700;

% Defines the wavelength range used for the comparison of functions distance from the
median.
sl = 300:1:500;

% In each iteration, optimization of variables c and d starts from c = 1.0 and d
% is randomly selected in the range d0l <= d <= d0h.
c0 = 1.0;
d0l = 0.011;
d0h = 0.084;
```

```
% Defines the number of iterations (integer) performed to optimize the variables c and d.
montestps = int16(1000);

% Defines level of confidence interval at 95%.
loc = 95;

% Initializes a variable for the number of wavelengths (integer) in the data.
lcnt = int16(length(l));

% Initializes an array for values of the estimated photomineralization over spectral range
l.
% Results for each iteration are stored at rows. The four additional positions on each row
% are used to store the optimized c, d, the cumulative distance over the spectral range to
% the median of all iterations and the squared relative difference between the measured and
% the estimated photomineralization, respectively.
fvals = zeros(montestps,lcnt + 4);
% Optarg variable initialized to disable printing from each fminsearch iteration.
optarg = optimset('Display','off');
% Initializes a vector for storing the estimated photomineralization over spectral range l
% with the optimized c and d.
f_opt = zeros(1,lcnt);
% Initialized an array for storing the confidence interval values over the spectral range l.
% The first row contains the upper and the second contains the lower limit.
cnf_int = zeros(2,lcnt);
% Initializes an integer variable defining the number of iterations to include around the
% median in the selection of the confidence interval values.
loc_eps = int16((((100.0 - loc) / 100.0) * montestps) / 2.0);
% Initializes an array for storing the extremums for all the optimized functions of
estimated
% photomineralization over the spectral range in 1nm intervals.
f_var = zeros(2,lcnt);
f_var(1,1:lcnt) = realmin;
f_var(2,1:lcnt) = realmax;

% Loads data from file containing a matrix of the spectral photons absorption by
% solution (absp) and the amount of photoproduced DIC (pmzmes) after irradiation.
load 20150701_AQY_Kuiva.mat;

% The unit for absQ is mol photons m-2 nm-1 exposure-1.
absp = absQ(:,20);

% The measured amount of DIC photoproduction is expressed as pmzmes for each
% experimental trail. The trail 1 is selected here.
% DIC is calculated from the measured DIC photoproduct (mol m-3 exposure-1) by multiplying
it
% with L, the mean optical path length inside sample vial (0.0105 m). The unit for DIC is
mol
% C m-2 exposure-1.
pmzmes = DIC(20,:);

% In each iteration, the starting value of c is c0 (= 1.0) and d is randomly selected
within
% the range d0l <= d <= d0h.
% The optimization is performed by fminsearch, searching to minimize the squared relative
% difference between the measured and the estimated photomineralization. The fminsearch is
```

```
% unconstrained and any optimization results
% negative c or d values are discarded as physically non-representative.
for n = 1:montestps

    % Sets (cd_opt) negative to simulate a do-while-loop. This way the while-block will be
    % executed at least once.
    cd_opt = [-1, -1];
    exitflag = 0;

    % While-block calls fminsearch on 'funBaltic' to minimize residual (ress), optimizing
    % variables c and d.
    % The starting values for iteration are set to the vector (cd). This block will repeat
    % in case of a negative c, d or if the exit condition of fminsearch (exitflag) is not 1.
    while (cd_opt(1) < 0 || cd_opt(2) < 0 || exitflag ~= 1)
        cd(1) = c0;
        cd(2) = d0l + ((d0h-d0l)*rand);
        [cd_opt,fval,exitflag,output] = fminsearch(@(x) funBaltic(x,absp,pmzmes,l), cd,
optarg);
    end

    % Stores the function values at 1nm intervals to fvals. Also stores the optimized c, d
    % and squared relative difference between the measured and the estimated
    %photomineralization.
    [ress,pmzest,fitl] = funBaltic(cd_opt,absp,pmzmes,l);
    fvals(n,1:lcnt) = fitl;
    fvals(n,lcnt + 1) = cd_opt(1);
    fvals(n,lcnt + 2) = cd_opt(2);
    fvals(n,lcnt + 4) = ress;
end

% Collects the extremums of optimized c (indices 1,2) and d (indices 3,4) to cd_extr.
% These are used for reporting purposes only.
cd_extr = zeros(1,4);
cd_extr(1) = min(fvals(:,lcnt + 1));
cd_extr(2) = max(fvals(:,lcnt + 1));
cd_extr(3) = min(fvals(:,lcnt + 2));
cd_extr(4) = max(fvals(:,lcnt + 2));

% Generates the median of photomineralizations over the set of optimized functions for each
% 1-nm step over the spectral range l.
mdf = median(fvals);

% Builds the cumulative, absolute differences between the median of photomineralizations
for
% the set of functions and each of the optimized functions over the spectral range sl.
Stores
% the value at the corresponding row in the array fvals, at the third additional position.
for n = 1:lcnt
    for m = 1:montestps

        if(n >= sl(1) && n <= sl(end))
            fvals(m,lcnt + 3) = fvals(m,lcnt + 3) + abs(fvals(m,n) - mdf(n));
        end
        % Uses the same loops to collect the extremums of the estimated
photomineralizations
        % in the set of optimized functions over the spectral range to the array f_var,
```

```
        % with maximums in the first row.
        if (fvals(m,n) > f_var(1,n))
            f_var(1,n) = fvals(m,n);
        end
        if (fvals(m,n) < f_var(2,n))
            f_var(2,n) = fvals(m,n);
        end
    end
end

% Selects the closest match to the median in the set of the optimized functions by finding
% the smallest cumulative difference (as calculated in the previous step).
mdfit = [realmax, 0];
for n = 1:montestps
    if fvals(n,lcnt + 3) < mdfit(1)
        mdfit(1) = fvals(n,lcnt + 3);
        % Stores the index (referring to fvals) of the best matching function to mdfit(2).
        mdfit(2) = n;
    end
end

% Sets optimized c, d variables and the residual. Stores the values of the selected
function
% in f_opt over the spectral range defined in l.
cd_opt(1) = fvals(mdfit(2),lcnt + 1);
cd_opt(2) = fvals(mdfit(2),lcnt + 2);
residual = fvals(mdfit(2),lcnt + 4);
f_opt = fvals(mdfit(2),1:lcnt);

% Sorts the values of all the optimized functions over spectral range l in descending order.
% Collects the confidence interval values over the spectral range l into the cnf_int matrix.
% Values are selected (((CI% - 100%) / 100) * montestps) / 2; i.e. for 95% 25 ranks from
both
% extremums.
[fvals_sort, sort_index] = sort(fvals,'descend');
cnf_int(1,1:lcnt) = fvals_sort(loc_eps,1:lcnt);
cnf_int(2,1:lcnt) = fvals_sort((montestps - loc_eps),1:lcnt);

% Prints results.
pmzmes       % For comparison pmzmes is reported.
residual     % Squared relative difference between measured and estimated
photomineralization.
cd_opt       % The optimized (c) and (d).
cd_extr      % The extremums of optimized c and d in the generated set of functions.
```

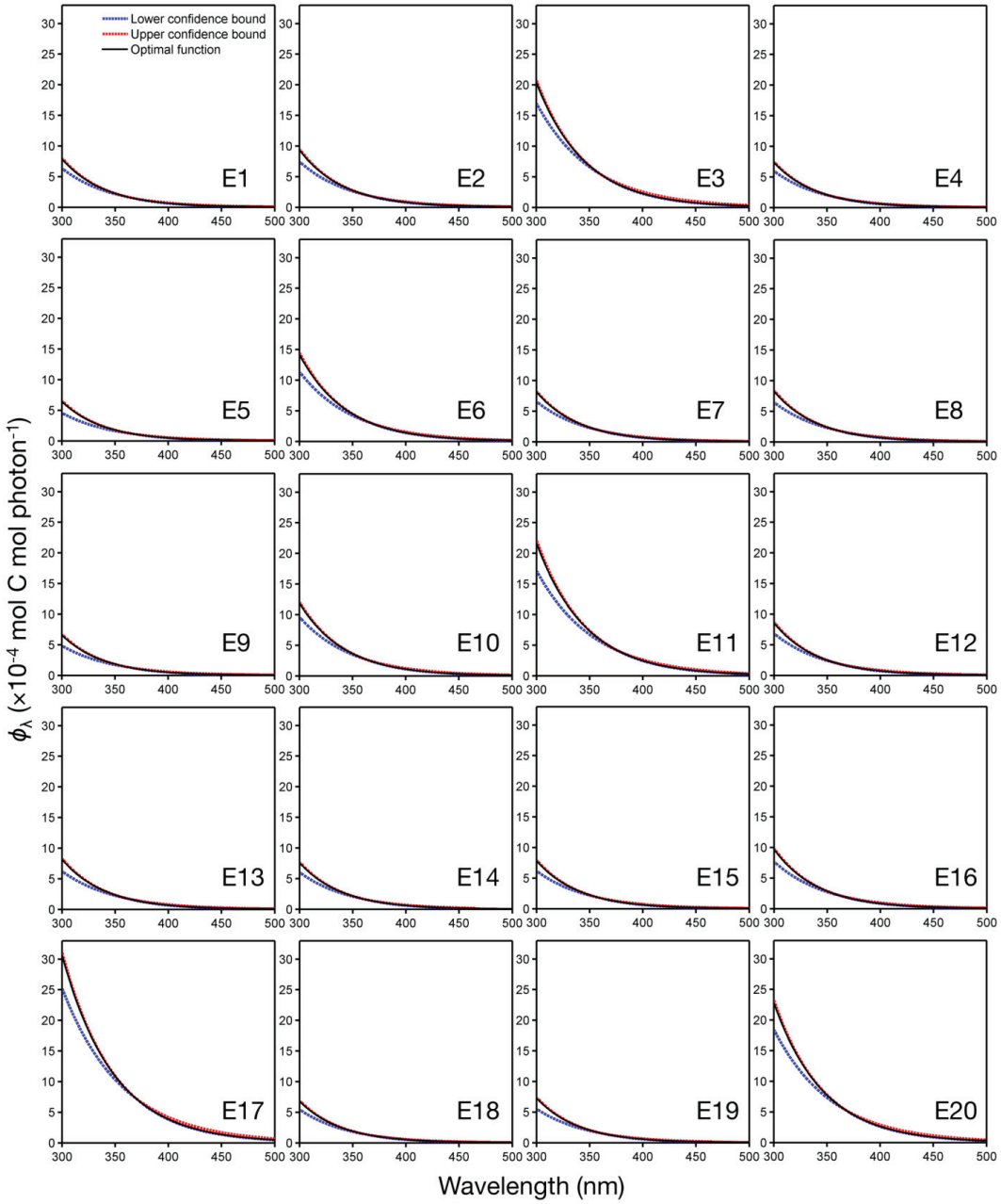

Figure S5. The best estimates for ϕ_λ (black line) with 95% confidence intervals for fitting (red and blue lines) of the 20 experiments (E1–E20). The best estimates are very close to the upper 95% confidence interval bound, and thus one of these curves may be poorly visible.

The uncertainty of iterations is shown as the 95% confidence intervals for ϕ_λ in each experiment (Figure S5). The iteration error was largest at the shortest wavelengths and decreased towards longer wavelengths. The best estimate of ϕ_λ was very close to the upper confidence bound and therefore that bound is not clearly visible in Figure S5.

Because this study reports only the best estimates for *c* and *d* (Table S7), we evaluated the uncertainty of those by determining ϕ_λ consecutively ten times for the experiments #5, #8, #13 and #17 (Table S4). These experiments represent the lowest (#5), the median (#8 and #13) and the largest (#17) value of ϕ_{330} in the experiments of this study. Among the consecutive determinations, the values of *c* and *d* defining ϕ_λ varied only minimally (Table S4). The coefficient of variation was less than 0.6 % for ϕ_λ at the spectral range from 300 nm to 500 nm (data not shown). This error related to the fitting of the best estimates is much lower than e.g., the analytical uncertainty in determination of DIC photoproduction (reported in Table S7).

Table S4. The parameters *c* and *d* for the four selected experiments determined in 10 consecutive runs of *fitBaltic.m* script.

	Consecutive determinations									
	1	2	3	4	5	6	7	8	9	10
Expr. 5										
c	1.395	1.420	1.383	1.420	1.419	1.396	1.415	1.403	1.417	1.421
d	0.0256	0.0257	0.0256	0.0257	0.0257	0.0256	0.0257	0.0256	0.0257	0.0257
Expr. 8										
c	1.413	1.414	1.426	1.430	1.428	1.414	1.428	1.442	1.435	1.427
d	0.0248	0.0248	0.0248	0.0248	0.0248	0.0248	0.0248	0.0249	0.0249	0.0248
Expr. 13										
c	1.431	1.432	1.418	1.398	1.425	1.414	1.429	1.417	1.422	1.414
d	0.0249	0.0249	0.0249	0.0248	0.0249	0.0249	0.0249	0.0249	0.0249	0.0249
Expr. 17										
c	1.553	1.483	1.542	1.539	1.540	1.545	1.550	1.543	1.498	1.490
d	0.0208	0.0206	0.0207	0.0207	0.0207	0.0207	0.0207	0.0207	0.0207	0.0206

Table S5. The absorption coefficients of CDOM at 330 nm (a_{330}) in the SPE-DOM solutions (10 mg DOM L^{-1}) and the photochemistry-induced change in a_{330} (Δa_{330}).

Expr.	pH	[Fe][a]	a_{330}[b]			Δa_{330}[c]
			Init.	Dark	Irra.	
		(μmol L^{-1})	(m^{-1})	(m^{-1})	(m^{-1})	(m^{-1})
1	4.18	0.04	16.23	16.17	13.70	−2.47
2	5.17	0.04	15.70	15.62	13.50	−2.12
3	5.98	0.04	17.15	17.21	14.11	−3.10
4	6.01	0.04	18.31	18.12	15.41	−2.71
5	7.12	0.04	17.47	17.09	13.86	−3.23
6	5.08	6.04	26.05	26.21	21.63	−4.58
7	7.46	6.04	27.81	27.93	22.45	−5.48
8	4.01	17.37	23.84	23.61	13.33	−10.28
9	5.87	17.37	25.47	25.66	22.25	−3.41
10	8.05	17.37	27.41	27.41	17.71	−9.70
11	4.00	18.04	23.65	23.82	11.24	−12.58
12	5.90	18.04	25.49	25.06	22.18	−2.88
13	8.10	18.04	26.62	26.61	22.90	−3.71
14	4.22	30.04	26.02	NA	14.54	−11.48
15	4.41	30.04	35.40	35.28	22.45	−12.83
16	6.85	30.04	28.77	28.69	25.36	−3.33
17	9.42	30.04	38.28	37.01	34.08	−2.93
18	4.26	34.71	34.41	31.30	21.75	−9.55
19	6.29	34.71	32.35	32.31	30.39	−1.92
20	7.70	34.71	33.58	33.50	27.36	−6.14

[a][Fe] represents the concentration of Fe introduced to solutions, with the exception of 0.04 μmol L^{-1}, which refers to the measured concentration from the solutions of SPE-DOM without introduced Fe. [b]The absorption coefficient of CDOM at 330 nm (a_{330}) of initial (Init.), dark control (Dark), and irradiated (Irra.) solution. [c]$\Delta a_{330} = a_{330\_Irra} - a_{330\_Dark}$. NA = Data not available.

Table S6. Spectral properties of CDOM and photochemistry-induced changes in the spectral properties.[b]

Expr.	pH	[Fe][a]	$S_{275–295}$			$\Delta S_{275–295}$	$S_{350–400}$			$\Delta S_{350–400}$	S_R			ΔS_R
			Init.	Dark	Irra.		Init.	Dark	Irra.		Init.	Dark	Irra.	
		(μmol L^{-1})	(nm^{-1})	(nm^{-1})	(nm^{-1})	(nm^{-1})	(nm^{-1})	(nm^{-1})	(nm^{-1})	(nm^{-1})				
1	4.18	0.04	0.0138	0.0138	0.0149	0.0011	0.0200	0.0203	0.0193	−0.00095	0.690	0.682	0.773	0.091
2	5.17	0.04	0.0134	0.0135	0.0151	0.0016	0.0191	0.0200	0.0192	−0.00076	0.703	0.675	0.783	0.108
3	5.98	0.04	0.0130	0.0130	0.0147	0.0016	0.0181	0.0179	0.0170	−0.00092	0.716	0.728	0.863	0.136
4	6.01	0.04	0.0134	0.0133	0.0148	0.0014	0.0190	0.0195	0.0183	−0.00120	0.707	0.684	0.807	0.123
5	7.12	0.04	0.0129	0.0129	0.0152	0.0022	0.0179	0.0184	0.0187	0.00032	0.721	0.703	0.811	0.108
6	5.08	6.04	0.0110	0.0110	0.0123	0.0012	0.0185	0.0184	0.0178	−0.00064	0.593	0.600	0.692	0.092
7	7.46	6.04	0.0109	0.0109	0.0123	0.0014	0.0171	0.0170	0.0164	−0.00061	0.636	0.642	0.749	0.107
8	4.01	17.37	0.0118	0.0119	0.0158	0.0039	0.0177	0.0177	0.0189	0.00115	0.668	0.668	0.836	0.168
9	5.87	17.37	0.0114	0.0115	0.0126	0.0011	0.0177	0.0177	0.0166	−0.00102	0.647	0.651	0.755	0.104
10	8.05	17.37	0.0112	0.0112	0.0139	0.0027	0.0162	0.0162	0.0168	0.00062	0.688	0.690	0.825	0.135
11	4.00	18.04	0.0113	0.0113	0.0150	0.0037	0.0174	0.0172	0.0175	0.00033	0.648	0.657	0.856	0.199
12	5.90	18.04	0.0112	0.0111	0.0124	0.0013	0.0181	0.0183	0.0179	−0.00037	0.620	0.608	0.693	0.085
13	8.10	18.04	0.0112	0.0112	0.0123	0.0012	0.0176	0.0175	0.0165	−0.00097	0.637	0.637	0.744	0.107
14	4.22	30.04	0.0109	NA	0.0142	0.0142	0.0174	NA	0.0175	0.01745	0.628	NA	0.814	0.186
15	4.41	30.04	0.0100	0.0098	0.0122	0.0023	0.0170	0.0164	0.0155	−0.00090	0.589	0.600	0.784	0.185
16	6.85	30.04	0.0109	0.0108	0.0120	0.0011	0.0180	0.0181	0.0178	−0.00025	0.605	0.600	0.671	0.071
17	9.42	30.04	0.0097	0.0096	0.0101	0.0006	0.0153	0.0146	0.0134	−0.00122	0.634	0.652	0.755	0.102
18	4.26	34.71	0.0087	0.0089	0.0097	0.0008	0.0141	0.0145	0.0123	−0.00215	0.618	0.616	0.788	0.171
19	6.29	34.71	0.0103	0.0103	0.0109	0.0005	0.0208	0.0208	0.0194	−0.00141	0.494	0.496	0.558	0.063
20	7.70	34.71	0.0105	0.0104	0.0111	0.0007	0.0198	0.0200	0.0186	−0.00148	0.528	0.518	0.597	0.079

[a]See Table S5 for further explanation. [b]$S_{275–295}$ and $S_{350–400}$ are the spectral slope coefficients at two spectral ranges, S_R is their slope ratio. The photochemistry-induced changes (Δ) are calculated as the difference between the irradiated and the dark control samples.

Table S7. Photoproduction rates of DIC (DICpr) and the apparent quantum yield spectrum for DIC photoproduction (ϕ_λ)

Expr.	pH	[Fe] [a] (μmol L^{-1})	DICpr [b] (μmol C L^{-1} h^{-1})	ϕ_λ [c]			
				c (mol C mol photon^{-1})	*d* (nm^{-1})	ϕ_{330} ($\times10^{-4}$ mol C mol photon^{-1})	CV (%)
1	4.18	0.04	1.72 ± 0.08	1.427	0.0250	3.70	5.76
2	5.17	0.04	1.78 ± 0.11	1.417	0.0249	3.85	7.06
3	5.98	0.04	1.79 ± 0.07	1.398	0.0251	3.55	4.44
4	6.01	0.04	1.82 ± 0.14	1.403	0.0252	3.45	8.54
5	7.12	0.04	1.97 ± 0.67	1.415	0.0248	3.92	9.74
6	5.08	6.04	4.43 ± 0.45	1.450	0.0237	5.84	2.93
7	7.46	6.04	2.35 ± 0.55	1.421	0.0256	3.07	5.87
8	4.01	17.37	4.72 ± 0.04	1.478	0.0219	10.57	1.39
9	5.87	17.37	3.40 ± 0.08	1.439	0.0245	4.49	2.88
10	8.05	17.37	2.65 ± 0.18	1.434	0.0250	3.72	6.82
11	4.00	18.04	10.40 ± 0.11	1.553	0.0208	16.48	3.61
12	5.90	18.04	3.45 ± 0.10	1.429	0.0243	4.66	3.62
13	8.10	18.04	2.38 ± 0.10	1.421	0.0255	3.16	4.74
14	4.22	30.04	8.42 ± 0.19	1.490	0.0216	11.95	3.65
15	4.41	30.04	6.70 ± 0.10	1.459	0.0231	7.12	1.67
16	6.85	30.04	2.73 ± 0.10	1.425	0.0253	3.41	4.59
17	9.42	30.04	3.22 ± 0.07	1.398	0.0256	2.97	4.53
18	4.26	34.71	12.08 ± 0.80	1.454	0.0217	11.24	2.60
19	6.29	34.71	3.57 ± 0.60	1.432	0.0247	4.07	4.36
20	7.70	34.71	3.35 ± 0.66	1.432	0.0249	3.87	5.06

[a]See Table S5. [b]The analytical uncertainty of DIC photoproduction rate (values after ±) is the sum of standard deviations of replicated determination of DIC in the irradiated and the dark control samples. [c]The parameters *c* and *d* define the spectral apparent quantum yield (eq. 2). ϕ_{330} represents AQY at 330 nm; coefficient of variation (CV) refers to the analytical uncertainty for the determination of ϕ_{330}, defined as the cumulative standard deviation related to the determination of DICpr and the absorption coefficient of CDOM.

Regression analyses

The dependencies of optical properties and photochemical transformations on [Fe] and pH were explored with regression models containing predictor variables alone, together, or accounting for their interaction (Tables S8–18). To make [Fe] and pH comparable in the regression analyses, the pH value was transformed to the concentration of hydrogen ions $[H^+]$ $(= 10^{-pH})$ (mol L^{-1}) and to the same unit used for [Fe] (mol L^{-1}). For the visualization of models, $[H^+]$ was expressed in log-scale as pH $(= -\log[H^+]$; Figures 1–3). The general form of the used regression equation is:

$$Y = a + b1\,[\mathrm{Fe}] + b2\,[H^+] + b3\,[\mathrm{Fe}]\,[H^+] \quad \text{(S17)}$$

where Y is the dependent variable, a is the intercept, $b1$ is the regression coefficient for [Fe], $b2$ is the regression coefficient for $[H^+]$, and $b3$ is the regression coefficient for the interaction between [Fe] and $[H^+]$. The dependent variables (Y) included optical properties of dark control (_Dark) and their changes caused by photobleaching, DIC photoproduction rate, and the parameters (c, d and ϕ_{330}) related to ϕ_λ.

Tables S8–18 show the coefficients of regression models, the adjusted coefficients of determination (adjusted R^2), root mean squared errors (RMSE), degrees of freedom (df), and corrected Akaike Information Criterion (AICc) values.[33, 34] The statistically significant ($p < 0.05$) terms are bolded. The most parsimonious models were selected based on the lowest AICc value and are marked with * in Tables S8–18. The selection was limited to models that do not contain nonsignificant predictor.

Table S8. Regression models and assessment values for the absorption coefficient of CDOM at 330 nm in the dark control samples, a_{330_Dark} (m^{-1}). The table shows the coefficients of regression for the terms [Fe] (coefficient *b1*), [H^+] (coefficient *b2*), and the interaction of [Fe] and [H^+] (coefficient *b3*) in eight competing models. The table reports the adjusted coefficients of determination (adjusted R^2), root mean squared errors (RMSE), the degrees of freedom (*df*), and the corrected Akaike Information Criterion (AICc) values for each model.[33, 34] Statistically significant ($p < 0.05$) terms are bolded. The most parsimonious model including only significant predictor terms was selected based on the lowest AICc value and is marked with *.

Term	Coef.	Model							
		1	2*	3	4	5	6	7	8
Intercept	*a*	**25.73**	**18.52**	**26.13**	**19.15**	**25.13**	**18.60**	**25.99**	**19.05**
[Fe]	*b1*		**4.21×10^5**		**4.32×10^5**		**4.59×10^5**		**4.39×10^5**
[H^+]	*b2*			-1.83×10^4	-3.73×10^4			**-1.61×10^5**	-3.04×10^4
[Fe] [H^+]	*b3*					1.42×10^9	-1.71×10^9	**7.69×10^9**	-3.90×10^8
adjusted R^2		0	0.737	−0.045	0.766	−0.086	0.760	0.148	0.767
RMSE		6.24	3.11	6.21	2.85	6.15	2.89	5.45	2.85
df		19	18	18	17	18	17	17	16
AICc		135	110	137	109	137	110	135	113

Table S9. Regression models and assessment values for the spectral slope coefficient of CDOM in dark control samples, $S_{275–295\_Dark}$ (nm^{-1}). The parameters are explained in Table S8.

Term	Coef.	Model							
		1	2*	3	4	5	6	7	8
Intercept	*a*	**1.14×10^{-2}**	**1.29×10^{-2}**	**1.14×10^{-2}**	**1.28×10^{-2}**	**1.16×10^{-2}**	**1.29×10^{-2}**	**1.14×10^{-2}**	**1.26×10^{-2}**
[Fe]	*b1*		**−88.34**		**−89.49**		**−88.09**		**−76.25**
[H^+]	*b2*			−0.15	3.79			**40.46**	17.72
[Fe] [H^+]	*b3*					-6.13×10^5	-1.12×10^4	**-2.19×10^6**	-7.81×10^5
adjusted R^2		0	0.738	-0.056	0.733	0.015	0.723	0.349	0.774
RMSE		0.00131	0.00065	0.00131	0.00064	0.00123	0.00065	0.0010	0.0006
df		19	18	18	17	18	17	17	16
AICc		−204	−229	−201	−227	−204	−226	−209	−226

Table S10. Regression models and assessment values for the spectral slope ratio in the dark control sample, S_{R_Dark} (dimensionless). The parameters are explained in Table S8.

Term	Coef.	Model							
		1	2*	3	4	5	6	7	8
Intercept	*a*	**0.64**	**0.69**	**0.63**	**0.68**	**0.64**	**0.69**	**0.63**	**0.69**
[Fe]	*b1*		**-3.13×10^3**		**-3.24×10^3**		**-3.67×10^3**		**-3.85×10^3**
$[H^+]$	*b2*			2.20×10^2	3.63×10^2			8.77×10^2	-2.70×10^2
[Fe] $[H^+]$	*b3*					-1.26×10^6	2.38×10^7	-3.53×10^7	3.55×10^7
adjusted R^2		0	0.493	−0.037	0.516	−0.117	0.556	−0.031	0.562
RMSE		0.056	0.039	0.055	0.037	0.056	0.035	0.054	0.035
df		19	18	18	17	18	17	17	18
AICc		−54	−66	−51	−65	−51	−66	−50	−63

Table S11. Regression models and assessment values for the photochemistry-induced change in the absorption coefficient of CDOM at 330 nm, Δa_{330} (m^{-1}). The parameters are explained in Table S8.

Term	Coef.	Model							
		1	2	3	4	5*	6	7	8
Intercept	*a*	**5.72**	**3.74**	**4.07**	**2.55**	**3.91**	**3.57**	**3.98**	**3.67**
[Fe]	*b1*		1.16×10^5		9.41×10^4		2.44×10^4		1.96×10^4
$[H^+]$	*b2*			**7.53×10^4**	**7.12×10^4**			-1.30×10^4	-7.16×10^3
[Fe] $[H^+]$	*b3*					**4.25×10^9**	**4.08×10^9**	**4.75×10^9**	**4.39×10^9**
adjusted R^2		0	0.114	0.437	0.521	0.676	0.682	0.680	0.683
RMSE[c]		3.71	3.40	2.71	2.42	2.00	1.98	1.98	1.97
df		19	18	18	17	18	17	17	16
AICc		114	113	104	103	92	95	95	98

Table S12. Regression models and assessment values for the photochemistry-induced change in the spectral slope coefficient at 275–295 nm, $\Delta S_{275-295}$ (nm^{-1}). The parameters are explained in Table S8.

Term	Coef.	Model							
		1	2	3	4	5	6*	7	8
Intercept	*a*	**1.69×10^{-3}**	**1.84×10^{-3}**	**1.25×10^{-3}**	**1.50×10^{-3}**	**1.32×10^{-3}**	**1.79×10^{-3}**	**1.25×10^{-3}**	**1.72×10^{-3}**
[Fe]	*b1*		−8.77		−14.95		**−33.06**		−29.80
$[H^+]$	*b2*			**19.84**	**20.50**			13.76	4.88
[Fe] $[H^+]$	*b3*					**8.62×10^5**	**1.09×10^6**	3.27×10^5	8.76×10^5
adjusted R^2		0.000	-0.042	0.421	0.429	0.338	0.512	0.406	0.519
RMSE		0.00099	0.00099	0.00073	0.00071	0.00076	0.00066	0.0007	0.0007
df		19	18	18	17	18	17	17	16
AICc		−215	−213	−224	−223	−223	−226	−222	−222

Table S13. Regression models and assessment values for the photochemistry-induced change in the spectral slope ratio, ΔS_R (dimensionless). The parameters are explained in Table S8.

Term	Coef.	Model							
		1	2	3	4	5	6*	7	8
Intercept	*a*	**0.12**	**0.12**	**0.10**	**0.10**	**0.10**	**0.11**	**0.10**	**0.12**
[Fe]	*b1*		3.25×10^2		70.9		**-8.46×10^2**		**-1.12×10^3**
$[H^+]$	*b2*			**8.48×10^2**	**8.44×10^2**			−72.5	-4.06×10^2
[Fe] $[H^+]$	*b3*					**4.67×10^7**	**5.25×10^7**	**4.95×10^7**	**7.01×10^7**
adjusted R^2		0	−0.044	0.487	0.457	0.716	0.787	0.717	0.816
RMSE		0.040	0.040	0.028	0.028	0.020	0.017	0.020	0.016
df		19	18	18	17	18	17	17	16
AICc		−68	−65	−79	−76	−92	−95	−89	−94

Table S14. Regression models and assessment values for DIC photoproduction rate (mol C L^{-1} h^{-1}). The parameters are explained in Table S8.

Term	Coef.	Model							
		1	2	3	4	5*	6	7	8
Intercept	*a*	**4.15×10^{-6}**	**2.11×10^{-6}**	**2.89×10^{-6}**	1.23×10^{-6}	**2.65×10^{-6}**	**1.98×10^{-6}**	**2.81×10^{-6}**	**2.27×10^{-6}**
[Fe]	*b1*		**0.116**		**0.103**		4.72×10^{-2}		3.42×10^{-2}
$[H^+]$	*b2*			**5.72×10^{-2}**	**5.27×10^{-2}**			-2.97×10^{-2}	-1.96×10^{-2}
[Fe] $[H^+]$	*b3*					**3.52×10^{3}**	**3.20×10^{3}**	**4.68×10^{3}**	**4.05×10^{3}**
adjusted R^2		0	0.237	0.410	0.604	0.775	0.817	0.812	0.830
RMSE		2.90×10^{-6}	2.46×10^{-6}	2.17×10^{-6}	1.72×10^{-6}	1.30×10^{-6}	1.17×10^{-6}	1.19×10^{-6}	1.13×10^{-6}
df		19	18	18	17	18	17	17	16
AICc		−449	−452	−457	−463	−478	−479	−478	−477

Table S15. Regression models and assessment values for the AQY of DIC photoproduction at 330 nm, ϕ_{330} (mol C mol $photon^{-1}$). The parameters are explained in Table S8.

Term	Coef.	Model							
		1	2	3	4	5*	6	7	8
Intercept	*a*	**5.76×10^{-4}**	**4.32×10^{-4}**	**3.70×10^{-4}**	**2.79×10^{-4}**	**3.76×10^{-4}**	**4.11×10^{-4}**	**3.64×10^{-4}**	**3.83×10^{-4}**
[Fe]	*b1*		8.37		5.63		−2.49		−1.20
$[H^+]$	*b2*			**9.36**	**9.11**			2.29	1.93
[Fe] $[H^+]$	*b3*					**4.69×10^{5}**	**4.86×10^{5}**	**3.81×10^{5}**	**4.03×10^{5}**
adjusted R^2		0	0.035	0.716	0.742	0.866	0.873	0.879	0.881
RMSE		0.00037	0.00035	0.00019	0.00018	0.00013	0.00012	0.00012	0.00012
df		19	18	18	17	18	17	17	16
AICc		−255	−254	−278	−278	−294	−292	−293	−290

Table S16. Regression models and assessment values for the pre-exponential parameter describing the spectral AQY for DIC photoproduction, c (mol C mol photon^{-1}; eq. 1), which also describes the AQY at the reference wavelength 0 nm (ϕ_0). The parameters are explained in Table S8.

Term	Coef.	Model							
		1	2	3	4	5*	6	7	8
Intercept	*a*	**1.44**	**1.42**	**1.42**	**1.41**	**1.42**	**1.42**	**1.42**	**1.42**
[Fe]	*b1*		8.21×10^2		5.74×10^2		−54.2	4.46×10^2	3.04×10^2
[H^+]	*b2*			**8.46×10^2**	**8.20×10^2**				5.36×10^2
[Fe] [H^+]	*b3*					**3.88×10^7**	**3.92×10^7**	2.15×10^7	1.59×10^7
adjusted R^2		0	0.039	0.631	0.657	0.615	0.616	0.671	0.681
RMSE		0.035	0.034	0.021	0.020	0.021	0.021	0.019	0.019
df		19	18	18	17	18	17	17	16
AICc		−72	−71	−90	−90	−91	−88	−91	−88

Table S17. Regression models and assessment values for the spectral slope coefficient of AQY for DIC photoproduction, d (nm^{-1}; eq. 1). The parameters are explained in Table S8.

Term	Coef.	Model							
		1	2	3	4	5*	6	7	8
Intercept	*a*	**0.02**	**0.02478**	**0.02**	**0.03**	**0.02**	**0.02**	**0.02**	**0.02**
[Fe]	*b1*		−36.0		−25.3		7.47		5.00
[H^+]	*b2*			**−36.6**	**−35.5**			−5.19	−3.69
[Fe] [H^+]	*b3*					**-1.89×10^6**	**-1.95×10^6**	**-1.69×10^6**	**-1.79×10^6**
adjusted R^2		0	0.050	0.691	0.727	0.892	0.896	0.897	0.898
RMSE		0.0015	0.0015	0.0008	0.0007	0.0005	0.0004	0.0004	0.0004
df		19	18	18	17	18	17	17	16
AICc		−200	−199	−221	−222	−244	−241	−241	−238

Table S18. Regression models and assessment values for photochemistry-induced change in the spectral slope coefficient of CDOM at 350–400 nm, $\Delta S_{350\text{-}400}$ (nm^{-1}). The parameters are explained in Table S8. No model was chosen here since no one was better than the constant model containing only intercept.

Term	Coef.	Model							
		1	2	3	4	5	6	7	8
Intercept	*a*	$\mathbf{-6.19 \times 10^{-4}}$	-3.84×10^{-4}	$\mathbf{-8.02 \times 10^{-4}}$	-5.36×10^{-4}	$\mathbf{7.24 \times 10^{-4}}$	-4.01×10^{-4}	$\mathbf{-7.97 \times 10^{-4}}$	-5.28×10^{-4}
[Fe]	*b1*		−13.68		−16.42		−22.66		−16.98
$[H^+]$	*b2*			8.37	9.09			13.57	8.51
[Fe] $[H^+]$	*b3*					2.47×10^5	4.02×10^5	-2.80×10^5	3.27×10^4
adjusted R^2		0	-0.002	0.082	0.110	0.055	0.076	0.050	0.110
RMSE		0.00078	0.00076	0.00073	0.00069	0.00076	0.00071	0.0007	0.0007
df		19	18	18	17	18	17	17	16
AICc		−225	−223	−225	−223	−223	−223	−222	−220

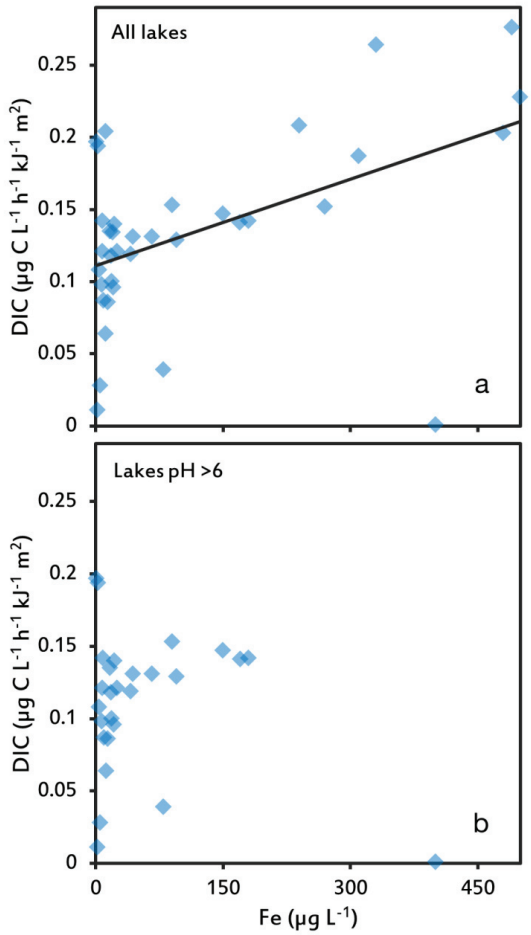

Figure S6. DIC photoproduction rates normalized for total absorbed energy (µg C L^{-1} h^{-1} kJ^{-1} m^2) in lake water samples with different concentrations of Fe.[35] (a) The dots represent all lakes (n = 36; pH 4.5–9.5) examined by Bertilsson and Tranvik (2000). The line represents a significant linear fit on data from individual lakes ($y = 0.00020x + 0.111$, $R^2 = 0.24$, $t = 3.3$, $df = 34$, $p = 0.002$). (b) Same as (a) but for a subset of 27 lakes with pH > 6 ($y = -0.00019x + 0.118$, $R^2 = 0.05$, $t = -1.18$, $df = 25$, $p = 0.25$).

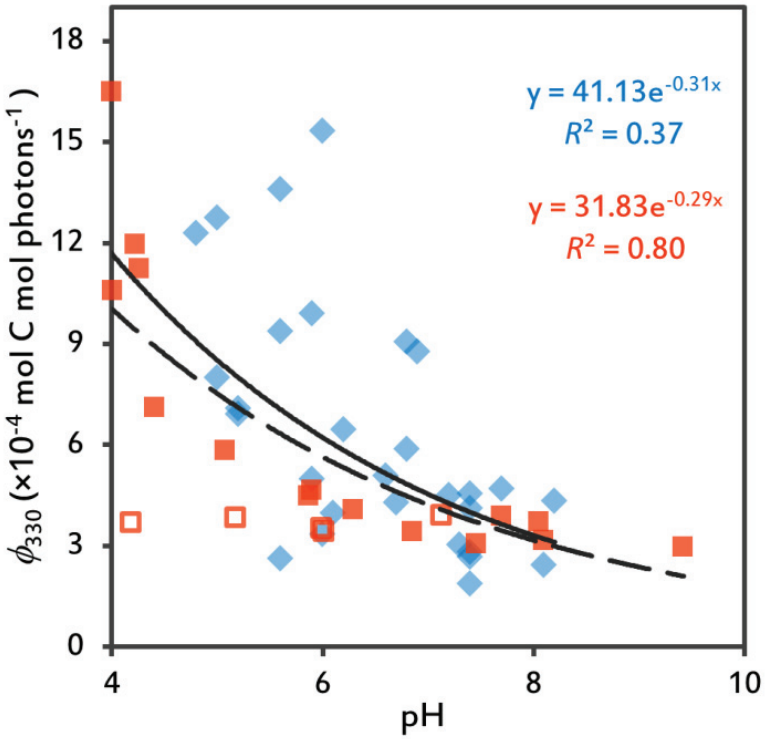

Figure S7. ϕ_{330} and pH reported earlier in lakes (◆) compared to those observed in this study (SPE-DOM from Lake Kuivajärvi with (■) or without (□) added Fe; Table S7). The published values are from two humic lakes in Finland,[17, 27] a reservoir in Alabama,[28] five Swedish lakes,[24] Lake Ersjön (Sweden) over a period of six months,[25] and 16 different types of lakes round the world[26]. Each dot represents ϕ_{330} calculated from the parameters describing ϕ_λ. The equations and curves describe the dependence of ϕ_{330} on pH in earlier studies (blue equation) and in the SPE-DOM solutions with introduced Fe in this study (red equation).

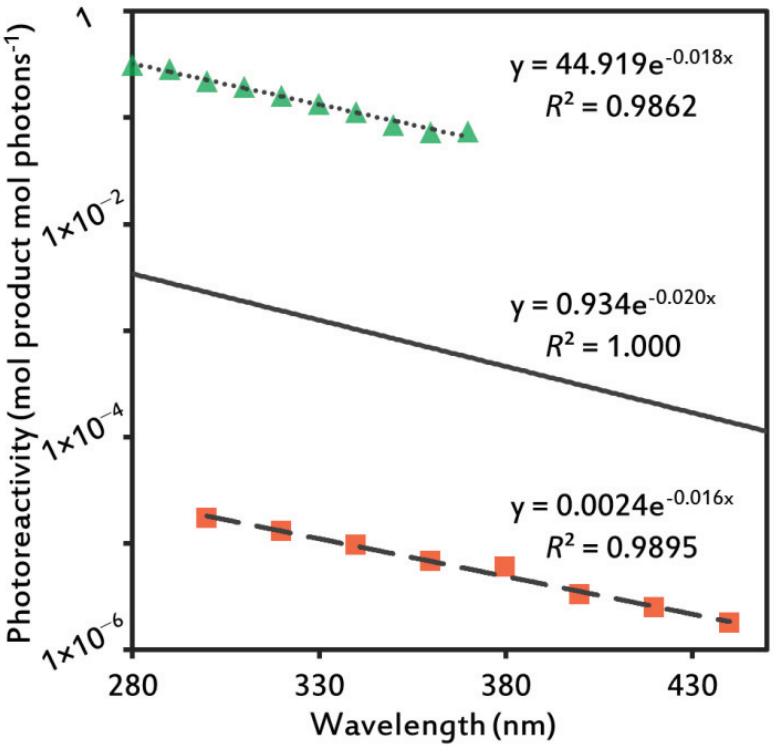

Figure S8. The spectral dependence of photochemical reactivity in three reactions based on the photoreduction of Fe(III). (1) The quantum yields for photoproduction of hydroxyl radicals (HO·) from $Fe(III)OH^{2+}$ (·▲·; Table 1 in Benkelberg et al. 1995).[18] (2) Fe-stimulated ϕ_λ (▬; Figure 5 this study). (3) The photoreductive dissolution of lepidocrocite normalized to photon flux (-■-; Table S2 in Borer et al. 2009).[19] The dots show the photoreactivity at narrow (4 nm or 20 nm) spectral bands. The regression lines and the equations show the spectral dependence expressed as an exponential equation. Note the log-scaled Y-axis. The coefficients of determination ($R^2 > 0.98$) indicated that the exponential equation describes the spectral dependence of reactions well. Although the magnitude of reactivity differed considerably among the reactions, their spectral slope coefficients are similar: (1) 0.018 nm^{-1}, (2) 0.020 nm^{-1}, and (3) 0.016 nm^{-1}.

References

1. Faust, B.C.; Zepp, R.G. Photochemistry of aqueous iron(III)-polycarboxylate complexes: roles in the chemistry of atmospheric and surface waters. *Environ. Sci. Technol.* **1993,** *27* (12), 2517–2522.

2. Voelker, B.M.; Morel, F.M.M.; Sulzberger, B. Iron redox cycling in surface waters: effects of humic substances and light. *Environ. Sci. Technol.* **1997,** *31* (4), 1004–1011.

3. Cho, I.; Zoh, K. Photocatalytic degradation of azo dye (Reactive Red 120) in TiO_2/UV system: Optimization and modeling using a response surface methodology (RSM) based on the central composite design. *Dyes Pigm.* **2007,** *75* (3), 533–543.

4. Khataee, A.R.; Zarei, M.; Asl, S.K. Photocatalytic treatment of a dye solution using immobilized TiO2 nanoparticles combined with photoelectro-Fenton process: Optimization of operational parameters. *J. Electroanal. Chem.* **2010,** *648* (2), 143–150.

5. Stamatis, N.; Antonopoulou, M.; Hela, D.; Konstantinou, I. Photocatalytic degradation kinetics and mechanisms of antibacterial triclosan in aqueous TiO_2 suspensions under simulated solar irradiation. *J. Chem. Technol. Biotechnol.* **2014,** *89* (8), 1145–1154.

6. Lenth, R.V. Response-Surface Methods in R, using rsm. *J. Stat. Softw.* **2009,** *32* (7), 1–17.

7. Gustafsson, C.; Gschwend, P.M. Aquatic colloids: Concepts, definitions, and current challenges. *Limnol. Oceanogr.* **1997,** *42* (3), 519–528.

8. Gustafsson, Ö; Widerlund, A.; Andersson, P.S.; Ingri, J.; Roos, P.; Ledin, A. Colloid dynamics and transport of major elements through a boreal river — brackish bay mixing zone. *Mar. Chem.* **2000,** *71* (1–2), 1–21.

9. Ingri, J.; Widerlund, A.; Land, M.; Gustafsson, Ö; Andersson, P.; Öhlander, B. Temporal variations in the fractionation of the rare earth elements in a boreal river; the role of colloidal particles. *Chem. Geol.* **2000,** *166* (1–2), 23–45.

10. Neubauer, E.; Köhler, S.J.; von, d.K.,Frank; Laudon, H.; Hofmann, T. Effect of pH and stream order on iron and arsenic speciation in boreal catchments. *Environ. Sci. Technol.* **2013,** *47* (13).

11. Chen, K.; Chen, T.; Chan, Y.; Cheng, C.; Tzou, Y.; Liu, Y.; Teah, H. Stabilization of natural organic matter by short-range-order iron hydroxides. *Environ. Sci. Technol.* **2016,** *50* (23), 12612–12620.

12. Karlsson, T.; Persson, P. Complexes with aquatic organic matter suppress hydrolysis and precipitation of Fe(III). *Chem. Geol.* **2012,** *322–323* (0), 19–27.

13. Philippe, A.; Schaumann, G.E. Interactions of dissolved organic matter with natural and engineered inorganic colloids: a review. *Environ. Sci. Technol.* **2014,** *48* (16), 8946–8962.

14. Gustafsson, J.P.; Berggren Kleja, D. Modeling salt-dependent proton binding by organic soils with the NICA-Donnan and Stockholm Humic models. *Environ. Sci. Technol.* **2005,** *39* (14), 5372–5377.

15. Xiao, Y.; Sara-Aho, T.; Hartikainen, H.; Vähätalo, A.V. Contribution of ferric iron to light absorption by chromophoric dissolved organic matter. *Limnol. Oceanogr.* **2013,** *58* (2), 653–662.

16. Gao, H.; Zepp, R.G. Factors influencing photoreactions of dissolved organic matter in a coastal river of the southeastern United States. *Environ. Sci. Technol.* **1998,** *32* (19), 2940–2946.

17. Vähätalo, A.V.; Salkinoja -Salonen, M.; Taalas, P.; Salonen, K. Spectrum of the quantum yield for photochemical mineralization of dissolved organic carbon in a humic lake. *Limnol. Oceanogr.* **2000,** *45* (3), 664–676.

18. Benkelberg, H.; Warneck, P. Photodecomposition of iron (III) hydroxo and sulfato complexes in aqueous solution: wavelength dependence of OH and SO_4^- quantum yields. *J. Phys. Chem.* **1995,** *99* (14), 5214–5221.

19. Borer, P.; Sulzberger, B.; Hug, S.J.; Kraemer, S.M.; Kretzschmar, R. Photoreductive dissolution of iron(III) (hydr)oxides in the absence and presence of organic ligands: Experimental studies and kinetic modeling. *Environ. Sci. Technol.* **2009,** *43* (6), 1864–1870.

20. Rundel, R.D. Action spectra and estimation of biologically effective UV radiation. *Physiol. Plantarum* **1983,** *58* (3), 360–366.

21. Johannessen, S.C.; Miller, W.L. Quantum yield for the photochemical production of dissolved inorganic carbon in seawater. *Mar. Chem.* **2001,** *76* (4), 271–283.

22. Bélanger, S.; Xie, H.; Krotkov, N.; Larouche, P.; Vincent, W.F.; Babin, M. Photomineralization of terrigenous dissolved organic matter in Arctic coastal waters from 1979 to 2003: Interannual variability and implications of climate change. *Global Biogeochem. Cycles* **2006,** *20* (4), DOI: 10.1029/2006GB002708.

23. White, E.M.; Kieber, D.J.; Sherrard, J.; Miller, W.L.; Mopper, K. Carbon dioxide and carbon monoxide photoproduction quantum yields in the Delaware Estuary. *Mar. Chem.* **2010,** *118* (1–2), 11–21.

24. Koehler, B.; Landelius, T.; Weyhenmeyer, G.A.; Machida, N.; Tranvik, L.J. Sunlight-induced carbon dioxide emissions from inland waters. *Global Biogeochem. Cycles* **2014,** *28* (7), DOI: 10.1002/2014GB004850.

25. Groeneveld, M.; Tranvik, L.; Natchimuthu, S.; Koehler, B. Photochemical mineralisation in a boreal brown water lake: considerable temporal variability and minor contribution to carbon dioxide production. *Biogeosciences* **2016,** *13* (13), 3931–3943.

26. Koehler, B.; Broman, E.; Tranvik, L.J. Apparent quantum yield of photochemical dissolved organic carbon mineralization in lakes. *Limnol. Oceanogr.* **2016,** DOI: 10.1002/lno.10366.

27. Aarnos, H.; Ylöstalo, P.; Vähätalo, A.V. Seasonal phototransformation of dissolved organic matter to ammonium, dissolved inorganic carbon, and labile substrates supporting bacterial biomass across the Baltic Sea. *J. Geophys. Res. Biogeosci.* **2012,** DOI: 10.1029/2010JG001633.

28. Vähätalo, A.V.; Wetzel, R.G. Photochemical and microbial decomposition of chromophoric dissolved organic matter during long (months–years) exposures. *Mar. Chem.* **2004,** *89* (1–4), 313–326.

29. Cory, R.M.; Ward, C.P.; Crump, B.C.; Kling, G.W. Sunlight controls water column processing of carbon in arctic fresh waters. *Science* **2014,** *345* (6199), 925–928.

30. Vachon, D.; Lapierre, J.; del Giorgio, P.A. Seasonality of photochemical dissolved organic carbon mineralization and its relative contribution to pelagic CO_2 production in northern lakes. *J. Geophys. Res. Biogeosci.* **2016,** *121* (3), 864–878.

31. Reader, H.E.; Miller, W.L. Variability of carbon monoxide and carbon dioxide apparent quantum yield spectra in three coastal estuaries of the South Atlantic Bight. *Biogeosciences* **2012,** *9* (11), 4279–4294.

32. Powers, L.C.; Miller, W.L. Photochemical production of CO and CO_2 in the Northern Gulf of Mexico: Estimates and challenges for quantifying the impact of photochemistry on carbon cycles. *Mar. Chem.* **2015,** *171*, 21–35.

33. Anderson, D.R.; Burnham, K.P.; White, G.C. AIC model selection in overdispersed capture-recapture data. *Ecology* **1994,** *75* (6), 1780–1793.

34. Burnham, K.P.; Anderson, D.R. Multimodel inference: understanding AIC and BIC in model selection. *Socio. Meth. Res.* **2004,** *33* (2), 261–304.

35. Bertilsson, S.; Tranvik, L.J. Photochemical transformation of dissolved organic matter in lakes. *Limnol. Oceanogr.* **2000,** *45* (4), 753–762.

II

LINKING PHOTOCHEMICAL REACTIVITY OF DISSOLVED ORGANIC CARBON TO CATCHMENT PROPERTY AND WATER QUALITY IN BOREAL LAKES

by

Gu Y., Vuorio K., Perämäki, S., Tiirola M. & Vähätalo A.V.

Manuscript

III

AN INTER-LABORATORY COMPARISON OF THE APPARENT QUANTUM YIELD FOR PHOTOCHEMICAL DISSOLVED ORGANIC CARBON MINERALIZATION IN INLAND WATERS

by

Koehler B., Miller W.L., Cory R.M., Einarsdottir K., Gu Y., Powers L.C.,
Vähätalo A.V., Ward C.P. & Tranvik L.J.

Manuscript

IV

PHOTOCHEMICAL MINERALIZATION OF TERRIGENOUS DOC TO DISSOLVED INORGANIC CARBON IN OCEAN

by

Aarnos H., Gélinas, Y., Kasurinen V., Gu Y., Puupponen V. & Vähätalo A.V.

Submitted manuscript